Tom Coleman, Siew Hoon Wong, Matthew N. Podgorski, John B. Bruning, James J. De Voss, and Stephen G. Bell

Cytochrome P450 CYP199A4 from Rhodopseudomonas palustris catalyses heteroatom dealkylations, sulfoxidation and amide and cyclic hemiacetal formation

ACS Catalysis, 2018; 8(7):5915-5927

The Cytochrome P450 CYP199A4 from *Rhodopseudomonas palustris* catalyses heteroatom dealkylations, sulfoxidation and amide and cyclic hemiacetal formation

Tom Coleman,[1] Siew Hoon Wong,[2] Matthew N. Podgorski,[1] John B. Bruning,[3] James J. De Voss[*,2] and Stephen G. Bell*[*1]

1 Department of Chemistry, University of Adelaide, SA 5005, Australia;

2 School of Chemistry and Molecular Biosciences, University of Queensland, Brisbane, Qld, 4072, Australia;

3 School of Biological Sciences, University of Adelaide, SA 5005, Australia

Corresponding authors: Stephen Bell, stephen.bell@adelaide.edu.au; James De Voss j.devoss@uq.edu.au

ABSTRACT. The cytochrome P450 enzymes execute a range of selective oxidative biotransformations across many biological systems. The bacterial enzyme CYP199A4 catalyses the oxidative demethylation of 4-methoxybenzoic acid. The benzoic acid moiety of the molecule binds in the active site of the enzyme such that the functional group at the *para*-position is held close to the heme iron. Therefore, CYP199A4 has the potential to catalyse alternative monooxygenase reactions with different *para*-substituted benzoic acid substrates such as thioethers and alkylamines. The oxidation of 4-methyl- and 4-ethyl-thiobenzoic acids by CYP199A4 resulted in sulfur oxidation. 4-Ethylthiobenzoic acid sulfoxidation and 4-ethylbenzoic acid

hydroxylation by CYP199A4 occurred with high enantioselectivity (>74% enantiomeric excess). By way of contrast, CYP199A4 catalysed exclusive oxidative N-demethylation over N-oxide formation with 4-methyl- and 4-dimethyl-aminobenzoic acids. Unexpectedly acetamide formation by CYP199A4 competes with dealkylation in the turnover of 4-ethyl- and diethyl-aminobenzoic acids. No oxidative dealkylation was observed with 3,4-ethylenedioxybenzoic with only hydroxylation to form a cyclic hemiacetal being detected. The X-ray crystal structures of four substrate-bound forms of the enzyme were solved and revealed subtle changes in the location of the *para* substituent which, when combined with the reactivity of the substituents, provided a basis for understanding the changes in selectivity. Furthermore, in the 4-ethylthiobenzoic acid bound structure the active site residue Phe298 moves to accommodate the substituent which points away from the heme iron. As such the CYP199A4 enzyme provides ready access to a combination of structural, binding and activity data with which to study a variety of reactions which are catalysed by the P450 superfamily of enzymes.

KEYWORDS biocatalysis, cytochrome P450 enzymes, dealkylation, heteroatom oxidation, crystal structures, C–H bond oxidation, enzyme mechanism.

Introduction

The heme-dependent cytochrome P450 (CYP) monooxygenase enzymes typically catalyse the insertion of an oxygen atom derived from dioxygen into unactivated carbon-hydrogen bonds.[1-6] There is strong experimental and theoretical evidence that the ubiquitous hydroxylation reaction of P450s proceeds via the electrophilic ferryl intermediate (Cpd I).[7, 8] However, while theory favours Cpd I involvement in the majority of P450 reactions, experimental studies have suggested that earlier intermediates of the catalytic cycle, including the electrophilic ferric-hydroperoxide (Cpd 0) and the nucleophilic ferric-peroxo anion, could also have in role in other P450-catalysed monooxygenase activity (Scheme 1). These intermediates have been proposed to play a part in epoxidation, sulfoxidation and other less common transformations such as Baeyer Villiger-like oxidations and carbon-carbon bond cleavage.[9-16]

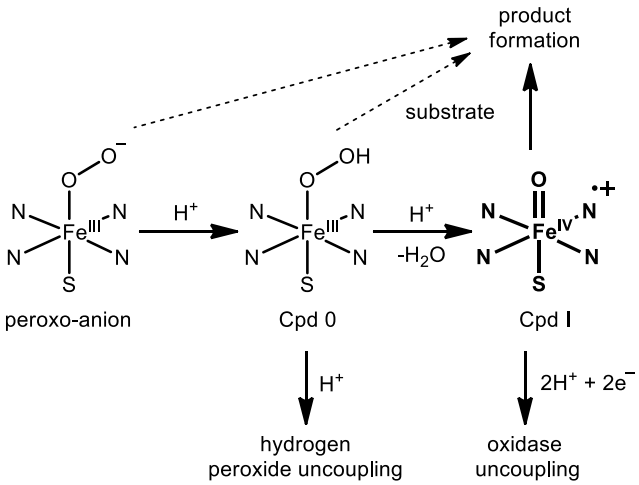

Scheme 1 The potential active oxidants of cytochrome P450 which could lead to product formation and the main uncoupling pathways arising from them.

CYP199A4, from *Rhodopseudomonas palustris* strain HaA2, is able to demethylate 4-methoxybenzoic acid and 4-methoxycinnamic acid, and demethenylate 3,4-methylenedioxybenzoic acid with complete selectivity.[17-19] It reacts with *para*-substituted alkylbenzoic acids, such as 4-ethyl- and 4-isopropyl-benzoic acids, to form a mixture of alkene and alcohol products through discrete hydroxylation and desaturation pathways.[17, 20] These activities are supported by a ferredoxin (HaPux; [2Fe-2S]) and a ferredoxin reductase (HaPuR; FAD-dependent) both of which are also from the *R*. *palustris* HaA2 bacterium. This class I electron

transfer chain mediates heme reduction and uses NADH as the source of the reducing equivalents. When CYP199A4 was paired with these electron transfer partners, the activities of oxidative O-demethylation, hydroxylation and desaturation of *para*-substituted benzoic acids were high and the loss of reducing equivalents due to uncoupling side reactions (i.e. NADH consumption without organic product formation) was low (Scheme 1).[17, 21-23]

The high activity and ease of use of the CYP199A4 enzyme means it is eminently suitable for biocatalytic applications involving C–H bond activation as well as studies on the mechanism of action of cytochrome P450 enzymes.[17, 20, 24-26] Adding to its desirability, CYP199A4 has high chemo- and substrate specificity for oxidation of the *para* substituent of methoxy-substituted benzoic acids. Alterations to the benzene ring and carboxylate group or removal of the *para*-substituent all reduced the substrate binding and monooxygenase activity of CYP199A4.[17, 20, 27] However, replacement of the methoxy group with alternate substituents is tolerated.[17, 20, 27] This high substrate regioselectivity can be related to how the substrate is bound in the enzyme active site. The crystal structure of several substrate-bound forms of CYP199A4 have been solved including those of 4-methoxybenzoic (PDB: 4DO1), 4-ethylbenzoic (PDB: EGM) and 3,4-dimethoxybenzoic (PDB: 4EGN) acids. These crystal structures reveal that the carboxylate group forms direct and indirect hydrogen bonds with hydrophilic arginine and serine residues. The benzene ring interacts hydrophobically with the side chains of phenylalanine and other hydrophobic residues (e.g. Phe182 and Phe185). These binding interactions hold the substrate in such an orientation that the *para* substituent is held over the heme iron and substituents at the *ortho* and *meta* positions point away from the heme.[18, 20] This accounts for the high level of selectivity for the *para* position in, for example, the oxidative demethylation of 3,4-dimethoxybenzoic acid which generated 4-hydroxy-3-methoxybenzoic acid as the sole product.[17, 20]

As CYP199A4 would bind different *para*-substituted benzoic acids with the altered substituent held over the heme iron it is potentially an ideal enzyme with which to study and compare alternative P450 monooxygenase activities. Suitably substituted benzoic acids could be used to investigate and compare the

different monooxygenase reactions of this enzyme. Here we report the binding, turnover kinetics and the substrate-bound crystal structures of a range of *para*-substituted benzoic acids in which the substituent is an oxygen, nitrogen or sulfur containing moiety. For example, we compare the reactivity of CYP199A4 with 4-methoxy-, 4-methylthio-, and 4-methylamino-benzoic acids and differently substituted variants. This enables a comparison of heteroatom (O, N and S) dealkylation versus oxidation in which the minimal changes to the substrate have been made. We also show that this enzyme is able to efficiently catalyse a range of common and more unusual P450 supported biotransformations, generating the metabolites in good yields. The new structures provide valuable information on the positions of the sites of monooxygenase action in relation to the heme iron.

Experimental Section

General

General reagents and organic substrates were from Sigma-Aldrich, TCI, Fluorochem or VWR. *N*,*O*-Bis(trimethylsilyl)trifluoroacetamide with trimethylsilyl chloride (BSTFA + TMSCl, 99:1) was from Sigma-Aldrich. Buffer components, NADH and isopropyl-β-D-thiogalactopyranoside (IPTG) were from Astral Scientific, Australia. 3-(Methylsulfinyl)benzoic acid was obtained from Enamine Ltd. UV/Vis spectra and spectroscopic activity assays were recorded on an Agilent CARY-60 or Varian CARY-5000 spectrophotometer with temperature control (30 ± 0.5 °C). High Performance Liquid Chromatography (HPLC) analysis was performed on an Agilent 1260 Infinity Pump equipped with an autoinjector connected using an Agilent Eclipse Plus C18 column (250 mm x 4.6 mm, 5 μm). Gradients of 20 - 95%, 0 - 80% or 0 - 50% acetonitrile in water (0.1% trifluoroacetic acid, TFA) at a flow rate of 1 mL min^{-1} over 30 minutes were used. Gas Chromatography-Mass Spectrometry (GC-MS) was undertaken on a Shimadzu GC-17A using a QP5050A GC-MS detector equipped with a DB-5 MS fused silica column (30 m x 0.25 mm, 0.25 μm). The interface and injector were held at 280 °C and 250 °C, respectively. The oven temperature was held at 100 ºC for 1 min and then increased at 15 ºC min^{-1} up to 220 ºC. The chromatography retention times for the substrates and products (trimethylsilyl (TMS) derivatives for GC-MS) are given in the Supporting Information. Enantioselective chromatography of methyl 4-(1′-hydroxyethyl)-benzoate was performed using a CHIRALCEL®OJ column (Analytical: 250 mm, 4.6 mm, 5 μm, Daicel; Preparative: 250 mm, 20 mm, 5 μm, Daicel) using an isocratic run of 5% isopropanol in hexane (flow rate: Analytical 0.8 ml min^{-1}; Preparative 16 ml min^{-1}) and monitoring at 254 nm. For methyl 4-methylsulfinylbenzoate, analysis was performed with a CHIRALCEL®OD Analytical column (250 mm, 4.6 mm, 5 μm, Daicel) eluting isocratically 5% isopropanol in hexane at a flow rate of 0.8 ml min^{-1} and monitoring at 270 nm.

The expression, purification and characterisation of CYP199A4, HaPux and HaPuR were undertaken as described previously.[17, 18, 20] The CYP199A4 protein concentration was calculated using ε_{419} = 119 $mM^{-1}\,cm^{-1}$.[17, 18]

Substrate binding: spin state determination and binding titrations

The spin-state shift induced upon substrate binding was determined using a CYP199A4 concentration of 1.5 – 3.3 μM in 50 mM Tris, pH 7.4. Addition of 1μL aliquots of substrate (from a 100 mM stock) were performed until the spectrum did not change further. The percentage spin state shift was compared with a set of spectra calculated from the sum of the appropriate percentages of the spectra of the substrate-free (>95% low-spin) and camphor-bound (>95% high-spin) forms of wild-type CYP101A1 (P450cam) and estimated to approximately ±5%.

The binding affinity was determined by measuring the dissociation constant. The enzyme was diluted to 0.4 – 1.7 μM in 2.5 mL of 50 mM Tris, pH 7.4 and this was used to baseline the spectrophotometer. Aliquots of the substrate (0.5 – 2 μL) were added from 1, 10 or 100 mM stock solutions in ethanol or DMSO using a Hamilton syringe until the peak-to-trough difference of the Soret band did not change. The maximum Soret band peak-to-trough absorbance difference (Δ*A*) was recorded. The dissociation constants, K_d, were obtained by fitting Δ*A* against the added substrate concentration [S] using a hyperbolic function:

$$\Delta A = \frac{\Delta A_{max} \times [S]}{K_d + [S]}$$

ΔA_{max} is the maximum absorbance difference. All the *para*-substituted alkyloxy, alkylamino and alkylthio-benzoic acids exhibited a K_d of < 5 μM. Therefore this data were fitted to the Morrison tight binding quadratic equation:[28]

$$\frac{\Delta A}{\Delta A_{max}} = \frac{([E]+[S]+K_d) - \sqrt{\{([E]+[S]+K_d)^2 - 4[E][S]\}}}{2[E]}$$

ΔA_{max} is the maximum absorbance difference and [E] is the enzyme concentration.

Activity assays

In vitro NADH turnover rate assays were performed in a total volume of 1.2 mL containing 50 mM Tris, pH 7.4, 0.5 μM CYP199A4, 5 μM HaPux and 0.5 μM HaPuR. The buffer solution was

oxygenated and the enzymes were then added before equilibration at 30 °C for 2 min. NADH was added to a final A_{340} of ~ 2.00 (~ 320 μM concentration) and this absorbance was monitored over time. Substrates were added from a 100 mM stock solution in ethanol or DMSO to a concentration of 1 mM to initiate the reaction. The NADH oxidation rate was calculated using ε_{340} = 6.22 $mM^{-1}cm^{-1}$. The product formation rate and coupling efficiency were calculated by quantitating the amount of product in the turnover as described below.

The concentration of hydrogen peroxide generated during the NADH turnovers was assayed using a horseradish peroxidase (HRP)/phenol/4-aminoantipyrine (4-AP) method.[29] To 400 μL of the turnover mixture 200 μL of a solution of 50 mM phenol (pH 7.4, Tris buffer) and 200 μL of 5 mM 4-AP (pH 7.4, Tris buffer) were added. The absorbance of the resulting mixture at 510 nm was set to zero, and 1 μL of a 20 mg mL^{-1} solution of HRP was added. The absorbance at this wavelength was recorded again and used to calculate the concentration of hydrogen peroxide (ε_{510} = 6.58 mM^{-1} cm^{-1}).

Analysis of metabolites

The products arising from enzyme turnover were mostly identified via co-elution of chemical standards using HPLC or GC-MS of the trimethylsilyl chloride (TMSCl) derivatised forms.[17] For HPLC analysis 150 μL of the final reaction mixture was combined with 2 μL of an internal standard solution (20 mM 9-hydroxyflourene in ethanol) and 50 μL of acetonitrile.

For GC-MS analysis, 990 μL of the final reaction mixture was mixed with 10 μL of internal standard (10 mM 9-hydroxyfluorene) and 3 μL of 3 M HCl. These samples were extracted with ethyl acetate (3 x 400 μL) and the organic extracts combined. The extract was dried over $MgSO_4$ and the solvent was evaporated under a stream of dinitrogen. This dried sample was resuspended in 150 μL anhydrous acetonitrile. Excess (35 μL) BSTFA + TMCS (99:1) was added and the mixture left for at 2 hours to produce the derivatised carboxylic acid and the alcohol or amine groups, if formed. These reaction mixtures were injected directly into the GC-MS. Calibrations were

performed using fixed amounts of these standards to quantitate the level of product in the turnovers, either by HPLC or GC-MS.

The turnovers of 4-dimethylamino-, 4-ethylamino- and 4-diethylamino-benzoic acids contained products which required two P450 catalytic cycles to be completed. These were 4-aminobenzoic acid produced by double dealkylation in the cases of 4-dimethylamino- and 4-diethylamino-benzoic acids, and 4-acetamidobenzoic acid in the cases of 4-ethylamino- and 4-diethylamino-benzoic acids. In determining the total coupling efficiency of these turnovers, double the molar amount of NADH was assumed to be consumed during formation these products.

Synthesis, isolation and purification of products

To isolate the products of 3,4-ethylenedioxybenzoic and 4-ethylaminobenzoic acids for characterisation we utilised a whole-cell oxidation system comprising the plasmids pETDuet and pRSFDuet, as has been described previously.[17] The plasmids were transformed into BL21(DE3) *E. coli* cells and grown on LB plates containing the antibiotics ampicillin, 100 μg mL^{-1}, and kanamycin, 30 μg mL^{-1} ($LB_{amp/kan}$). A colony was added to 500 mL broth ($2xYT_{amp/kan}$) and grown at 37 ºC overnight at 150 rpm. The temperature was reduced to 25 °C, the shaker speed reduced to 120 rpm and protein production was started by the addition of 100 μM IPTG (from a 0.5 M stock in H_2O). The growths were continued for 24 hours before the cell pellet was harvested by centrifugation.[30] The cell pellet (~ 6 g cell wet weight L^{-1}) was resuspended in double the volume of *E. coli* minimal media (EMM)[30] and split into 200 mL aliquots in 2 L baffled flasks. The substrate was added to these cells to a final concentration of 2 mM and the reactions were then shaken at 160 rpm and 30 °C for 20 hours.

The cells were removed by centrifugation (as described above) and the supernatant was acidified before extraction with ethyl acetate (3 x 100 mL), washing with brine (100 mL) and drying over $MgSO_4$. The majority of solvent was removed using a rotary evaporator before using a stream of nitrogen. The products separated using an Agilent 1100 HPLC equipped with semi-prep Supelcosil LC-18 column (5 μm particle size, 25 cm × 10 mm). A gradient of 20 - 50% acetonitrile

(containing trifluoroacetic acid, 0.1%) in water (TFA, 0.1%) was used. UV detection at 240, 254 and 280 nm was used and the product containing fractions were combined. The acetonitrile and water were removed by lyophilisation. The extract dissolved in deuterated DMSO and a combination of ^{1}H and ^{13}C NMR experiments were used to identify the product (Supporting Information). These were acquired on an Agilent DD2 spectrometer operating at 500 MHz for ^{1}H and 126 MHz for ^{13}C.

The different enantiomers of methyl 4-(1′-hydroxyethyl)-benzoate were obtained by separating the racemic mixture of the enantiomers using enantioselective HPLC. The enantiomers were identified based upon comparison of their elution order and optical rotation with literature reports.[31, 32] However, these assignments were apparently based upon catalyst specificity and so formation of and ^{1}H NMR analysis of the corresponding (*R*)-α-methoxy-α-trifluoromethylphenylacetic acid esters (Mosher's Ester) of each enantiomer was undertaken to confirm its configuration.

(*R*) enantiomer: R_T 22.8 min (analytical conditions); $[\alpha]_D$ 38° (c 0.1, $CHCl_3$) Mosher's Ester ^{1}H NMR (400 MHz, $CDCl_3$) δ 1.56 (d, *J* = 7 Hz, 3H), 3.54 (brd s, 3H), 3.90 (s, 3H), 6.13 (q, *J* = 7 Hz, 1H) 7.31-7.43 and 7.99-8.02 (m, 9H).

(*S*) enantiomer: R_T 20.3 min (analytical conditions); $[\alpha]_D$ -37° (c 0.1, $CHCl_3$) Mosher's Ester ^{1}H NMR (400 MHz, $CDCl_3$) δ 1.62 (d, *J* = 7 Hz, 3H), 3.45 (brd s, 3H), 3.90 (s, 3H), 6.09 (q, *J* = 7 Hz, 1H) 7.26-7.41 and 7.94-7.96 (m, 9H).

The racemic mixtures of the 4-alkylthiobenzoic acids were generated by reacting them with hydrogen peroxide before derivatisation to the methyl esters.

Protein crystallisation and X-ray crystallography

Prior to use, glycerol was removed from CYP199A4 using a 5 mL gel filtration column (PD-10, GE Healthcare). For crystallisation, CYP199A4 was concentrated to 30 - 35 mg mL^{-1} in 50 mM Tris,

pH 7.4. Substrate was added to the protein from a 100 mM stock solution in EtOH/DMSO to a final concentration of 1 mM.

Crystals were obtained using the hanging-drop vapor diffusion method at 16 ^{o}C using 1 µL of protein with 1 µL of reservoir solution and equilibrated with 500 µL of the same reservoir solution. Rectangular plate-shaped crystals of approx. 300 µm by 150 µm by 20 µm were obtained in 1 week from 30 - 35 mg mL^{-1} CYP199A4 (containing 1 mM substrate) with a reservoir solution containing 0.2 M magnesium acetate tetrahydrate, and 20 - 23% w/v PEG-3,350 and 0.1 M Bis-Tris pH 5.25 - 5.5. Crystals were harvested using a Microloop or Micromount (MiTeGen), then cryoprotected by immersion in Parabar 10312 (Paratone-N, Hampton Research) and flash cooled in liq. N_2. X-ray diffraction data was collected at 100 K on the MX1 beamline at the Australian Synchrotron.[33, 34]

All diffraction data were indexed and integrated using iMosflm;[35] scaled, merged and R-free flags were added using Aimless,[36] both available in the CCP4 suite of programs.[37] The phase problem was solved using the molecular replacement method with Phaser in CCP4,[38] using 4-methoxybenzoic acid-bound CYP199A4 (PDB: 4DO1, with the 4-methoxybenzoic acid and heme ligands removed) as the initial search model. Electron density maps were obtained after initial model building and the model was rebuilt using Coot.[39] Structural refinements were performed over multiple iterations using Phenix Refine available in the Phenix suite of programs.[40] Composite Omit maps were generated using the appropriate program in Phenix. In the case of 4-methylaminobenzoic acid, a Feature-Enhanced Map (FEM) was generated to reduce model bias rather than a Composite Omit Map.[41] Detailed data collection and structural refinement statistics for the data sets are summarised in Table 1.

The coordinates for the crystal structures of the substrate-bound CYP199A4 combinations studied have been deposited in the Protein Data Bank (accession codes presented in Table 1).

Docking Studies

3-Methylaminobenzoic acid was docked into the active site of CYP199A4 (PDB: 5U6W) using the ICM-Pro software.[42] The ligand bound in the active site (4-methylaminobenzoic acid) was first modified to 3-methylaminobenzoic acid using the ICM 3D Ligand Editor. The 3-methylamino moiety was placed pointing away from the substrate as per the crystal structure of 3,4-dimethoxybenzoic acid bound CYP199A4 (PDB: 4EGN). Docking was performed using the docking module of ICM-Pro (Molsoft). The molecule reorientated into a lower energy configuration with this substituent pointing towards the heme. A higher energy (lower scoring) orientation had the 3-methylamino moiety pointing away the heme.

Table 1 Data collection and refinement statistics for the substrate bound CYP199A4 crystal structures: Where multiple values are presented, the overall value is presented first, while the value for the highest resolution (outer) shell in is parentheses.

Statistic	4-MethylthioBA	4-EthylthioBA	4-MethylaminoBA	4-EthoxyBA
PDB code	5KT1	5U6U	5U6W	5U6T
X-ray wavelength	0.9537	0.9537	0.9537	0.9537
Unit cell parameters	a = 44.07, b = 51.28, c = 79.98, α = 90.00, β = 91.82, γ = 90.00	a = 44.18, b = 51.35, c = 79.91, α = 90.00, β = 92.11, γ = 90.00	a = 44.37, b = 51.15, c = 78.92, α = 90.00, β = 91.98, γ = 90.00	a = 44.44, b = 51.42, c = 79.12, α = 90.00, β = 91.95, γ = 90.00
Space group	$P12_11$	$P12_11$	$P12_11$	$P12_11$
Molecules in asymmetric unit	1	1	1	1
Resolution range	44.05 – 2.01 (2.07 – 2.01)	44.15 – 1.79 (1.82 – 1.79)	44.34 – 2.63 (2.76 – 2.63)	44.42 – 1.94 (1.98 – 1.94)
<I/σ(I)>	7.2 (2.1)	12.0 (2.1)	6.9 (1.8)	8.4 (2.1)
Unique reflections	23479	33670	10517	26777
Completeness of data	99.7 (97.2)	99.8 (97.7)	98.6 (89.4)	99.8 (96.9)
Redundancy / multiplicity	7.1 (6.7)	7.4 (7.1)	7.4 (7.0)	7.4 (7.2)
R_{merge} (%)	29.7 (89.4)	10.7 (81.8)	25.0 (88.6)	16.8 (78.8)
R_{pim} (%)	11.9 (36.7)	4.2 (32.5)	9.9 (35.7)	6.6 (31.2)
$CC_{1/2}$ (%)	98.4 (82.8)	99.8 (97.7)	99 (77.9)	99.5 (77.4)
R_{work}	0.1555	0.1523	0.2243	0.1331
R_{free} (5% held)	0.2234	0.2021	0.2605	0.1842
Ramachandran favored (%)	97.2	97.2	97.7	98.0
Ramachandran outliers (%)	0	0.3	0	0
Rotamer outliers (%)	1.6	0.9	0.3	0.6
Omit map generation method	Composite Omit Map [43] 0.8 sigma, 1.6 Å carve	Composite Omit Map [43] 0.8 sigma, 1.6 Å carve	Feature-Enhanced Map [41] 1 sigma, 1.6 Å carve	Composite Omit Map [43] 0.8 sigma, 1.6 Å carve

Results

Substrate binding and product formation

An array of benzoic acids with oxygen, nitrogen and sulfur containing substituents at the *para*-position were screened for binding to and oxidation by CYP199A4 (Figure 1).

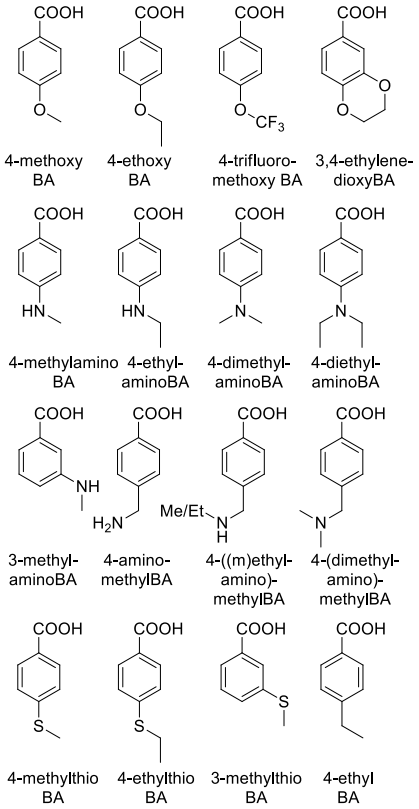

Figure 1 Substrates of CYP199A4 investigated in this study

Oxygen-containing substituents: As with 4-methoxybenzoic acid, 4-ethoxybenzoic acid bound tightly to CYP199A4 and induced a ≥95% shift of the enzyme spin state to the high-spin (HS) form, indicative of binding in the active site (Table 2, Figure S1, Figure S2). It was oxidatively demethylated to yield 4-hydroxybenzoic acid as the sole product but the activity, as measured by product formation rate (PFR, 527 nmol.nmol-CYP^{-1}.min^{-1}, henceforth abbreviated to min^{-1}), was lower than observed for 4-methoxybenzoic acid (Scheme 2, Table 2, Figure S3. Figure S4, Figure S5).

Table 2 Substrate binding parameters and catalytic turnover activity data for CYP199A4 with various substrates.

Substrate	% HS	K_d (μM)	*N*[a]	PFR[b]	C (%)[c]	H_2O_2 (%)
***para*- O, N, S and alkyl substituted**						
4-methoxybenzoic acid[g]	≥95%	0.22 ±	1340 ± 28	1220 ±	91 ± 2	2 ± 0.2

		0.02		120		
4-ethoxybenzoic acid	95%	0.17 ± 0.02	527 ± 10	527 ± 10	100 ± 8	≤ 1
4-trifluoromethoxybenzoic acid	≥95%	0.43 ± 0.05	294 ± 8	-[d]	-[d]	4 ± 2
3,4-methylenedioxybenzoic acid[g]	70%	0.17 ± 0.05	265 ± 7	158 ± 19	59 ± 7	-
3,4-ethylenedioxybenzoic acid	70%	50 ± 1.5	437 ± 7	332 ± 7	76 ± 2	< 2
4-methylaminobenzoic acid	70%	1.6 ± 0.07	923 ± 200	669 ± 15	64 ± 2	3 ± 0.6
4-ethylaminobenzoic acid	40%	0.92 ± 0.02	197 ± 8	112 ± 10[f]	57 ± 3[f]	-
4-dimethylaminobenzoic acid	50%	20 ± 2	284 ± 4	239 ± 16[e]	84 ± 4[e]	-
4-diethylaminobenzoic acid	70%	11 ± 1	332 ± 17	298 ± 8[f]	90 ± 4[f]	-
4-methylthiobenzoic acid	70%	2.3 ± 0.3	1430 ± 180	1180 ± 130	83 ± 3	2 ± 0.4
4-ethylthiobenzoic acid	10%[h]	0.99 ± 0.05	132 ± 6	64 ± 6	50 ± 3	-
4-ethylbenzoic acid[g]	≥95%	0.34 ± 0.02	812 ± 7	515 ± 88	63 ± 10	2 ± 0.1
***meta*- O, N and S substituted**						
3-methylaminobenzoic acid	10%	31 ± 1	255 ± 2	175 ± 1	69 ± 1	4 ± 0.2
3-methylthiobenzoic acid	30%	33 ± 0.5	56 ± 0.2	37 ± 1	66 ± 2	~1%
3-methoxybenzoic acid[g]	40%	69 ± 2	498 ± 5	-[d]	-[d]	2 ± 0.7

The data are presented as a mean ± S.D. with $n \geq 3$ and the rates are given as nmol.nmol-CYP^{-1}.min^{-1}. The reaction mixtures contained 0.5 μM P450, 5 μM HaPux and 0.5 μM HaPuR. The average leak rate was 9.0 nmol.nmol-CYP^{-1}.min^{-1}. [a] NADH oxidation activity. [b] PFR: product formation rate defines the number of product forming catalytic cycles completed over the time period. [c] C is the coupling efficiency which is the proportion of NADH consumed in the reaction that led to the formation of products expressed as a percentage. H_2O_2 is the percentage of NADH converted to hydrogen peroxide via this uncoupling pathway. [d] no detectable product observed. [e] these coupling efficiencies were calculated on the basis that two P450 catalytic cycles are required for the double dealkylation of these substrates. [f] these coupling efficiencies were calculated on the basis that two P450 catalytic cycles are required for acetamide formation (and double dealkylation when relevant) of these substrates. (–) indicates that this value was not determined. [g] Data published previously.[17, 20, 27] [h] Note the Soret maxima shifted from 418 to 419 nm for 4-ethylthiobenzoic acid (a type I difference spectrum is still obtained – Figure S2).

The coupling efficiency, which is the measure of the reducing equivalents that are channeled into organic substrate oxidation rather than unproductive oxygen reduction reactions, approached 100% (Table 2).[17, 18, 20] 4-Trifluoromethoxybenzoic acid bound to CYP199A4 with high affinity (K_d = 0.43 μM) and engendered a

≥95% shift to the HS state. The NADH oxidation activity (294 min^{-1}) was lower than that observed for both alkyloxybenzoic acids and, as would be expected due to the strong C–F bonds, no product was formed. Additionally only low quantities of hydrogen peroxide could be detected in these turnovers (3% of the total reducing equivalents added) suggesting that the oxidase uncoupling pathway (four electron reduction of O_2 to water) was the major pathway in catalytic consumption of the reducing equivalents (Scheme 1).[5, 21]

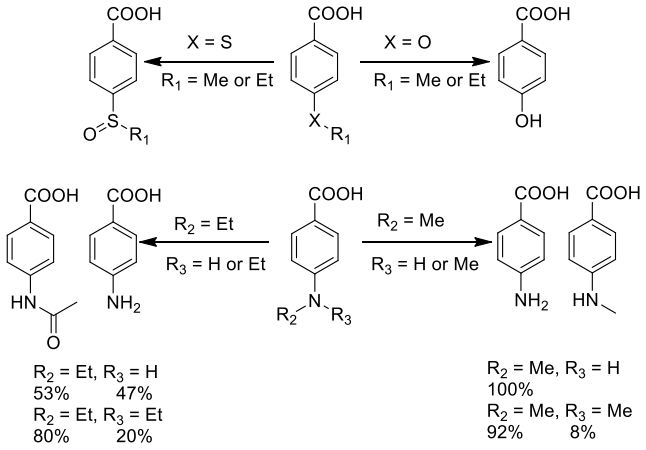

Scheme 2 The products formed from the CYP199A4 catalysed oxidation of different substrates.

CYP199A4 can catalyse the efficient oxidative demethenylation of 3,4-methylenedioxybenzoic acid producing formic acid as a product.[27] The larger substrate 3,4-ethylenedioxybenzoic acid bound to CYP199A4 with a much lower affinity (250-fold less tightly) but induced a similar spin state shift (70%, Table 2). The CYP199A4-catalysed oxidation of the ethylendioxy substrate was efficient (Table 2) and generated a single product, which was isolated and identified by NMR as a cyclic hemiacetal, 6-carboxy-2,3-dihydro-2-hydroxy-1,4-benzodioxin (Scheme 3, Table 2, Figure S3, Figure S4, Figure S6).

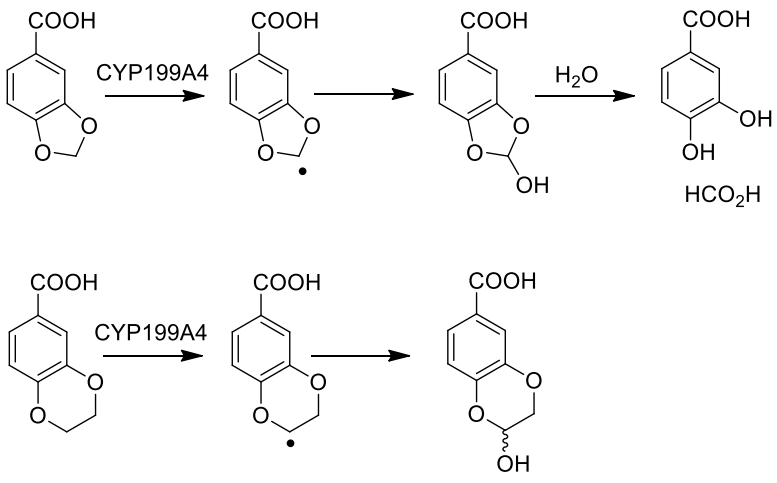

Scheme 3 The products formed from the CYP199A4 catalysed oxidation of 3,4-methylenedioxy- and 3,4-ethylenedioxy-benzoic acid.[27]

Nitrogen-containing substituents: 4-Methylaminobenzoic acid bound tightly to CYP199A4 inducing a 70% type I HS shift but with lower affinity (K_d 1.6 μM) than 4-methoxybenzoic acid (Table 2, Figure S1, Figure S2). As expected 3-methylaminobenzoic acid bound to CYP199A4 with lower affinity (31 ± 1 μM) and induced a decreased spin state shift (20%, Table 2). The addition of 4-ethylaminobenzoic acid resulted in a reduced modification of the spin state (40% HS) but bound with higher affinity than the 4-methylamino analogue (K_d 0.92 μM; Table 2, Figure S1, Figure S2). The observed oxidation activity of CYP199A4 toward *para*-substituted alkylamino benzoic acids was lower than toward the equivalent alkoxybenzoic acids (Table 2).

4-Methylaminobenzoic acid was dealkylated by CYP199A4 generating 4-aminobenzoic acid as the sole product with reasonable coupling efficiency (Table 2, Scheme 2, Figure S4). 3-Methylaminobenzoic acid was also oxidised by CYP199A4 to generate significant quantities of the demethylation metabolite as the sole product (Figure S4). While this occurred with lower activity relative to the *para*-substituted isomer the coupling efficiency and product formation rate were higher than expected, when compared to the *meta*-substituted methoxybenzoic acid (Table 2).[27] When this substrate was docked into CYP199A4 it preferred to bind with the 3-methylamino group oriented towards the heme, rationalising the observed levels of product formation (Figure S7).

The turnover of 4-ethylaminobenzoic was slower and less efficient than 4-methylaminobenzoic acid (Table 2). Two products were generated in roughly equal amounts, one coeluting with 4-aminobenzoic acid while the other, which was formed in a slight excess (53% of product), was isolated by semi-prep HPLC purification and assigned by NMR and MS as 4-acetamidobenzoic acid. (Scheme 2, Figure S4, Figure S5, Figure S6). This assignment was subsequently confirmed by HPLC coelution with an authentic product standard (Figure S4).

4-Dimethyl- and 4-diethyl-aminobenzoic acids bound to CYP199A4 with a 10-fold lower affinity than the 4-methylamino and 4-ethylamino equivalents (Table 2, Figure S2). The type I spin state shift of CYP199A4 induced by 4-diethylaminobenzoic acid (70% HS) was greater than

observed with 4-ethylaminobenzoic acid but that of 4-dimethylaminobenzoic acid (50% HS) was lower than that of 4-methylaminobenzoic acid (Table 2, Figure S1). The changes in NADH oxidation activity and product formation rate of the tertiary amine derivatives compared to their secondary amine equivalents were in line with the modification in the spin state. As such, the NADH oxidation activity of CYP199A4-catalysed oxidation of the 4-diethylamino species was greater than that of 4-ethylaminobenzoic acid while the rate of oxidation of the 4-dimethylamino compound was lower than 4-methylaminobenzoic acid (Table 2).

Only products arising from dealkylation of 4-dimethylaminobenzoic acid were identified. The double dealkylation product, 4-aminobenzoic acid, was the major metabolite with only a small amount of the intermediate secondary amine, 4-methylbenzoic acid, observed (~8% of the product) despite an excess of the starting material still remaining (Table 2 and Figure S4). In the turnover of diethylaminobenzoic acid, 4-aminobenzoic acid and 4-acetamidobenzoic acid were the two major products (Scheme 2). No significant levels of 4-ethylaminobenzoic acid, or a peak that could be assigned to 4-(*N*-ethyl)-acetamidobenzoic acid, was detected in the HPLC or GC analysis (Figure S4). There was also no evidence of any product arising from N-oxidation in any of the turnovers of the alkylaminobenzoic acids.

4-Aminomethylbenzoic acid induced a very small type I shift to the high-spin form and a binding affinity more than four orders of magnitude weaker than 4-methylaminobenzoic acid (Table S1, Figure S1, Figure S2). Similar results were obtained with 4-(dimethylamino)methylbenzoic and 4-(ethylamino)methylbenzoic acids, while the addition of 4-(methylamino)methylbenzoic acid resulted in a small red shift in the Soret band to 420 nm (Figure S1). Little catalytic activity was observed in the turnovers with these substrates (Table S1). Terephthalic acid and 4-formylbenzoic acid were detected by HPLC and GC-MS analysis (Figure S4 and S5) and the latter could arise from the hydrolysis of a carbinolamine intermediate arising from benzylic C-H bond hydroxylation, and the former by further oxidation of the formyl product (Table S1, Figure S3, Figure S4). No other products which could be conclusively assigned as arising from CYP199A4 activity were observed.

Sulfur-containing substituents: 4-Methyl- and 4-ethyl-thiobenzoic acids both induced a type I spin state shift upon addition to CYP199A4 but the magnitude of the shifts, 70% and 10% respectively, were lower than the equivalent alkoxybenzoic acids (Table 2, Figure S1). The spin state shifts and binding affinities (K_d 2.3 μM, methylthio and 1.0 μM, ethylthio) were similar to those of the equivalent 4-alkylamino benzoic acids (Table 2, Figure S2). 4-Ethylthiobenzoic acid bound with higher affinity than 4-methylthiobenzoic acid despite the significantly lower shift in the spin state observed (Table 2).

The rate of NADH oxidation with 4-methylthiobenzoic acid was higher than that with 4-methoxybenzoic acid. In contrast, that found for 4-ethylthiobenzoic acid was lower than those of 4-ethoxy- and 4-ethylamino-benzoic acids (Table 2). The major products from both 4-alkylthiobenzoic acids arose from S-oxidation, initially identified by GC-MS analysis (*m*/*z* = 256.05 versus substrate 240.05 for 4-methylthiobenzoic acid (Scheme 2, Figure S5)). Little or no 4-mercaptobenzoic acid, arising from P450-catalysed dealkylation, was detected with either thioether (~1% of the dealkylation product was detected in each turnover and in controls lacking the P450 enzyme; Figure S4). The product formation rate of S-oxidation with 4-methylthiobenzoic acid was comparable to that of demethylation of 4-methoxybenzoic acid, both being in excess of 1000 min^{-1}, due to a slightly lower coupling efficiency (Table 2). There was a sharp drop in the activity of CYP199A4 with 4-ethylthiobenzoic acid predominantly due to the reduced NADH oxidation rate (Table 2).

3-Methylthiobenzoic acid bound to CYP199A4 with lower affinity (33 ± 0.5 μM) and induced a reduced spin state shift (30%, Table 2) than the corresponding *para*-substituted isomer. It was oxidised by CYP199A4 to 3-methylsulfinylbenzoic acid with a reasonably high coupling efficiency (66%) but the rate of sulfoxidation was substantially reduced (37 ± 1 min^{-1}, Table 2 and Figure S4).

The alkylsulfinylbenzoic acid products arising from *S*-oxidation are chiral. We therefore set out to determine the enantioselectivity of the reactions. The methyl esters of both *para*-substituted alkylsulfinylbenzoic acids were synthesised for enantioselective HPLC analysis. The enantiomers

of the methylsulfinyl metabolites could not be separated preventing further analysis but they did confirm the identity of the turnover product. The ethylsulfinyl benzoic acids were resolved by enantioselective HPLC. Analysis of the methyl esters of the products from CYP199A4 catalysed oxidation revealed that there was a significant excess of one enantiomer (91:9, Figure S8). In order to compare the enantioselectivity of the sulfoxidation reaction to hydroxylation we determined the enantioselectivity of the known CYP199A4-catalysed oxidation of 4-ethylbenzoic acid to 4-(1′-hydroxyethyl)-benzoic acid.[13,14] Enantioselective HPLC demonstrated that the α-hydroxylated metabolite produced was predominantly one enantiomer (87:13, Figure S8). This was shown to be the *S*-enantiomer by comparison with literature and by *de novo* analysis of the Mosher's esters of chromatographically resolved enantiomers of methyl 4-(1′-hydroxyethyl)-benzoate (see experimental section for the experimental details and results).

Crystal structure analysis

The binding and oxidative activity of CYP199A4 with *para*-substituted benzoic acids with oxygen, nitrogen and sulfur containing moieties and the switch from O- and N-demethylation to S-oxidation provides an opportunity to understand how P450-substrate interactions may control these reactions. The orientation of the substrate in the active site and the position of the substituents in relation to the reactive iron-oxo intermediate would be expected to impact the formation of products which arise from different monooxygenase activities (heteroatom oxidation versus dealkylation pathways). X-ray crystal structures were solved for the substrate-bound forms of CYP199A4 with 4-ethoxy- (PDB: 5U6T), 4-methylamino- (PDB: 5U6W), 4-methylthio- (PDB: 5KT1) and 4-ethylthio-benzoic acid (PDB: 5U6U) to complement the available structural data on the 4-methoxy- (PDB: 4DO1) and 4-ethyl-benzoic acid (PDB: 4EGM) bound forms of CYP199A4 (Figure 2). The data processing and refinement statistics are provided in Table 1.

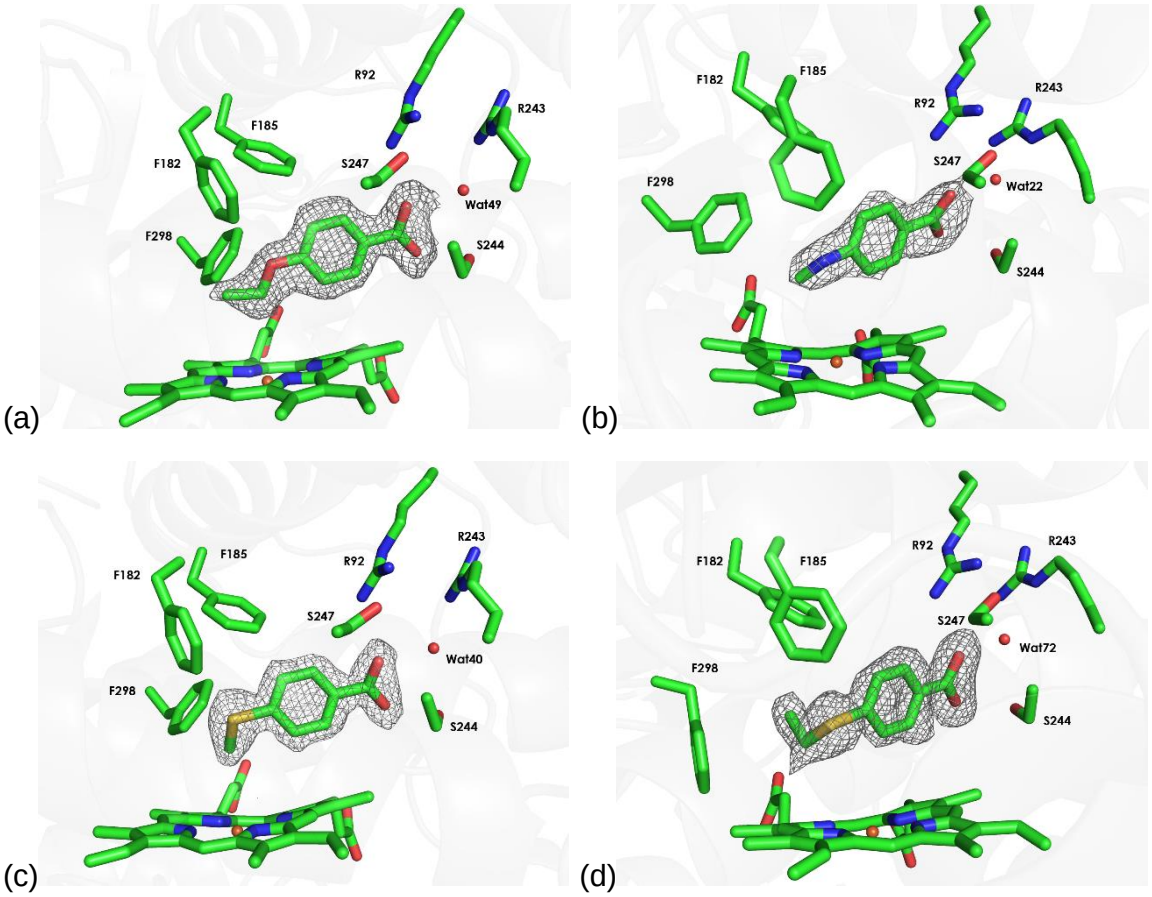

Figure 2: Omit maps for the active site of various substrate-bound CYP199A4 crystal structures. In each, the 2*mF*o – *DF*c density of the substrate is shown contoured as a grey mesh. The heme, substrate and the active site residues are shown in green. The water molecule involved in the hydrogen bonding network is shown as a red sphere. The contour level and carve radius of each structure is displayed in Table 1. Shown are (a) 4-ethoxybenzoic acid, (b) 4-methylaminobenzoic acid, (c) 4-methylthiobenzoic acid and (d) 4-ethylthiobenzoic acid.

For all the crystal structures of the CYP199A4–substrate complexes determined here, the asymmetric unit contained a single molecule, which could be traced from residues 17 to 409. The structures of these substrate-bound complexes of CYP199A4 displayed a high similarity to that of CYP199A4 bound with 4-methoxybenzoic acid (Figure S9). All displayed a closed conformation and contained a bound ion, modelled as chloride, close to the enzyme surface, which shields the active site from the external solvent.[18, 44] The tertiary structures of the enzyme in the different substrate-bound complexes are superimposable on one another. The r.m.s.d. for all resolved C^{α} atoms between these molecules is <0.60 Å (measured over 393 atoms).

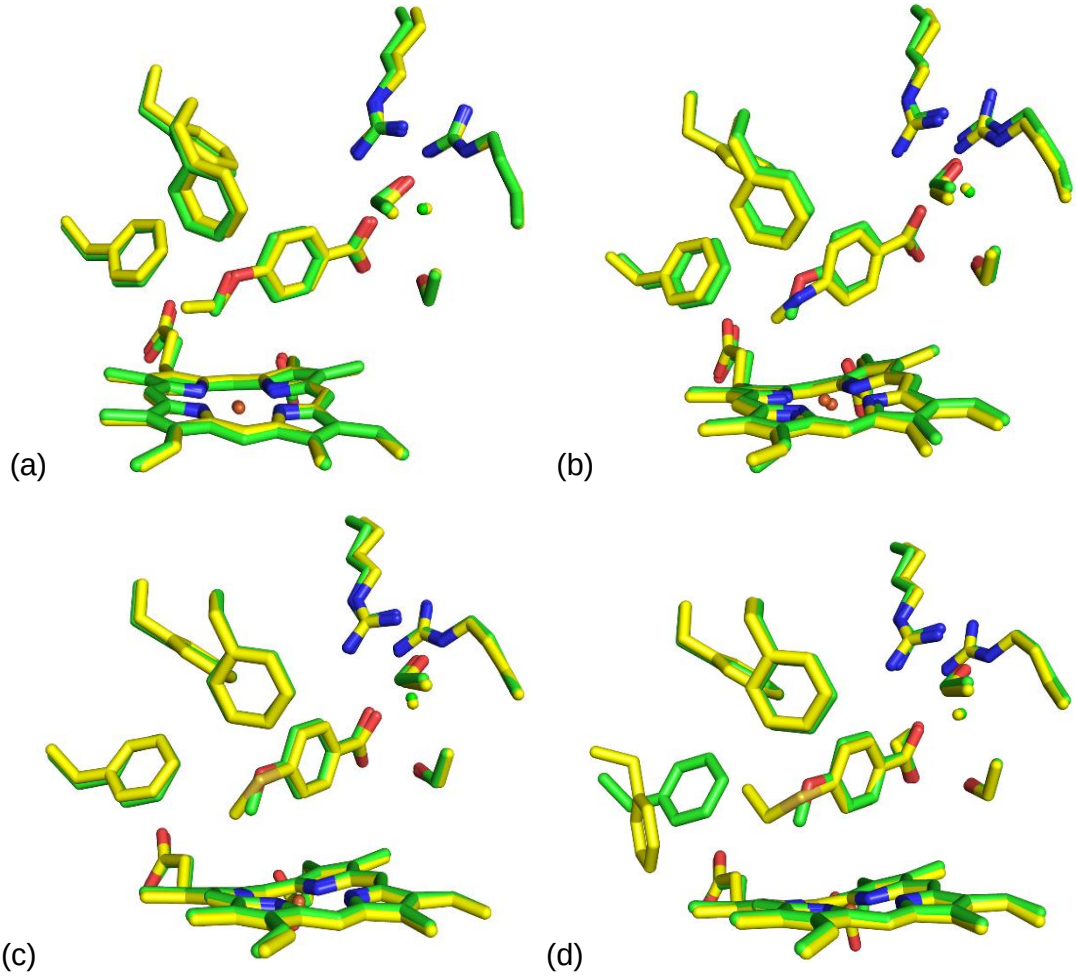

Figure 3: Overlay of the structures of 4-methoxybenzoic acid (green) with determined structures (yellow) of (a) 4-ethoxybenzoic acid, (b) 4-methylaminobenzoic acid, (c) 4-methylthiobenzoic acid and (d) 4-ethylthiobenzoic acid. Water molecules in the active site are shown as spheres in the structure's respective color.

In all the new structures the water molecule that is part of the hydrogen bonding network to the carboxylic acid group of the substrate is found in an almost identical position to that in the 4-methoxybenzoic acid structure (Figure 3). In addition, for all structures except 4-ethylthiobenzoic acid, the positions of all the active site residues are virtually unchanged (Figure 3). These crystal structures should therefore provide insight into the observed monooxygenase activity and regioselectivity of the oxidations catalysed by CYP199A4 with the different substrates.

4-Ethoxybenzoic acid, which undergoes deethylation, is oriented similarly in the active site to 4-methoxybenzoic acid (Figure 3a). The methylene of the ethyl substituent is the closest substrate atom to the heme iron at a comparable distance to the methyl of 4-methoxybenzoic acid (4.2 Å versus 4.1 Å). The methyl carbon points towards Val295 and is further from the heme iron

(4.3 Å, Table S2). When the position of the oxygen of the Cpd I intermediate was considered (modelled 1.6 Å from the Fe)[45, 46] the methyl group was 0.2 Å further away than the more reactive methylene group (Table S2). No products were observed that arise from H abstraction from the stronger C–H bonds of the methyl group.

4-Methylaminobenzoic acid undergoes exclusive N-dealkylation despite the observation that N-oxides are common products arising from P450 oxidations. The 4-methylamino moiety of the substrate is orientated differently in relation to the heme iron compared to 4-methoxybenzoic acid (the dihedral angle is 50.0° versus 2.1° and the angle in relation to Fe=O bond of Cpd I was 133.0° versus 140.7°; Figure 3b and Table S2). The distance from the methyl group to the heme iron is almost identical to that of 4-methoxybenzoic acid (4.1 Å, Figure 3b). However, the nitrogen is significantly closer to the heme and the Cpd I oxygen atom than the oxygen in 4-methoxybenzoic acid (4.2 Å versus 5.2 Å and 3.0 versus 3.6 Å, respectively; Table S2). Despite this change, there was no observed N-oxidation product in the turnovers nor was there any spectroscopic evidence that the nitrogen atom was interacting with the heme iron.

4-Methylthiobenzoic acid undergoes S-oxidation. Compared to bound 4-methoxybenzoic acid in the enzyme-substrate crystal structure, the 4-methylthio moiety is rotated in a manner more similar to that of the 4-methylaminobenzoic acid substrate (dihedral angle 33.9°, angle to Cpd I Fe=O 131.9°; Figure 3c and Table S2). This orientation results in the methyl group being further from the heme iron and therefore the oxygen of Cpd I than in the 4-methoxybenzoic acid structure (4.4 Å versus 4.1 Å and 3.3 Å versus 2.7 Å, respectively; Table S2). However, the reactive sulfur atom is closer to the heme iron and the iron-oxo moiety of Cpd I than the oxygen in the 4-methoxybenzoic acid structure (4.9 Å versus 5.2 Å and 3.4 Å versus 3.6 Å, respectively; Table S2). The sulfur atom is almost the same distance from the oxygen of Cpd I as the methyl group (3.4 versus 3.3 Å and at an angle of 162.5° compared to 131.9°, Table S2). This coupled with the increased orbital size, reactivity and electron density of sulfur must account for the change in the CYP catalysed reaction.

In the active site of 4-ethylthiobenzoic acid-bound CYP199A4, residue Phe298 moves to accommodate the ethylthio moiety (Figure 4). The side chain of the phenylalanine has rotated so that it no longer points towards the substrate but is now oriented towards the plane of the heme group (Figure 3d, Figure 4). This enables the methyl group of the ethylthio moiety to occupy the space vacated by the aromatic ring. The 4-ethylthio moiety is twisted (dihedral angle 55.2°) so that the sulfur is closer to the heme iron than the oxygen in 4-methoxybenzoic acid (4.7 Å versus 5.2 Å, 3.3 Å from Cpd I oxygen, Figure 3d, Table S2). The methylene carbon of the ethyl group is further from the heme iron and the Cpd I oxygen atom than the methyl of 4-methoxybenzoic acid (5.2 Å versus 4.1 Å and 4.0 Å versus 2.7 Å, respectively, Table S2) and of methylthiobenzoic acid (5.2 Å versus 4.5 Å and 4.0 Å versus 3.3 Å, Table S2). The methyl group is even further from the heme iron and Cpd I oxygen compared to the equivalent group in the 4-ethoxybenzoic acid bound structure (Figure 4a, 6.7 Å versus 4.3 Å and 5.5 Å versus 3.0 Å, respectively; Table S2).

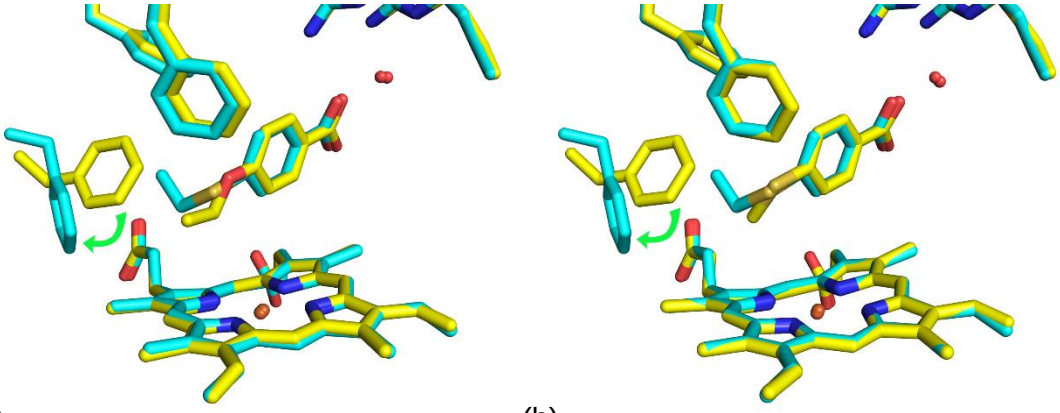

Figure 4: Overlays showing the movement of Phe298 residue in 4-ethylthiobenzoic acid structure. Shown are (a) comparison of 4-ethoxybenzoic acid structure (yellow) and 4-ethylthiobenzoic acid structure (blue), and (b) comparison of 4-methylthiobenzoic acid structure (yellow) and 4-ethylthiobenzoic acid structure (blue). Arrow (green) shows movement of the Phe298 residue between the structures.

The increased distance of 4-ethylthiobenzoic acid from the heme iron compared to the other substrates in the substrate bound crystal structures may increase the solvent accessibility accounting for the lower spin state shift, although there was no evidence of any water molecules interacting with the heme iron in the crystal structure. The orientation of the substrate shows that

one face of the sulfur would be significantly closer to the heme iron than the other which could explain the high enantioselectivity of sulfoxidation.

Discussion

CYP199A4 binds and selectively oxidises *para*-methoxy-substituted benzoic acids and closely related substrates.[17, 20, 27] The current work confirms that a range of *para*-substituted benzoic acids can be accommodated within the active site of CYP199A4, and the nature of the substituent influences the binding affinity of the enzyme. Within the sets of O-, N- and S- containing *para*-substituted benzoic acids the rate of NADH oxidation, and as a consequence the product formation rate, tended to follow the trend seen in the shift to the high spin state upon substrate binding. This shift is often used as an indicator of displacement of the heme-bound water ligand, a required step early in the catalytic cycle. The relative rates of NADH oxidation and product formation suggest that the reactions are gated by substrate binding.[47, 48] N-dealkylation, S-oxidation and acetamide and cyclic hemiacetal formation can be added to this CYP enzyme's known hydroxylation, O-dealkylation and desaturation activities. Oxidative O-demethylation is the most rapid reaction catalysed by CYP199A4, followed by sulfoxidation, hydroxylation and then N-demethylation.

Two main mechanistic pathways have been proposed for heteroatom dealkylation by P450s. N-Dealkylation reactions can proceed in the same way as hydroxylation and O-dealkylations, with hydrogen abstraction followed by radical rebound at the carbon alpha to the heteroatom (HAT).[49] This yields an unstable, hydroxylated product which then decomposes to give the dealkylated product.[49] It has been proposed that N-dealkylation reactions catalysed by heme proteins may also occur via an initial single electron transfer (SET) from the heteroatom to compound I (Cpd I) to give a cation radical.[50] Subsequent proton abstraction and radical rebound can give the dealkylated product.[11, 49, 51] The current view, which is supported by large intramolecular isotope effects for amide N-dealkylations (> 13), DFT studies and the lack of ring opening products with N-cyclopropyl substrates, is that a HAT mechanism occurs for N-dealkylation.[52-56] DFT calculations on selected *para*-substituted N,N-dimethylanilines showed that the radical cation arising from the first single electron transfer on the SET pathway was significantly higher in energy than its radical counterpart on the HAT pathway[57] and that

dealkylation products can arise from either of the two spin-states of Cpd I depending on the nature of the substrate's substituent.[51, 57, 58]

Some unusual major metabolites were observed during this work, including the isolable, stable cyclic hemiacetal from 3,4-diethylenedioxy benzoic acid. The isolation of the cyclic hemiacetal is probably due to the fact it is more stable than its non-cyclic counterparts that decompose to yield the dealkylated ether; this stability is analogous to that seen for the 6-membered cyclic hemiacetal form of sugars. The observation of high levels of an acetamide product with the N-ethylbenzoic acids, though not the N-methyl equivalents, was also unexpected. To the best of our knowledge this is the first report of an acetamide being formed from an ethylamine moiety as a result of P450 catalysed oxidation, although this transformation has been observed in whole-cell biotransformations of cyclic amines and *N*-methylanilines by a non-P450 enzyme.[59] Hemiacetals and carbinolamine (hemiaminal) intermediates normally react to form the aldehyde and alcohol/amine. Carbinolamine metabolites have been observed previously, for example, with cyclophosphamide and *N*-methylcarbazole.[60-63] It has been hypothesised that carbinolamine formation may be stabilised when delocalisation of the nitrogen lone pair to an adjacent carbonyl or aromatic group is possible, which would be the case here.[63] Acetamide formation could arise from further oxidation of the carbinolamine intermediate if it remained in the CYP199A4 active site.[64] By analogy 4-ketocyclophosphamide has been observed as a metabolite from P450 catalysed oxidation (arising from 4-hydroxycyclophosphamide).[63] With CYP199A4 the carbinolamine intermediate could be held in the active site and may be more stable in the ethyl, rather than the methyl substituted amines. Theoretically, the acetamide could be formed from oxidation of an imine intermediate which can be formed in P450 reactions but the conditions required for this chemical transformation are quite harsh.[65] These monooxygenase activities may be found in natural product synthetic pathways; for example in plants which have highly specialised and selective P450 enzymes.[66, 67]

The ability of CYP199A4 to catalyse the multistep reaction required for amide formation is also observed in the formation of *para*-aminobenzoic acid from the dialkylaminobenzoic acids.

Presumably this proceeds via initial carbinolamine formation, decomposition to the monoalkylaminobenzoic acid and then a second round of P450 catalysed oxidative N-dealkylation. The production of the acetamide from diethylaminobenzoic acid supports the presence of ethylaminobenzoic acid as an intermediate. The fact that no *N*-ethylacetamidobenzoic acid is formed is presumably because the dialkylamino substituted benzoic acids bind much less tightly to CYP199A4 and so the initial carbinolamine intermediate would be released and decompose to the alkylamino compound before being further oxidised.

The excellent fit and high binding affinity for the benzoic acids with the active site of CYP199A4 may help the formation of unusual metabolites such as the acetamidobenzoic acid. In drug metabolising P450s, which have large, more open substrate binding pockets, the carbinolamine intermediate may have a lower affinity and dealkylation is preferred. Given the tight binding, high product formation activity and coupling efficiencies, CYP199A4 would be a good system with which to conduct further mechanistic investigations on N-dealkylation and acetamide formation.

No products arising from heteroatom oxidation of any of the alkyl amine substrates were detected. This could be due to the closer approach of the β-nitrogen atom in the substituent of these substrates to the heme, as inferred by low spin state shifts and the red shift in the Soret band of CYP199A4 with 4-(methylamino)methylbenzoic acid. The lack of significant product formation activity with the aminomethylbenzoic acids could also reflect the fact that these substrates are likely to be protonated (pKa 9-10) under the reaction conditions, unlike the aminobenzoic acids (pKa 4-5) and so do not bind as effectively to CYP199A4.

By way of contrast, little to no dealkylation activity was observed for either of the thioether substrates with S-oxidation being the major product. The results also agree with experimental and theoretical work. These found that sulfoxidation is favored over S-dealkylation but the equivalent N-dealkylation reaction has lower barriers than N-oxidation. [68-70] Experimental evidence suggests that the mechanism of sulfoxidation may involve a different oxidant to that involved in C–H bond hydroxylation and oxidative dealkylation.[16, 71] Initially it was proposed that this may be Cpd 0, the

hydroperoxy species, but theory suggests this is a weak oxidant.[72, 73] Recently, the ferric hydrogen peroxide complex was proposed using theory to have the potential to catalyse sulfoxidation.[74]

The effect of the substrate on the CYP199A4 structure was most pronounced for 4-ethylthiobenzoic acid where the phenyl ring of Phe298 moves to accommodate the ethyl group of the *para* substituent. 4-Ethoxybenzoic acid bound in a similar orientation to 4-methoxybenzoic acid with little to no movement of the active site residues. The X-ray crystal structures show that even these single atom changes have an effect on the orientation of the *para* substituent in the active site of CYP199A4. The binding and position of the benzoic acid component of the substrate is however tightly controlled. In 4-methoxybenzoic acid the dihedral angle of the methoxy group places the substituent in the plane of the benzene ring so the methyl group points towards the heme iron. With the other substrates, the orientation of the methylamino and methylthio groups changes and the methyl group is oriented away from the heme, resulting in the heteroatom being closer to the reactive centre. In the case of the thioethers this would facilitate sulfoxidation. Despite the closer approach of the nitrogen in 4-methylaminobenzoic acid bound structure no N-oxidation products were detected in agreement with the energetics of the reaction. It is important to consider that the *para* substituents could have some mobility in the enzyme active site and that minor structural changes may occur after the oxygen binding and activation steps of the catalytic cycle.

Conclusion

We have established that CYP199A4 can catalyse efficient N-demethylation and acetamide formation from (di)alkylaminobenzoic acids and the sulfoxidation of alkylthiobenzoic acids. CYP199A4 also promoted the formation of cyclic hemiacetal metabolites. The efficient catalysis of multiple reactions using a single P450 system would allow the mechanism of different P450 activities to be investigated in unprecedented detail. The CYP199A4 system could be used to study P450 oxidation mechanisms that are as yet unclear using *para*-substituted benzoic acids. The benzoic acid skeleton will serve to position a *para* substituent close to the reactive iron-oxo moiety during reaction and should allow the study of uncommon P450-catalysed transformations. 4-Methoxybenzoic acid, 4-methylaminobenzoic acid and 4-methylthiobenzoic acid were chosen for study to compare the O-demethylation, N-demethylation and sulfoxidation activity of CYP199A4. These substrates ensure that the minimum structural changes are made to the substrate with only the identity of the heteroatom at the *para* substituent being changed. The structural data provides important information on how the relevant parts of the substrate are held and orientated relative to the heme iron. This information would be critical for accurate theoretical studies on these systems. CYP199A4 and appropriate active site mutants of the enzyme could also be used to probe the role of the active oxidant(s) in different oxidative P450 catalytic reactions. For example, sulfoxidation has been proposed to occur via Cpd 0 or a hydrogen peroxide complex. Using different substrates, isotopic analogues and mutants the oxidant(s) responsible for these reactions can be investigated.

Corresponding Author

Stephen G. Bell, Department of Chemistry, University of Adelaide, SA 5005, Australia; email: stephen.bell@adelaide.edu.au

Author Contributions

The manuscript was written through contributions of all authors. All authors have given approval for the final version of the manuscript.

Funding Sources

Australian Research Council DP140103229

Supporting Information. Additional substrate binding parameters and catalytic turnover activity data for CYP199A4, details of the distances and angles of pertinent substrate atoms from the heme iron in the crystal structures of CYP199A4, spin state shift assays, dissociation constant analysis, examples of NADH oxidation assays, HPLC and GC-MS analysis of the *in vitro* turnovers, NMR spectra and details of isolated products, computational docking studies with 3-methylaminobenzoic acid, enantioselective HPLC data and structures of the Cα chains of different CYP199A4 crystal structures. This information is available free of charge on the ACS Publications website.

Abbreviations

2xYT, 2x Yeast Extract Tryptone; 4-AP, 4-aminoantipyrine; amp, ampicillin; Bis-Tris, 2-Bis(2-hydroxyethyl)amino-2-(hydroxymethyl)-1,3-propanediol; BSTFA, *N*,*O*-bis(trimethylsilyl)trifluoroacetamide; Cpd 0, compound 0 the ferric hydroperoxy intermediate; Cpd I, iron(IV)−oxo porphyrin radical cation intermediate; CYP, cytochrome P450 enzyme; CYP199A4, cytochrome P450 enzyme from *Rhodopseudomonas palustris* strain HaA2; DMSO, dimethylsulfoxide; *E. coli*, *Escherichia coli*; EMM, *E. coli* minimal media; EtOH, ethanol; FAD, flavin adenine dinucleotide; FEM, feature enhanced maps; GC-MS, gas chromatography-mass spectrometry; HaPuR, FAD containing flavoprotein from *Rhodopseudomonas palustris* strain HaA2; HaPux; [2Fe-2S] ferredoxin from *Rhodopseudomonas palustris* strain HaA2; HAT, hydrogen abstraction; HPLC, high performance liquid chromatography; HRP, horseradish

peroxidase; HS, high spin; IPTG, isopropyl β-D-1-thiogalactopyranoside; kan, kanamycin; LB, lysogeny broth; LS, low spin; NADH, reduced nicotinamide adenine dinucleotide; PEG, polyethylene glycol; rpm, revolutions per minute; PFR, product formation rate; SET, single electron transfer; TFA, trifluoracetic acid; TMSCl, trimethylsilyl chloride; Tris, tris(hydroxymethyl)aminomethane.

Acknowledgements

This work was supported by ARC grant DP140103229 (to JJDV and SGB). SGB acknowledges the ARC for a Future Fellowship (FT140100355). The authors also acknowledge the award of an Australian Government Research Training Program Scholarships (PhD to TC and MPhil to MNP). We would like to thank the beamline scientists at MX1 for help with data collection. We acknowledge financial support from the Australian Synchrotron.

References

1. Ortiz de Montellano, P. R. *Cytochrome P450: Structure, Mechanism, and Biochemistry* 4th ed.; Springer International Publishing: Switzerland, 2015; p 912.

2. Ortiz de Montellano, P. R. Hydrocarbon hydroxylation by cytochrome P450 enzymes. *Chem. Rev.* **2010**, *110*, 932-948.

3. Sigel, A.; Sigel, H.; Sigel, R. *The Ubiquitous Roles of Cytochrome P450 Proteins*. John Wiley & Sons: Weinheim, 2007; Vol. 3, p 678.

4. Denisov, I. G.; Makris, T. M.; Sligar, S. G.; Schlichting, I. Structure and chemistry of cytochrome P450. *Chem. Rev.* **2005**, *105*, 2253-2277.

5. Mueller, E. J.; Loida, P. J.; Sligar, S. G. Twenty-five years of P450cam research. Mechanistic insights into oxygenase catalysis. In *Cytochrome P450: Structure, Mechanism, and Biochemistry*, 2nd ed.; Ortiz de Montellano, P. R., Ed. Plenum Press: New York, 1995; pp 83-124.

6. Poulos, T. L. Heme enzyme structure and function. *Chem. Rev.* **2014**, *114*, 3919-3962.

7. Rittle, J.; Green, M. T. Cytochrome P450 compound I: capture, characterization, and C-H bond activation kinetics. *Science* **2010**, *330*, 933-937.

8. Kumar, D.; de Visser, S. P.; Shaik, S. Multistate reactivity in styrene epoxidation by compound I of cytochrome p450: mechanisms of products and side products formation. *Chemistry* **2005**, *11*, 2825-2835.

9. Franke, A.; van Eldik, R. Spectroscopic and Kinetic Evidence for the Crucial Role of Compound 0 in the P450cam -Catalyzed Hydroxylation of Camphor by Hydrogen Peroxide. *Chemistry* **2015**, *21*, 15201-15210.

10. Jin, S.; Makris, T. M.; Bryson, T. A.; Sligar, S. G.; Dawson, J. H. Epoxidation of olefins by hydroperoxo-ferric cytochrome P450. *J. Am. Chem. Soc.* **2003**, *125*, 3406-3407.

11. Ortiz de Montellano, P. R.; De Voss, J. J. Oxidizing species in the mechanism of cytochrome P450. *Nat. Prod. Rep.* **2002**, *19*, 477-493.

12. Vaz, A. D.; McGinnity, D. F.; Coon, M. J. Epoxidation of olefins by cytochrome P450: evidence from site-specific mutagenesis for hydroperoxo-iron as an electrophilic oxidant. *Proc. Natl. Acad. Sci. U .S. A.* **1998**, *95*, 3555-3560.

13. Shaik, S.; Cohen, S.; Wang, Y.; Chen, H.; Kumar, D.; Thiel, W. P450 enzymes: their structure, reactivity, and selectivity-modeled by QM/MM calculations. *Chem. Rev.* **2010**, *110*, 949-1017.

14. Wang, B.; Li, C.; Dubey, K. D.; Shaik, S. Quantum mechanical/molecular mechanical calculated reactivity networks reveal how cytochrome P450cam and Its T252A mutant select their oxidation pathways. *J. Am. Chem. Soc.* **2015**, *137*, 7379-7390.

15. Akhtar, M.; Wright, J. N. Acyl-Carbon Bond Cleaving Cytochrome P450 Enzymes: CYP17A1, CYP19A1 and CYP51A1. In *Monooxygenase, Peroxidase and Peroxygenase Properties and Mechanisms of Cytochrome P450*, 2015/05/24 ed.; Hrycay, E. G.; Bandiera, S. M., Eds. Springer International Publishing: Cham, Switzerland, 2015; Vol. 851, pp 107-130.

16. Cryle, M. J.; De Voss, J. J. Is the ferric hydroperoxy species responsible for sulfur oxidation in cytochrome p450s? *Angew. Chem. Int. Ed. Engl.* **2006**, *45*, 8221-8223.

17. Bell, S. G.; Tan, A. B.; Johnson, E. O.; Wong, L. L. Selective oxidative demethylation of veratric acid to vanillic acid by CYP199A4 from *Rhodopseudomonas palustris* HaA2. *Mol. Biosyst.* **2010**, *6*, 206-214.

18. Bell, S. G.; Yang, W.; Tan, A. B.; Zhou, R.; Johnson, E. O.; Zhang, A.; Zhou, W.; Rao, Z.; Wong, L. L. The crystal structures of 4-methoxybenzoate bound CYP199A2 and CYP199A4: structural changes on substrate binding and the identification of an anion binding site. *Dalton Trans.* **2012**, *41*, 8703-8714.

19. Chao, R. R.; De Voss, J. J.; Bell, S. G. The efficient and selective catalytic oxidation of para-substituted cinnamic acid derivatives by the cytochrome P450 monooxygenase, CYP199A4. *RSC Adv.* **2016**, *6*, 55286-55297.

20. Bell, S. G.; Zhou, R.; Yang, W.; Tan, A. B.; Gentleman, A. S.; Wong, L. L.; Zhou, W. Investigation of the Substrate Range of CYP199A4: Modification of the Partition between Hydroxylation and Desaturation Activities by Substrate and Protein Engineering. *Chemistry* **2012**, *18*, 16677-16688.

21. Loida, P. J.; Sligar, S. G. Molecular recognition in cytochrome P450 - mechanism for the control of uncoupling reactions. *Biochemistry* **1993**, *32*, 11530-11538.

22. Bell, S. G.; McMillan, J. H.; Yorke, J. A.; Kavanagh, E.; Johnson, E. O.; Wong, L. L. Tailoring an alien ferredoxin to support native-like P450 monooxygenase activity. *Chem. Commun.* **2012**, *48*, 11692-11694.

23. Xu, F.; Bell, S. G.; Peng, Y.; Johnson, E. O.; Bartlam, M.; Rao, Z.; Wong, L. L. Crystal structure of a ferredoxin reductase for the CYP199A2 system from *Rhodopseudomonas palustris*. *Proteins* **2009**, *77*, 867-880.

24. Furuya, T.; Kino, K. Biocatalytic synthesis of dihydroxynaphthoic acids by cytochrome P450 CYP199A2. *Biosci. Biotechnol. Biochem.* **2009**, *73*, 2796-2799.

25. Furuya, T.; Kino, K. Discovery of 2-naphthoic acid monooxygenases by genome mining and their use as biocatalysts. *ChemSusChem* **2009**, *2*, 645-649.

26. Furuya, T.; Kino, K. Regioselective oxidation of indole- and quinolinecarboxylic acids by cytochrome P450 CYP199A2. *Appl. Microbiol. Biotechnol.* **2010**, *85*, 1861-1868.

27. Coleman, T.; Chao, R. R.; Bruning, J. B.; De Voss, J.; Bell, S. G. CYP199A4 catalyses the efficient demethylation and demethenylation of para-substituted benzoic acid derivatives. *RSC Adv.* **2015**, *5*, 52007 - 52018.

28. Williams, J. W.; Morrison, J. F. The kinetics of reversible tight-binding inhibition. *Methods Enzymol.* **1979**, *63*, 437-467.

29. Xu, F.; Bell, S. G.; Rao, Z.; Wong, L. L. Structure-activity correlations in pentachlorobenzene oxidation by engineered cytochrome P450cam. *Protein Eng. Des. Sel.* **2007**, *20*, 473-480.

30. Bell, S. G.; Harford-Cross, C. F.; Wong, L. L. Engineering the CYP101 system for in vivo oxidation of unnatural substrates. *Protein Eng.* **2001**, *14*, 797-802.

31. Guyon, C.; Métay, E.; Duguet, N.; Lemaire, M. Biphasic Glycerol/2-MeTHF, Ruthenium-Catalysed Enantioselective Transfer Hydrogenation of Ketones Using Sodium Hypophosphite as Hydrogen Donor. *Eur. J. Org. Chem.* **2013**, *2013*, 5439-5444.

32. Inagaki, T.; Phong, L. T.; Furuta, A.; Ito, J.-i.; Nishiyama, H. Iron- and Cobalt-Catalyzed Asymmetric Hydrosilylation of Ketones and Enones with Bis(oxazolinylphenyl)amine Ligands. *Chemistry* **2010**, *16*, 3090-3096.

33. Cowieson, N. P.; Aragao, D.; Clift, M.; Ericsson, D. J.; Gee, C.; Harrop, S. J.; Mudie, N.; Panjikar, S.; Price, J. R.; Riboldi-Tunnicliffe, A.; Williamson, R.; Caradoc-Davies, T. MX1: a bending-magnet crystallography beamline serving both chemical and macromolecular crystallography communities at the Australian Synchrotron. *J. Synchrotron Radiat.* **2015**, *22*, 187-190.

34. McPhillips, T. M.; McPhillips, S. E.; Chiu, H. J.; Cohen, A. E.; Deacon, A. M.; Ellis, P. J.; Garman, E.; Gonzalez, A.; Sauter, N. K.; Phizackerley, R. P.; Soltis, S. M.; Kuhn, P. Blu-Ice and the Distributed Control System: software for data acquisition and instrument control at macromolecular crystallography beamlines. *J. Synchrotron Radiat.* **2002**, *9*, 401-406.

35. Battye, T. G.; Kontogiannis, L.; Johnson, O.; Powell, H. R.; Leslie, A. G. iMOSFLM: a new graphical interface for diffraction-image processing with MOSFLM. *Acta Crystallogr. D Biol. Crystallogr.* **2011**, *67*, 271-281.

36. Evans, P. R.; Murshudov, G. N. How good are my data and what is the resolution? *Acta Crystallogr. D: Biol. Crystallogr.* **2013**, *67*, 1204-1214.

37. Winn, M. D.; Ballard, C. C.; Cowtan, K. D.; Dodson, E. J.; Emsley, P.; Evans, P. R.; Keegan, R. M.; Krissinel, E. B.; Leslie, A. G.; McCoy, A.; McNicholas, S. J.; Murshudov, G. N.; Pannu, N. S.; Potterton, E. A.; Powell, H. R.; Read, R. J.; Vagin, A.; Wilson, K. S. Overview of the CCP4 suite and current developments. *Acta Crystallogr. D: Biol. Crystallogr.* **2011**, *67*, 235-242.

38. McCoy, A. J.; Grosse-Kunstleve, R. W.; Adams, P. D.; Winn, M. D.; Storoni, L. C.; Read, R. J. Phaser crystallographic software. *J. Appl. Crystallogr.* **2007**, *40*, 658-674.

39. Emsley, P.; Lohkamp, B.; Scott, W. G.; Cowtan, K. Features and development of Coot. *Acta Crystallogr. D: Biol. Crystallogr.* **2010**, *66*, 486-501.

40. Adams, P. D.; P. V. Afonine, G. B., V. B. Chen I. W. Davis N. Echols J. J. Headd L.-W. Hung G. J. Kapral R. W. Grosse-Kunstleve A. J. McCoy N. W. Moriarty R. Oeffner R. J. Read D. C. Richardson J. S. Richardson T. C. Terwilliger; Zwart, P. H. PHENIX: a comprehensive Python-based system for macromolecular structure solution. *Acta Crystallogr. D: Biol. Crystallogr.* **2010**, *66*, 213-221.

41. Afonine, P. V.; Moriarty, N. W.; Mustyakimov, M.; Sobolev, O. V.; Terwilliger, T. C.; Turk, D.; Urzhumtsev, A.; Adams, P. D. FEM: feature-enhanced map. *Acta Crystallogr. D: Biol. Crystallogr.* **2015**, *71*, 646-666.

42. Abagyan, R.; Totrov, M.; Kuznetsov, D. ICM—A new method for protein modeling and design: Applications to docking and structure prediction from the distorted native conformation. *J. Comput. Chem.* **1994**, *15*, 488-506.

43. Terwilliger, T. C.; Grosse-Kunstleve, R. W.; Afonine, P. V.; Moriarty, N. W.; Zwart, P. H.; Hung, L. W.; Read, R. J.; Adams, P. D. Iterative model building, structure refinement and density modification with the PHENIX AutoBuild wizard. *Acta Crystallogr. D Biol. Crystallogr.* **2008**, *64*, 61-69.

44. Bell, S. G.; Xu, F.; Forward, I.; Bartlam, M.; Rao, Z.; Wong, L.-L. Crystal structure of CYP199A2, a para-substituted benzoic acid oxidizing cytochrome P450 from *Rhodopseudomonas palustris*. *J. Mol. Biol.* **2008**, *383*, 561-574.

45. Lonsdale, R.; Olah, J.; Mulholland, A. J.; Harvey, J. N. Does compound I vary significantly between isoforms of cytochrome P450? *J. Am. Chem. Soc.* **2011**, *133*, 15464-15474.

46. de Visser, S. P. What Factors Influence the Ratio of CH Hydroxylation versus CC Epoxidation by a Nonheme Cytochrome P450 Biomimetic? *J. Am. Chem. Soc.* **2006**, *128*, 15809-15818.

47. Honeychurch, M. J.; Hill, H. A. O.; Wong, L. L. The thermodynamics and kinetics of electron transfer in the cytochrome P450cam enzyme system. *FEBS Lett.* **1999**, *451*, 351-353.

48. Sligar, S. G. Coupling of spin, substrate, and redox equilibria in cytochrome P450. *Biochemistry* **1976**, *15*, 5399-5406.

49. Guengerich, F. P. Common and uncommon cytochrome P450 reactions related to metabolism and chemical toxicity. *Chem. Res. Toxicol.* **2001**, *14*, 611-650.

50. Shaffer, C. L.; Morton, M. D.; Hanzlik, R. P. N-dealkylation of an N-cyclopropylamine by horseradish peroxidase. Fate of the cyclopropyl group. *J. Am. Chem. Soc.* **2001**, *123*, 8502-8508.

51. Shaik, S.; Kumar, D.; de Visser, S. P.; Altun, A.; Thiel, W. Theoretical perspective on the structure and mechanism of cytochrome P450 enzymes. *Chem. Rev.* **2005**, *105*, 2279-2328.

52. Meyer, A. H.; Dybala-Defratyka, A.; Alaimo, P. J.; Geronimo, I.; Sanchez, A. D.; Cramer, C. J.; Elsner, M. Cytochrome P450-catalyzed dealkylation of atrazine by Rhodococcus sp. strain NI86/21 involves hydrogen atom transfer rather than single electron transfer. *Dalton Trans.* **2014**, *43*, 12175-12186.

53. Bhakta, M. N.; Wimalasena, K. Microsomal P450-catalyzed N-dealkylation of N,N-dialkylanilines: evidence for a C(alpha)-H abstraction mechanism. *J. Am. Chem. Soc.* **2002**, *124*, 1844-1845.

54. Roberts, K. M.; Jones, J. P. Anilinic N-oxides support cytochrome P450-mediated N-dealkylation through hydrogen-atom transfer. *Chemistry* **2010**, *16*, 8096-8107.

55. Shaffer, C. L.; Harriman, S.; Koen, Y. M.; Hanzlik, R. P. Formation of cyclopropanone during cytochrome P450-catalyzed N-dealkylation of a cyclopropylamine. *J. Am. Chem. Soc.* **2002**, *124*, 8268-8274.

56. Cerny, M. A.; Hanzlik, R. P. Cytochrome P450-catalyzed oxidation of N-benzyl-N-cyclopropylamine generates both cyclopropanone hydrate and 3-hydroxypropionaldehyde via hydrogen abstraction, not single electron transfer. *J. Am. Chem. Soc.* **2006**, *128*, 3346-3354.

57. Wang, Y.; Kumar, D.; Yang, C.; Han, K.; Shaik, S. Theoretical study of N-demethylation of substituted N,N-dimethylanilines by cytochrome P450: the mechanistic significance of kinetic isotope effect profiles. *J. Phys. Chem. B* **2007**, *111*, 7700-7710.

58. Li, C.; Wu, W.; Kumar, D.; Shaik, S. Kinetic isotope effect is a sensitive probe of spin state reactivity in C-H hydroxylation of N,N-dimethylaniline by cytochrome P450. *J. Am. Chem. Soc.* **2006**, *128*, 394-395.

59. Zheng, D.; Zhou, X.; Cui, B.; Han, W.; Wan, N.; Chen, Y. Biocatalytic α-Oxidation of Cyclic Amines and N-Methylanilines for the Synthesis of Lactams and Formamides. *ChemCatChem* **2017**, *9*, 937-940.

60. Kedderis, G. L.; Dwyer, L. A.; Rickert, D. E.; Hollenberg, P. F. Source of the oxygen atom in the product of cytochrome P-450-catalyzed N-demethylation reactions. *Mol. Pharmacol.* **1983**, *23*, 758.

61. Shea, J. P.; Valentine, G. L.; Nelson, S. D. Source of oxygen in cytochrome P-450 catalyzed carbinolamine formation. *Biochem. Biophys. Res. Commun.* **1982**, *109*, 231-235.

62. Perrin, L.; Loiseau, N.; Andre, F.; Delaforge, M. Metabolism of N-methyl-amide by cytochrome P450s: formation and characterization of highly stable carbinol-amide intermediate. *FEBS J.* **2011**, *278*, 2167-2178.

63. Rodriguez-Antona, C.; Ingelman-Sundberg, M. Cytochrome P450 pharmacogenetics and cancer. *Oncogene* **2006**, *25*, 1679-1691.

64. Upthagrove, A. L.; Nelson, W. L. Carbinolamines, imines, and oxazolidines from fluorinated propranolol analogs. (19)F NMR and mass spectral characterization and evidence for formation as intermediates in cytochrome P450-catalyzed N-dealkylation. *Drug Metabol. Dispos.* **2001**, *29*, 1114-1122.

65. An, G.-I.; Kim, M.; Kim, J. Y.; Rhee, H. Oxidation of aldimines to amides by m-CPBA and BF3·OEt2. *Tetrahedron Lett.* **2003**, *44*, 2183-2186.

66. Hamberger, B.; Bak, S. Plant P450s as versatile drivers for evolution of species-specific chemical diversity. *Philos. Trans. R. Soc. Lond. B. Biol. Sci.* **2013**, *368*, 20120426.

67. Mizutani, M.; Sato, F. Unusual P450 reactions in plant secondary metabolism. *Arch. Biochem. Biophys.* **2011**, *507*, 194-203.

68. Rydberg, P.; Ryde, U.; Olsen, L. Sulfoxide, Sulfur, and Nitrogen Oxidation and Dealkylation by Cytochrome P450. *J. Chem. Theory Comput.* **2008**, *4*, 1369-1377.

69. Alvarez, J. C.; Ortiz de Montellano, P. R. Thianthrene 5-oxide as a probe of the electrophilicity of hemoprotein oxidizing species. *Biochemistry* **1992**, *31*, 8315-8322.

70. Seto, Y.; Guengerich, F. P. Partitioning between N-dealkylation and N-oxygenation in the oxidation of N,N-dialkylarylamines catalyzed by cytochrome P450 2B1. *J. Biol. Chem.* **1993**, *268*, 9986-9997.

71. Volz, T. J.; Rock, D. A.; Jones, J. P. Evidence for two different active oxygen species in cytochrome P450 BM3 mediated sulfoxidation and N-dealkylation reactions. *J. Am. Chem. Soc.* **2002**, *124*, 9724-9725.

72. Sharma, P. K.; De Visser, S. P.; Shaik, S. Can a single oxidant with two spin states masquerade as two different oxidants? A study of the sulfoxidation mechanism by cytochrome p450. *J. Am. Chem. Soc.* **2003**, *125*, 8698-8699.

73. Lai, W.; Shaik, S. Can ferric-superoxide act as a potential oxidant in P450(cam)? QM/MM investigation of hydroxylation, epoxidation, and sulfoxidation. *J. Am. Chem. Soc.* **2011**, *133*, 5444-5452.

74. Wang, B.; Li, C.; Cho, K. B.; Nam, W.; Shaik, S. The Fe(III)(H2O2) Complex as a Highly Efficient Oxidant in Sulfoxidation Reactions: Revival of an Underrated Oxidant in Cytochrome P450. *J. Chem. Theory. Comput.* **2013**, *9*, 2519-2525.

Supporting information

The Cytochrome P450 CYP199A4 from *Rhodopseudomonas palustris* catalyses heteroatom dealkylations, sulfoxidation and amide and cyclic hemiacetal formation

Tom Coleman,[1] Siew Hoon Wong,[2] Matthew N. Podgorski,[1]John B. Bruning,[3] James J. De Voss[,2] and Stephen G. Bell[*,1]*

1 Department of Chemistry, University of Adelaide, SA 5005, Australia;

2 School of Chemistry and Molecular Biosciences, University of Queensland, Brisbane, Qld, 4072, Australia;

3 School of Biological Sciences, University of Adelaide, SA 5005, Australia

Corresponding authors: Stephen Bell, stephen.bell@adelaide.edu.au; James De Voss jdevoss@uq.edu.au

Index

Table S1 Substrate binding parameters and catalytic turnover activity data for CYP199A4 with various 4-aminomethylbenzoic acid derivatives. The data are given as mean ± S.D. with $n \geq 3$. The reaction mixtures (in 50 mM Tris, pH 7.4) contained 0.5 μM P450, 5 μM HaPux and 0.5 μM HaPuR. Rates are given as nmol.nmol-CYP^{-1}.min^{-1}. The leak rate of the system in the absence of the substrate was 9.0 nmol.nmol-CYP^{-1}.min^{-1}.

Substrate	**% HS**	***N*[a]**	**PFR[b]**	**C (%)[c],[d]**
4-aminomethylbenzoic acid	20%	13 ± 1	0.3 ± 0.003	2 ± 0.02
4-(methylamino)methylbenzoic acid	*(420 nm)[e]	24 ± 3	1.3 ± 0.06	5.6 ± 0.8
4-(dimethylamino)methylbenzoic acid	10%	24 ± 2	2.9 ± 0.2	12.2 ± 0.6
4-(ethylamino)methylbenzoic acid	<5%	15 ± 1	0.4 ± 0.05	2.9 ± 0.04

[a] NADH oxidation activity. [b] PFR: product formation rate defines the number of product forming catalytic cycles completed over the time period. [c] C is the coupling efficiency which is the percentage of NADH consumed in the reaction that led to the formation of products. H_2O_2 is the percentage of NADH converted to hydrogen peroxide via this uncoupling pathway. [d] The coupling values are based on the total amount of identified products in the turnovers. There were small amounts of both products (terephthalic acid and 4-formylbenzoic acid) in control turnovers containing no NADH or CYP199A4. However the overall product formations rates are significantly lower for these substrates compared to those in Table 1. [e] On addition of substrate the maximum absorption of the Soret peak is red shifted from 418 to 420 nm, however a Type I difference spectrum is still obtained.

Table S2 Overview of the distances (angstroms Å) and angles of pertinent substrate atoms from the heme iron in the crystal structure of CYP199A4 for various substrates. Also included are distances and angles from the likely position of the reactive oxygen of compound I.

Distance Å	**4-methoxy PDB:4DO1**	**4-ethoxy PDB:5U6T**	**4-methylamino PDB: 5U6W**	**4-methylthio PDB:5KT1**	**4-ethylthio PDB:5U6U**
C Me - Fe	4.1	4.2	4.1	4.4	5.2
C Me - O=Fe	2.7	2.8	3.1	3.3	4.0
C Et - Fe	-	4.3	-	-	6.7
C Et - O=Fe	-	3.0	-	-	5.5
X - Fe	(X=O) 5.2	(X=O) 5.1	(X=N) 4.2	(X=S) 4.9	(X=S) 4.7
X - O=Fe	3.6	3.6	3.0	3.4	3.3
Cx - closest F298 C	(X=Me) 3.8	(X=Me) 3.6	(X=Me) 3.5	(X=Me) 3.2	(X=Et) 4.0
Angle					
C_{04}-X-C Me	118.6	119.9	120.3	104.3	106.1
Dihedral C_{09}-C_{04}-X-C_{Me}	2.1	9.2	50.0	33.9	55.2
Fe=O-C_{Me}	140.7	144.8	133	131.9	133.7
Fe=O-X	158.3	163.4	158.4	162.5	159.2
Fe=O-C_{Et}	-	137.3	-	-	137.9

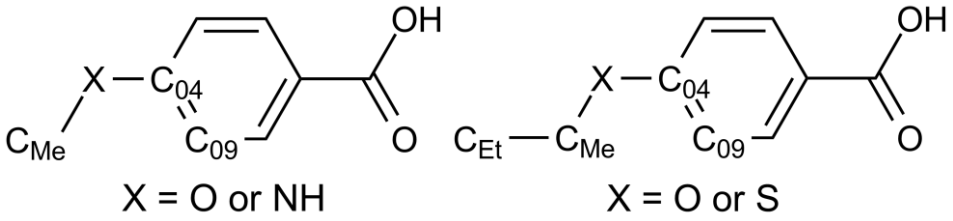

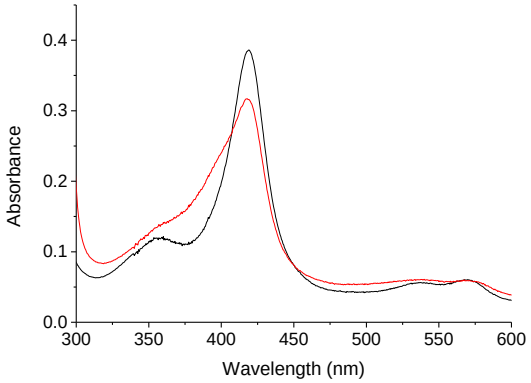

a) 4-aminomethylbenzoic acid

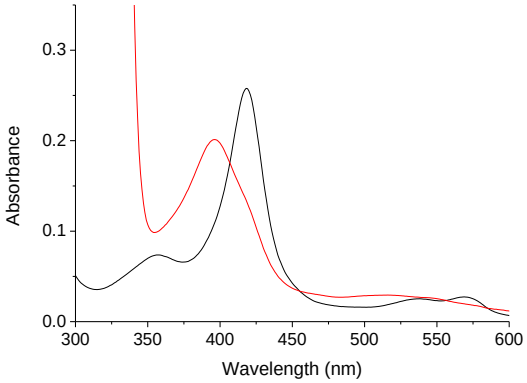

b) 4-diethylaminobenzoic acid

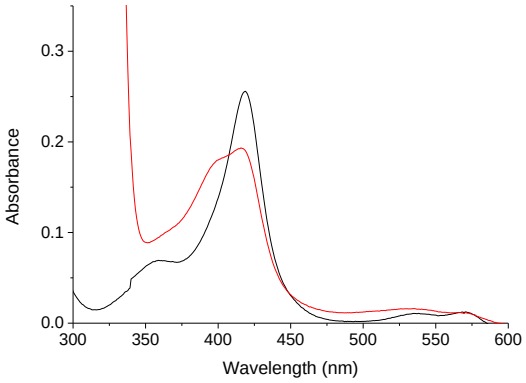

c) 4-dimethylaminobenzoic acid

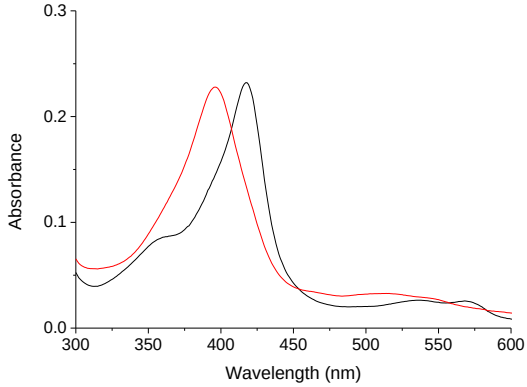

d) 4-ethoxybenzoic acid

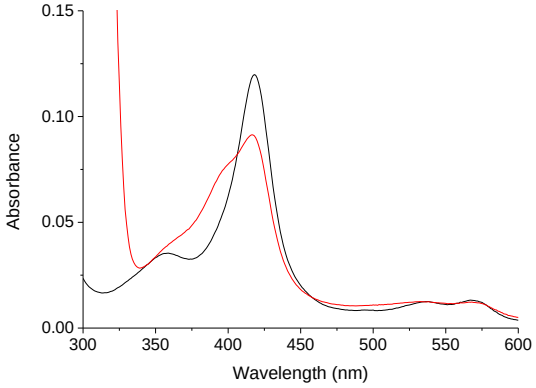

e) 4-ethylaminobenzoic acid

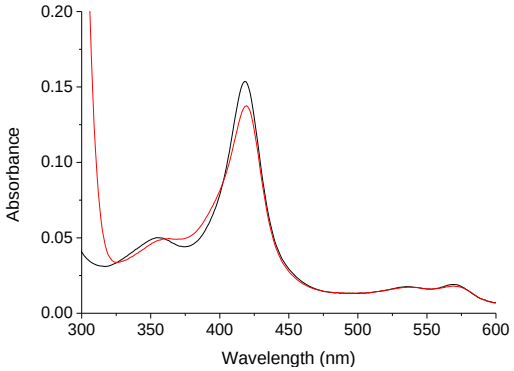

f) 4-ethylthiobenzoic acid

Note Soret Maxima shifted slightly from 418 to 419 nm for 4-ethylthiobenzoic acid (a type I difference spectrum is still obtained – Figure S2).

Figure S1 Spin state shift assays of CYP199A4 and a selection of substrates. The substrate free form is shown in black and the substrate bound form in red.

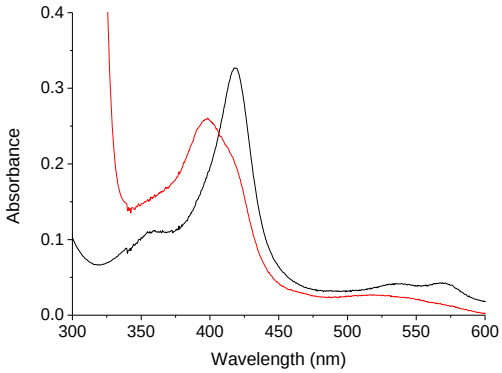

g) 4-methylaminobenzoic acid

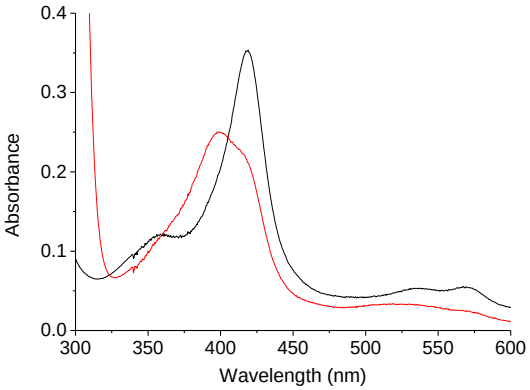

h) 4-methylthiobenzoic acid

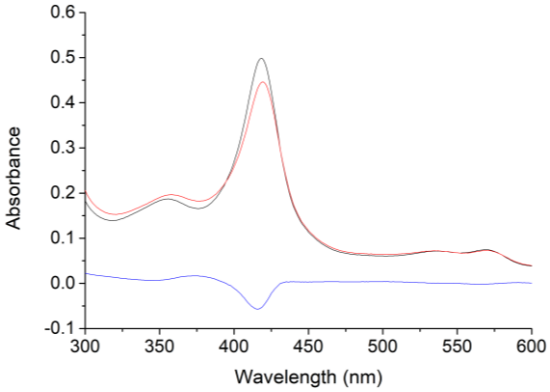

i) 4-(methylamino)methylbenzoic acid Note Soret Maxima shifted slightly from 418 to 420 nm but a type I difference spectrum is still obtained – blue spectrum).

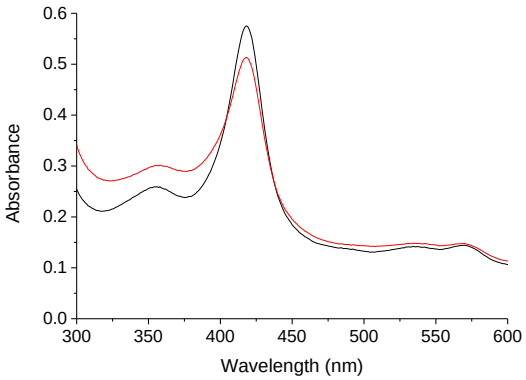

j) 4-(dimethylamino)methylbenzoic acid

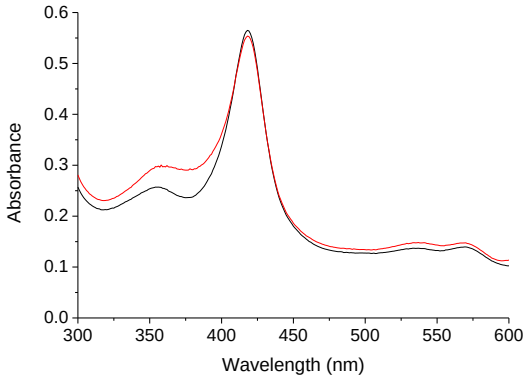

k) 4-(ethylamino)methylbenzoic acid

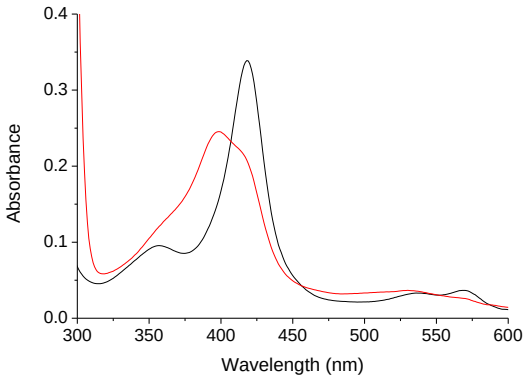

l) 3,4-ethylenedioxybenzoic acid

Figure S1 (continued) Spin state shift assays of CYP199A4 and a selection of substrates. The substrate free form is shown in black and the substrate bound form in red.

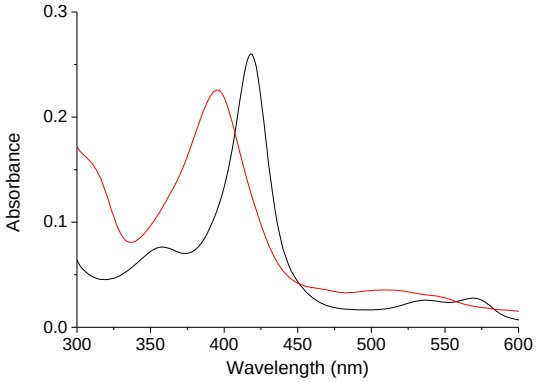

m) 4-trifluoromethoxybenzoic acid

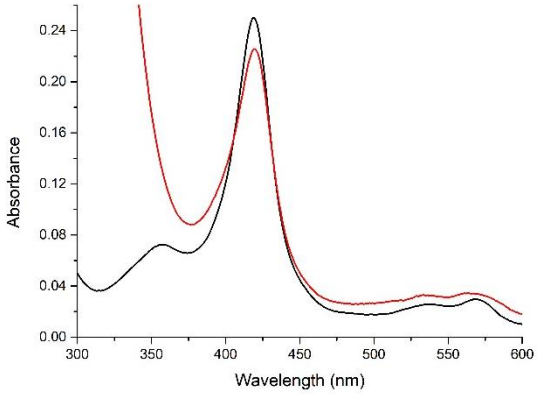

n) 3-methylaminobenzoic acid

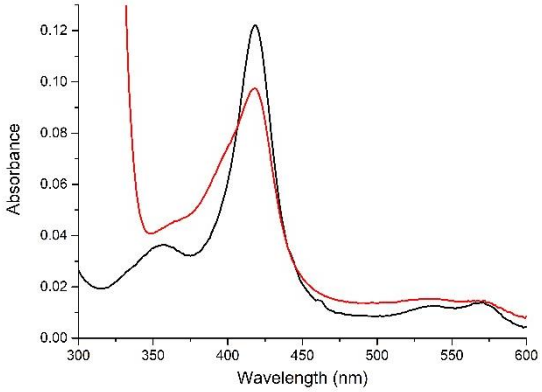

o) 3-methylthiobenzoic acid

Figure S1 (continued) Spin state shift assays of CYP199A4 and a selection of substrates. The substrate free form is shown in black and the substrate bound form in red.

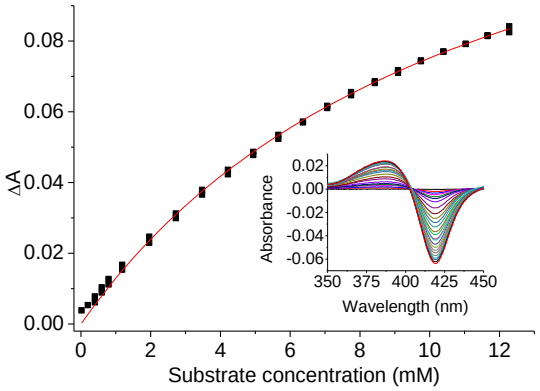

a) 4-aminomethylbenzoic acid
1.69 μM A_{419}/A_{386}

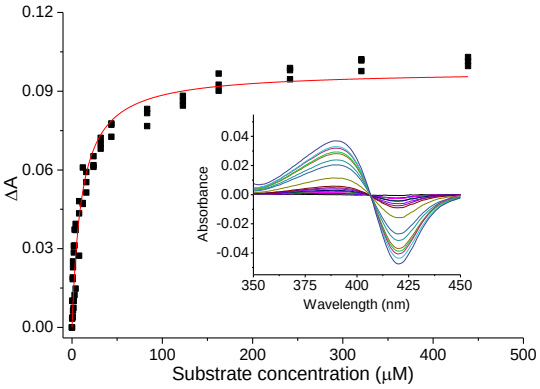

b) 4-diethylaminobenzoic acid
1.44 μM A_{420}/A_{390}

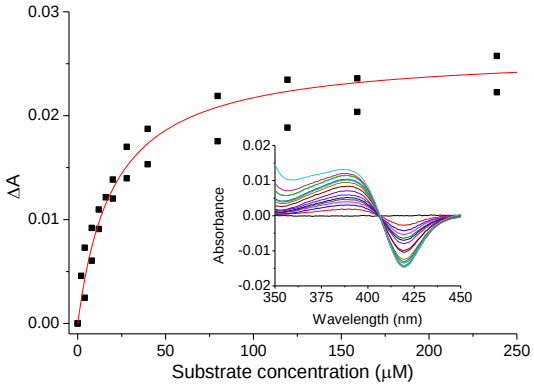

c) 4-dimethylaminobenzoic acid
0.39 μM A_{419}/A_{388}

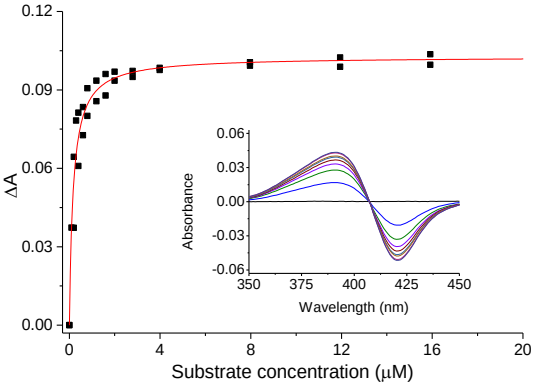

d) 4-ethoxybenzoic acid
0.89 μM A_{421}/A_{391}

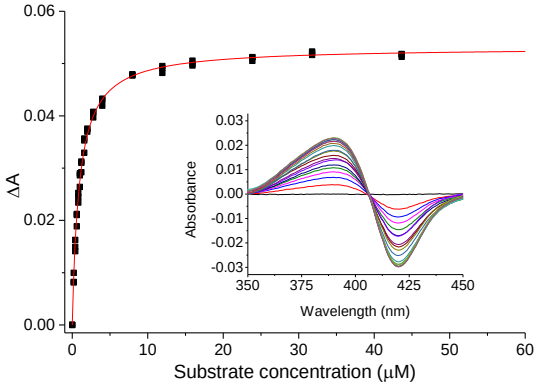

e) 4-ethylaminobenzoic acid
1.01 μM A_{420}/A_{390}

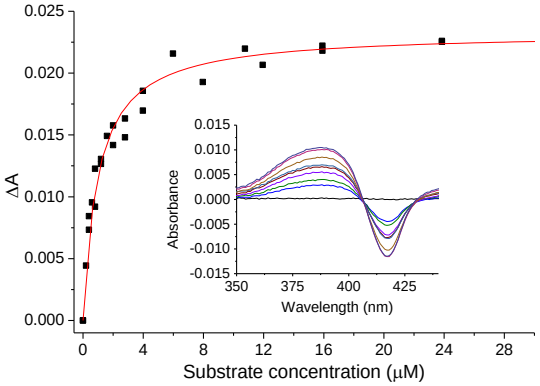

f) 4-ethylthiobenzoic acid
1.01 μM A_{417}/A_{387}

Figure S2 Dissociation constant analysis of CYP199A4 with selected substrates. The concentration of enzyme used is given as are the absorbances of the trough and the peak.

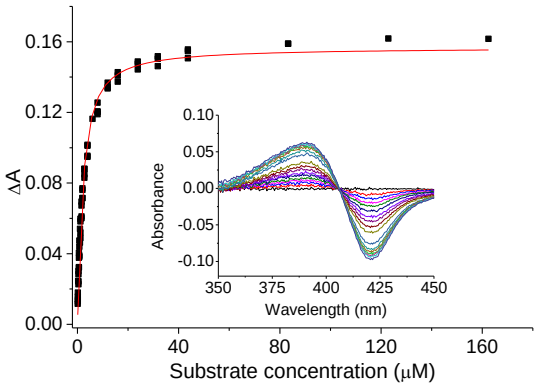

g) 4-methylaminobenzoic acid
1.41 μM A_{421}/A_{390}

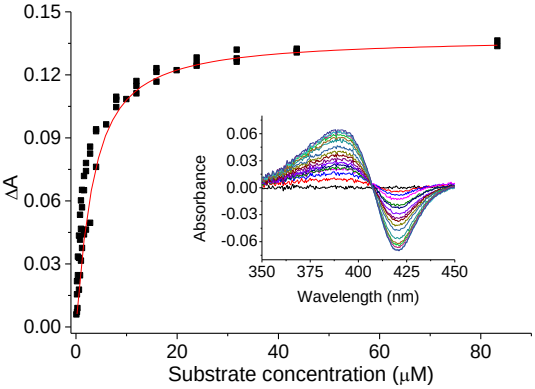

h) 4-methylthiobenzoic acid
1.50 μM A_{421}/A_{389}

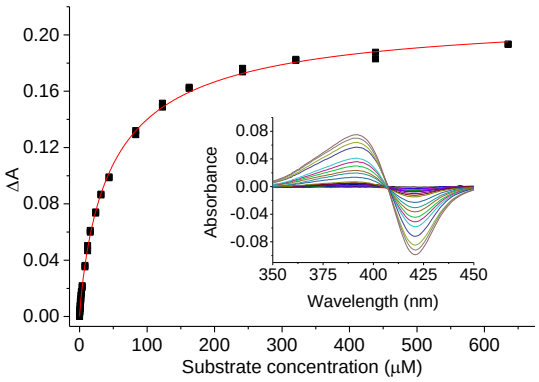

i) 3,4-ethylenedioxybenzoic acid
2.0 μM A_{421}/A_{392}

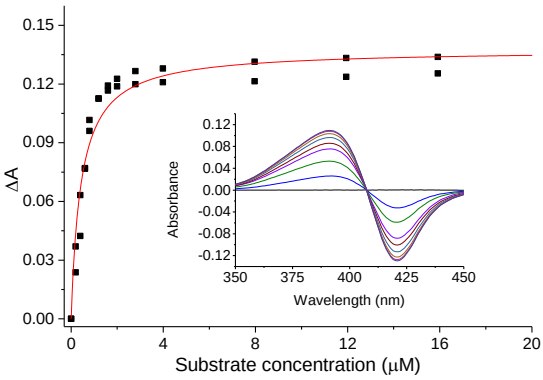

j) 4-trifluoromethoxybenzoic acid
1.50 μM A_{421}/A_{391}

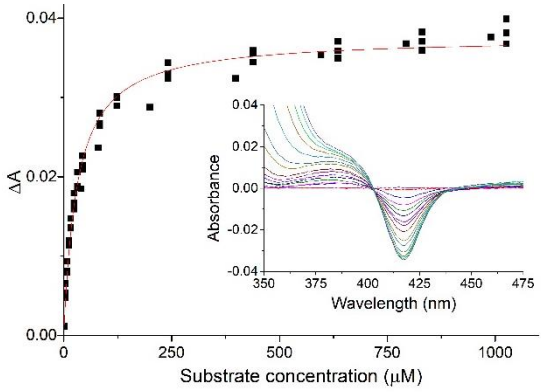

k) 3-methylaminobenzoic acid
2.0 μM
Due to interference of the substrate with the peak at 390 nm the reduction in the trough at 417 nm was used

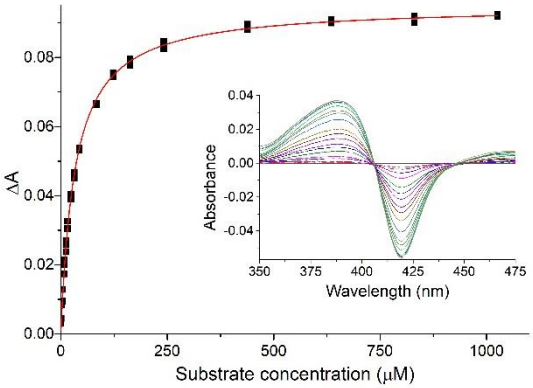

l) 3-methylthiobenzoic acid
2.2 μM A_{419}/A_{389}

Figure S2 (continued) Dissociation constant analysis of CYP199A4 with selected substrates. The concentration of enzyme used is given as are the absorbances of the trough and the peak.

Black = 4-methoxyBA, red = 4-methylaminoBA, blue = 4-methylthioBA

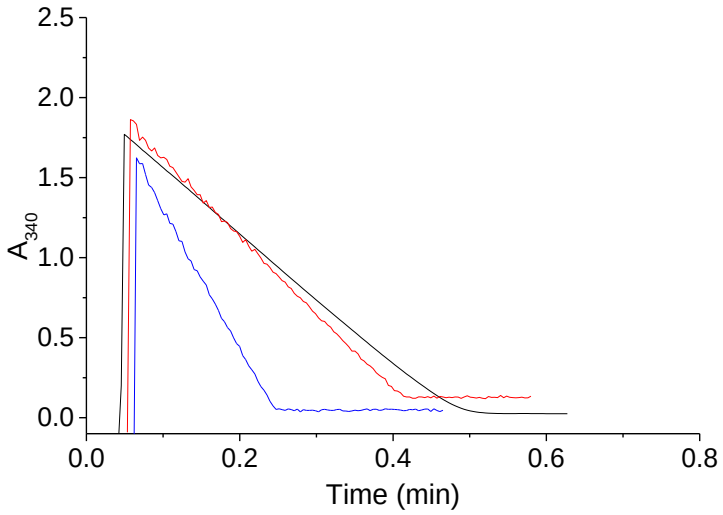

Black = 4-ethoxyBA, red = 4-aminomethylBA, blue = 4-ethylthioBA

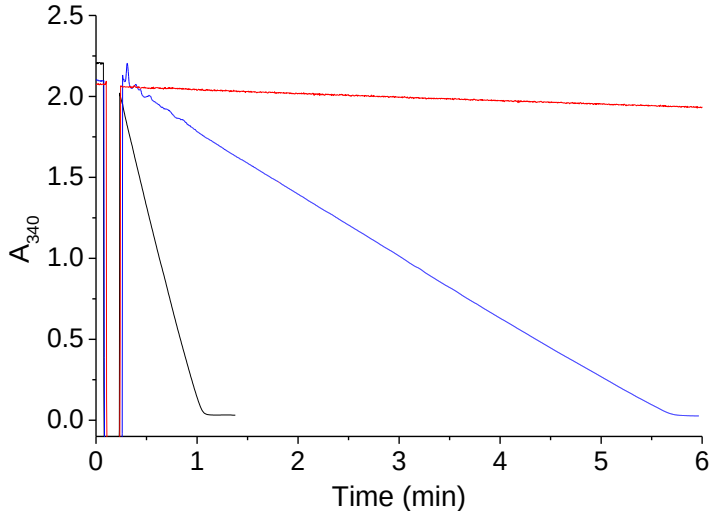

Figure S3 Examples of CYP199A4 catalysed NADH oxidation assays of selected substrates (Table 1).

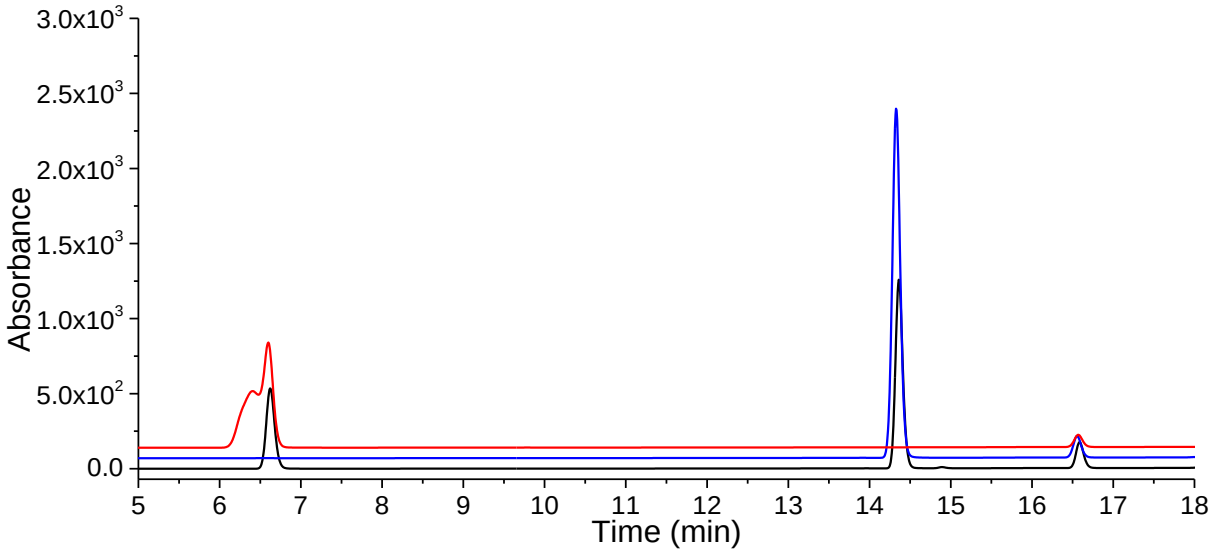

Figure S4 (a) HPLC analysis of the *in vitro* turnovers of 4-ethoxybenzoic acid with CYP199A4. For clarity the chromatograms have been offset along the y axis.

4-Ethoxybenzoic acid, 254 nm, 20-95% acetonitrile.

Black = *in vitro* turnover, blue = 4-ethoxyBA control, red = 4-hydroxyBA control. Internal standard shown at 16.6 min.

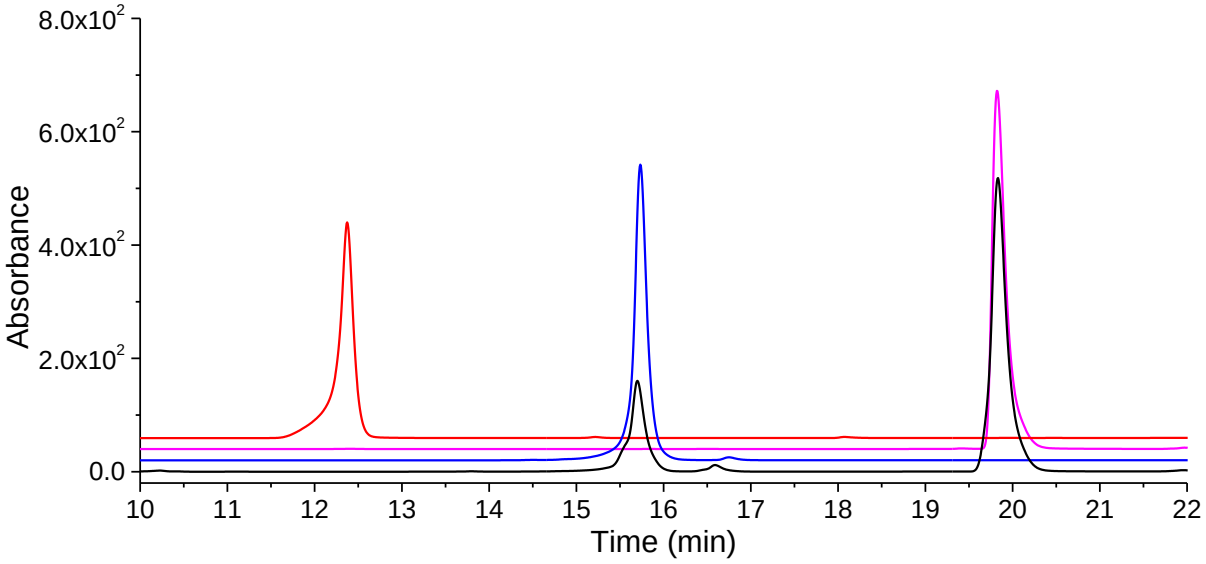

Figure S4 (b) HPLC analysis of the *in vitro* turnovers of 3,4-ethylenebenzoic acid with CYP199A4. For clarity the chromatograms have been offset along the y axis.

3,4-ethylenedioxybenzoic acid, 254 nm, 20-95% acetonitrile.

black = *in vitro* turnover, blue = isolated hydroxylation product, pink = substrate control, red = 3,4-dihydroxyBA control.

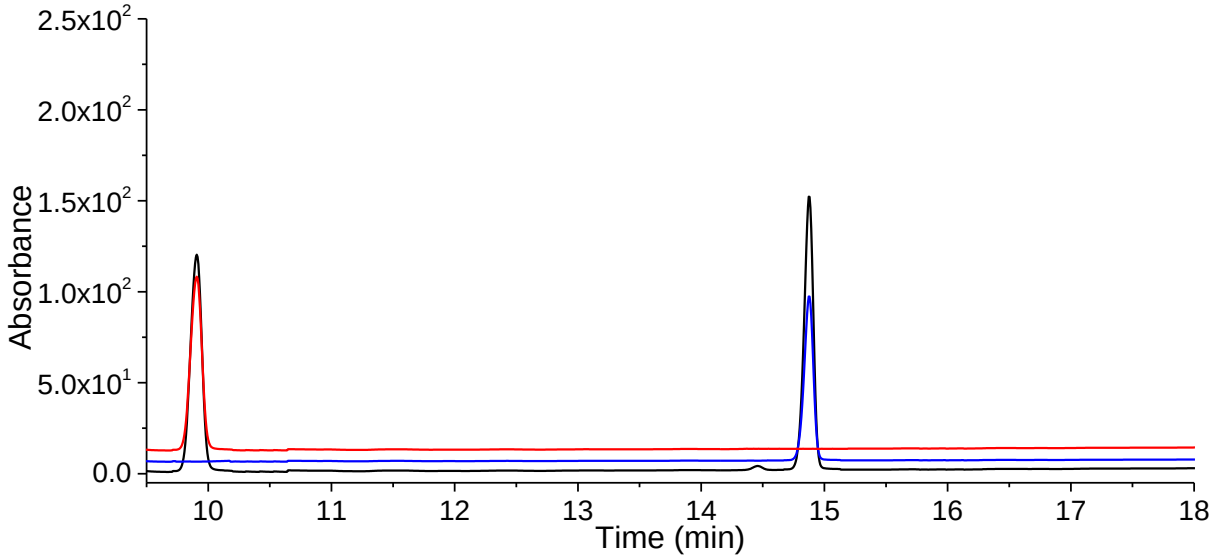

Figure S4 (c) HPLC analysis of the *in vitro* turnovers of 4-methylaminobenzoic acid with CYP199A4. For clarity the chromatograms have been offset along the y axis.

4-Methylaminobenzoic acid, 240 nm, 0-50% acetonitrile.

black = *in vitro* turnover, blue = 4-methylaminoBA control, red = 4-aminoBA control

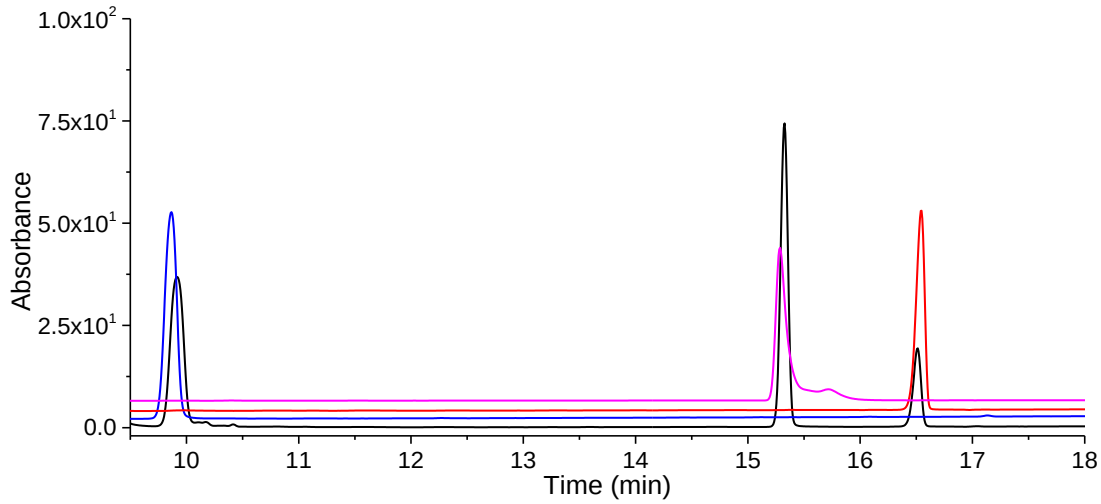

Figure S4 (d) HPLC analysis of the *in vitro* turnovers of 4-methylaminobenzoic acid with CYP199A4. For clarity the chromatograms have been offset along the y axis.

4-Ethylaminobenzoic acid, 254 nm, 0-50% acetonitrile.

black = *in vitro* turnover, blue = 4-aminoBA control, red = 4-ethylaminoBA control, pink = 4-acetamidoBA control.

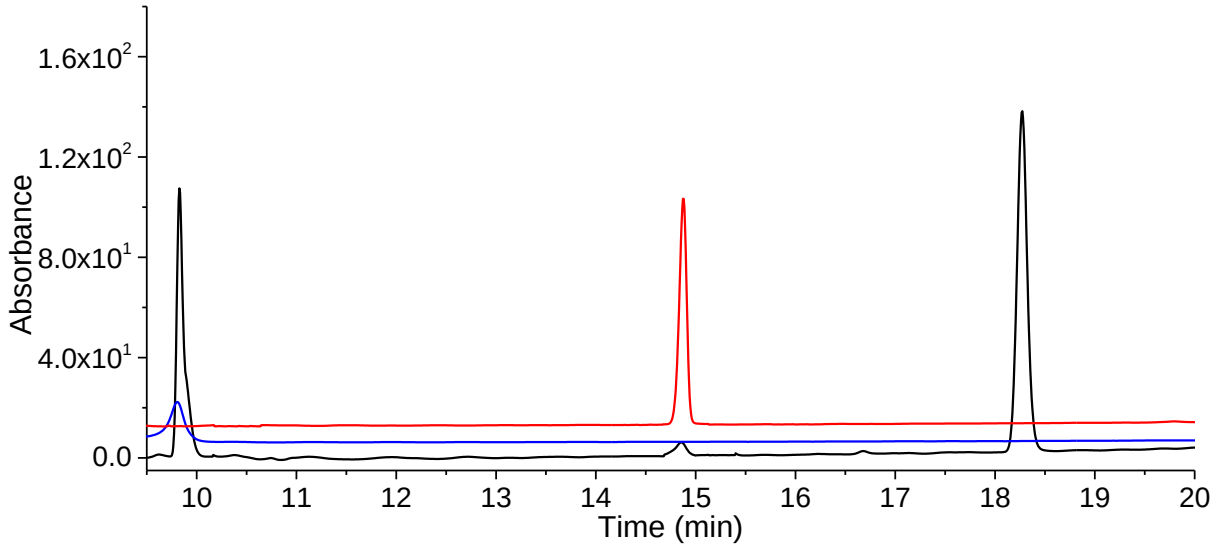

Figure S4 (e) HPLC analysis of the *in vitro* turnovers of 4-dimethylaminobenzoic acid with CYP199A4. For clarity the chromatograms have been offset along the y axis.

4-Dimethylaminobenzoic acid, 240 nm, 0-50% acetonitrile.

black = *in vitro* turnover, blue = 4-aminoBA control, red = 4-methylaminoBA control

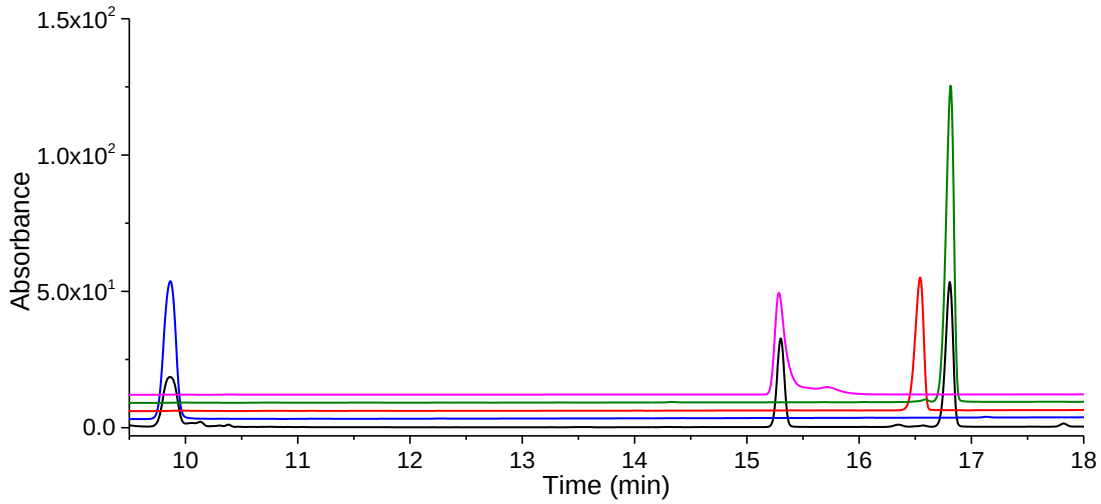

Figure S4 (f) HPLC analysis of the *in vitro* turnovers of 4-diethylaminobenzoic acid with CYP199A4. For clarity the chromatograms have been offset along the y axis.

4-Diethylaminobenzoic acid, 254 nm, 0-50% acetonitrile.

black = *in vitro* turnover, blue = 4-aminoBA control, red = 4-ethylaminoBA control, green = 4-diethylaminoBA control, pink = 4-acetamidoBA control.

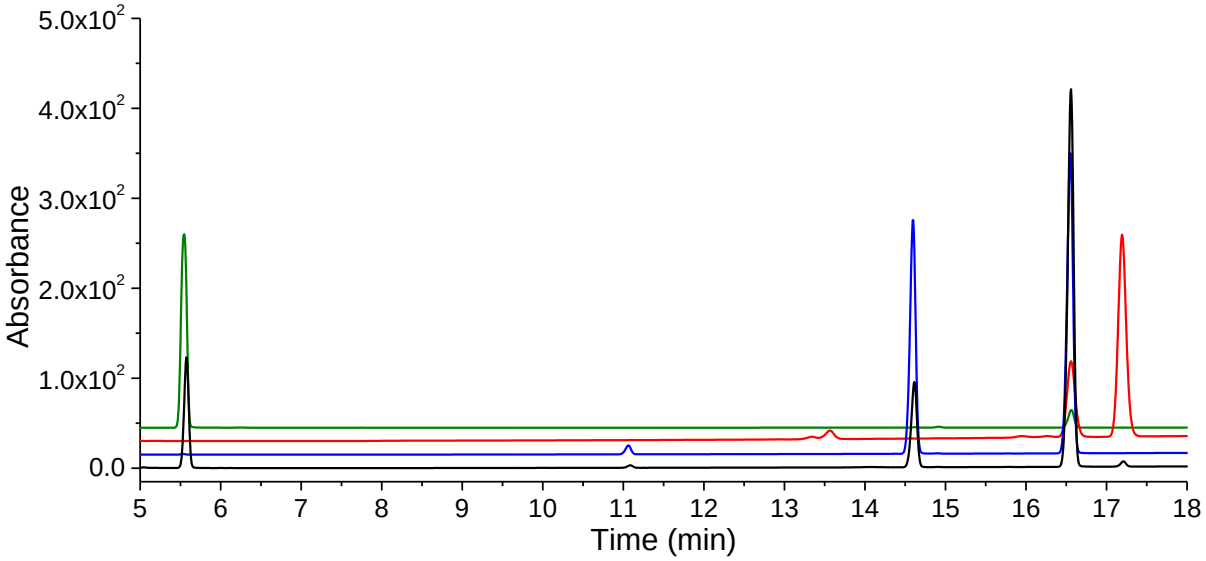

Figure S4 (g) HPLC analysis of the *in vitro* turnovers of 4-methylthiobenzoic acid with CYP199A4. For clarity the chromatograms have been offset along the y axis.

4-Methylthiobenzoic acid, 254 nm, 20-95% acetonitrile.

black = *in vitro* turnover, blue = 4-methylthioBA control, red = 4-mercaptobenzoic acid control, green = 4-methylsulfinyl benzoic acid control.

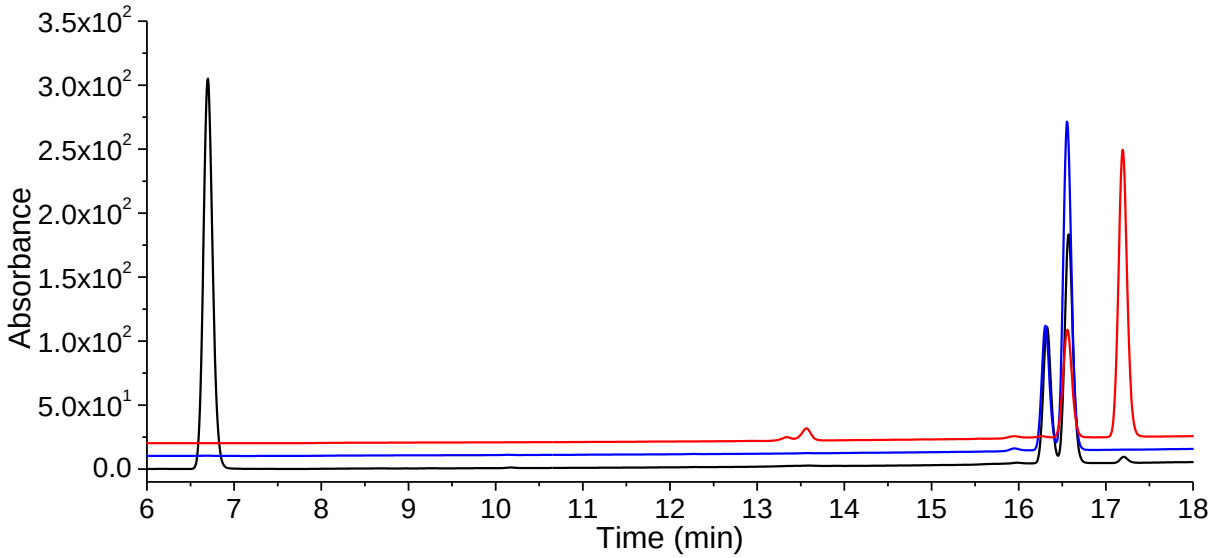

Figure S4 (h) HPLC analysis of the *in vitro* turnovers of 4-ethylthiobenzoic acid with CYP199A4. For clarity the chromatograms have been offset along the y axis.

4-Ethylthiobenzoic acid, 254 nm, 20-95% acetonitrile.

black = *in vitro* turnover, blue = 4-ethylthioBA control, red = 4-mercaptoBA control. Internal standard shown at 16.6 min.

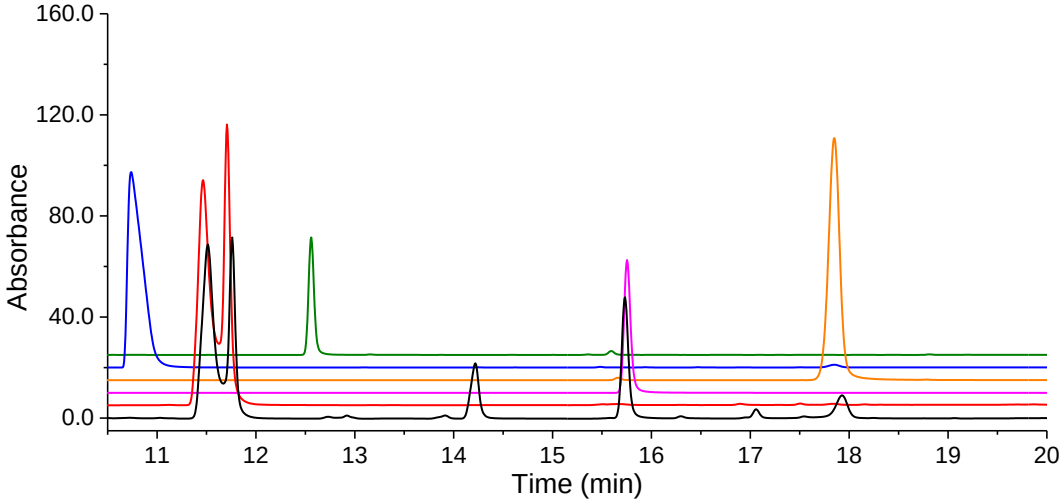

Figure S4 (i) HPLC analysis of the *in vitro* turnovers of 4-(methylamino)methylbenzoic acid with CYP199A4. For clarity the chromatograms have been offset along the y axis.

4-(methylamino)methylbenzoic acid, 254 nm, 0-50% acetonitrile,

black = *in vitro* turnover, red = substrate control, blue = 4-aminomethylbenzoic acid control, pink = terephthalic acid control, orange = 4-formylbenzoic acid control and green = monoamide terephthalic acid control.

The peak at 14.2 min is uncharacterised no equivalent additional peak could be detected/assigned in the GC-MS analysis.

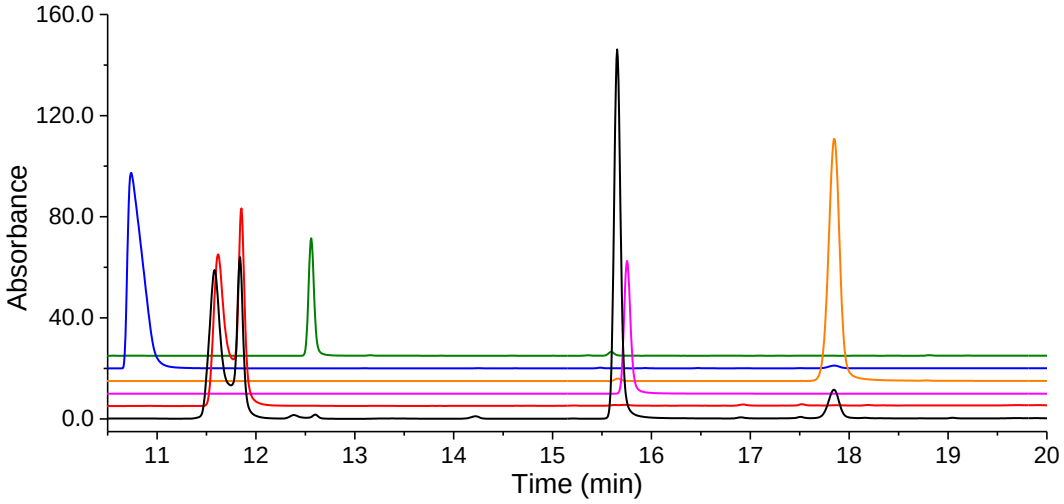

Figure S4 (j) HPLC analysis of the *in vitro* turnovers of 4-(dimethylamino)methylbenzoic acid with CYP199A4. For clarity the chromatograms have been offset along the y axis.

4-(dimethylamino)methylbenzoic acid, 254 nm, 0-50% acetonitrile,

black = turnover, red = substrate control, blue = 4-aminomethylbenzoic acid control, pink = terephthalic acid control, orange = 4-formylbenzoic acid control and green = monoamide terephthalic acid control.

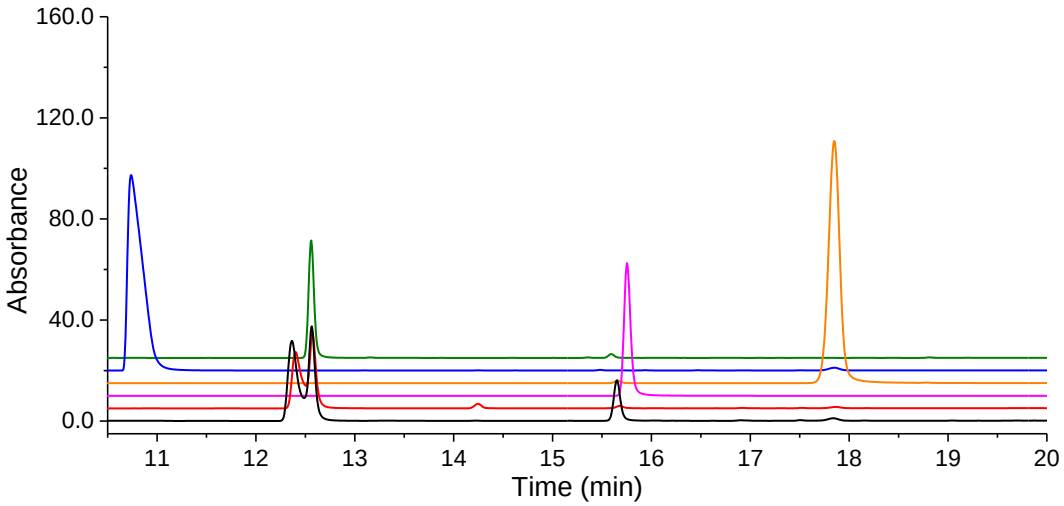

Figure S4 (k) HPLC analysis of the *in vitro* turnovers of 4-(ethylamino)methylbenzoic acid with CYP199A4. For clarity the chromatograms have been offset along the y axis.

4-(ethylamino)methylbenzoic acid, 254 nm, 0-50% acetonitrile,

black = turnover, red = substrate control, blue = 4-aminomethylbenzoic acid control, pink = terephthalic acid control, orange = 4-formylbenzoic acid control and green = monoamide terephthalic acid control.

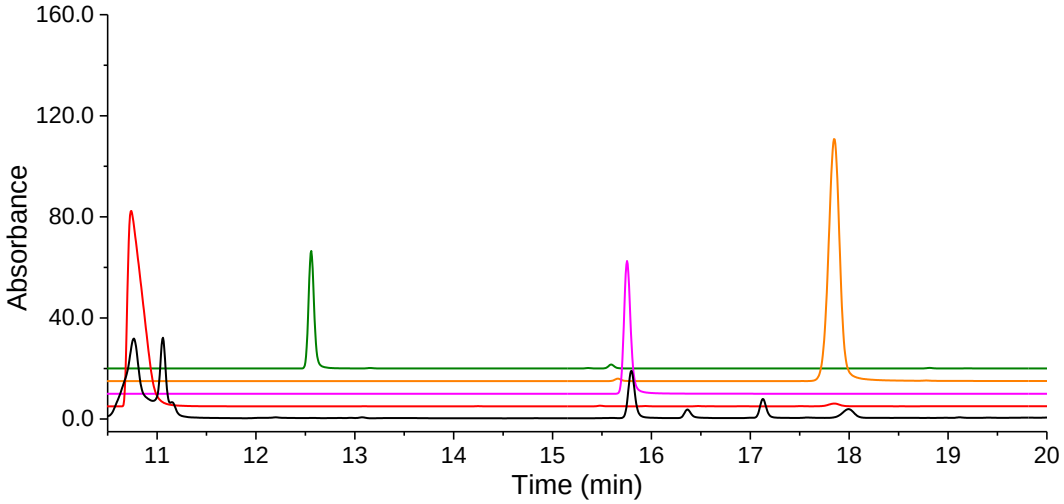

Figure S4 (l) HPLC analysis of the *in vitro* turnovers of 4-aminomethylbenzoic acid with CYP199A4. For clarity the chromatograms have been offset along the y axis.

4-aminomethylbenzoic acid, 254 nm, 0-50% acetonitrile,

black = turnover, red = substrate control, pink = terephthalic acid control, orange = 4-formylbenzoic acid control and green = monoamide terephthalic acid control. Note minor unidentified peaks at 16.4 min and 17.2 min.

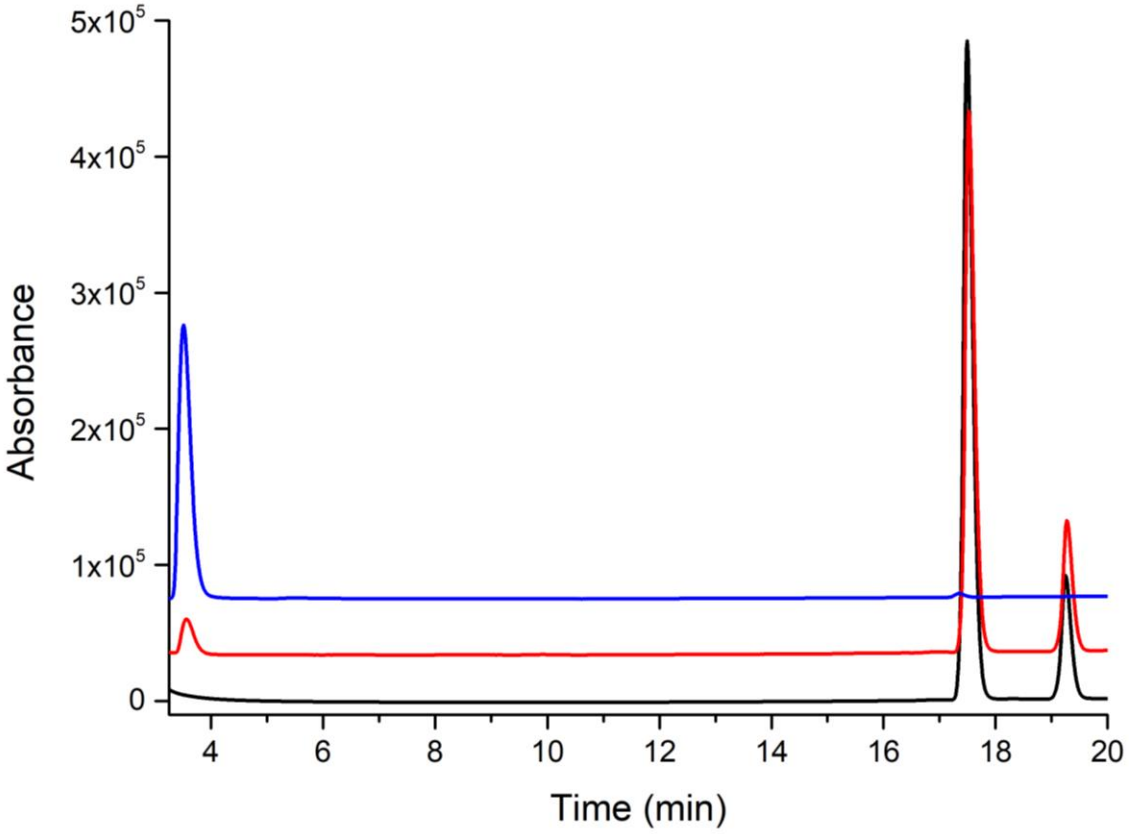

Figure S4 (m) HPLC analysis of the *in vitro* turnovers of 3-methylthiobenzoic acid with CYP199A4. For clarity the chromatograms have been offset along the y axis.

3-methylthiobenzoic acid HPLC, 254 nm, 20-95% acetonitrile

red = in vitro turnover, blue = chemically synthesised 3-(methylsulfinyl)benzoic acid standard and black = no P450 control reaction (**black**). The chromatograms have been offset along the *y*-axis.

Note for the 4-(methylamino)methylbenzoic acid, 4-(dimethylamino)methylbenzoic acid, 4-(ethylamino)methylbenzoic acid and 4-aminomethylbenzoic acid turnovers no peaks could be assigned to potential products before 10 minutes which were not present in controls (both no P450 and no NADH controls were run). It is important to note that peaks corresponding to terephthalic acid (RT 15.7 min) and formylbenzoic acid (RT 17.9 min) were also present in some of these controls but in much lower quantities than observed in the turnovers.

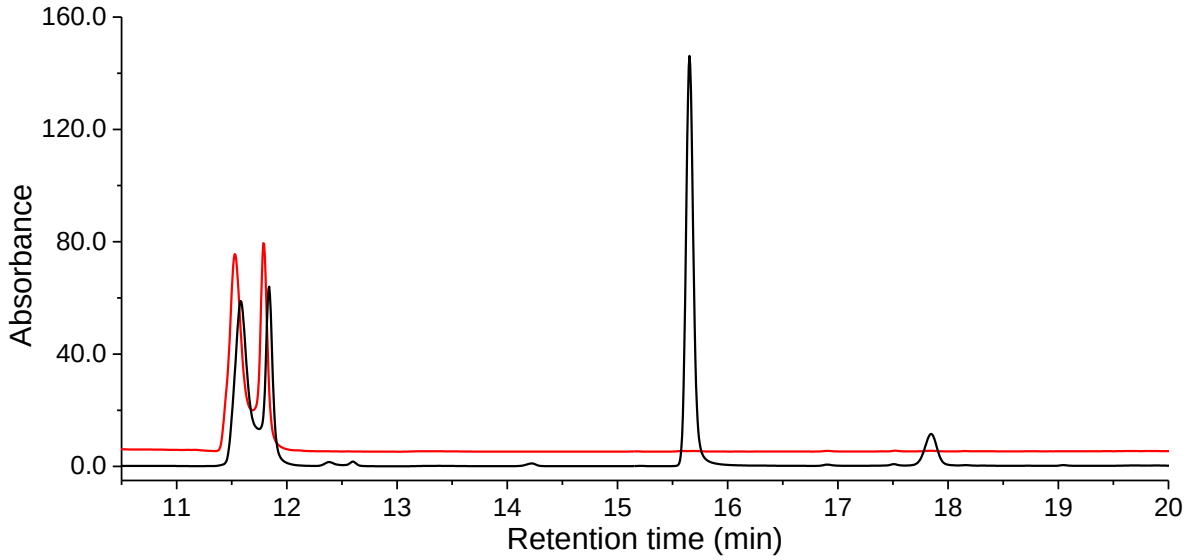

Figure S4 (n) HPLC analysis of the *in vitro* turnovers of 4-(dimethylamino)methylbenzoic acid with CYP199A4. For clarity the chromatograms have been offset along the y axis. black = *in vitro* turnover, red = no p450 control.

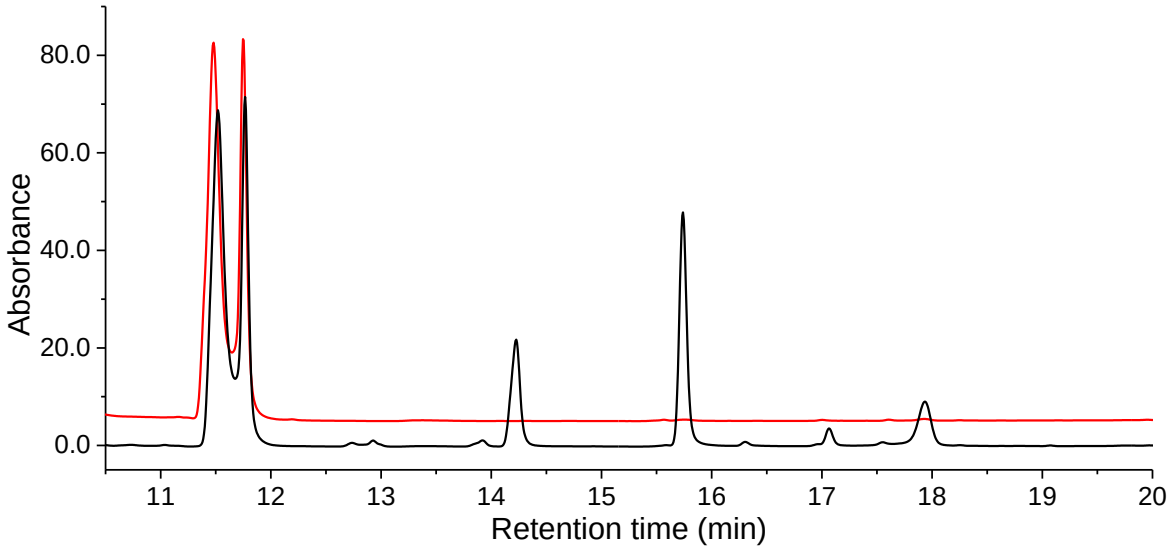

Figure S4 (o) HPLC analysis of the *in vitro* turnovers of 4-(methylamino)methylbenzoic acid with CYP199A4. For clarity the chromatograms have been offset along the y axis. black = *in vitro* turnover, red = no p450 control.

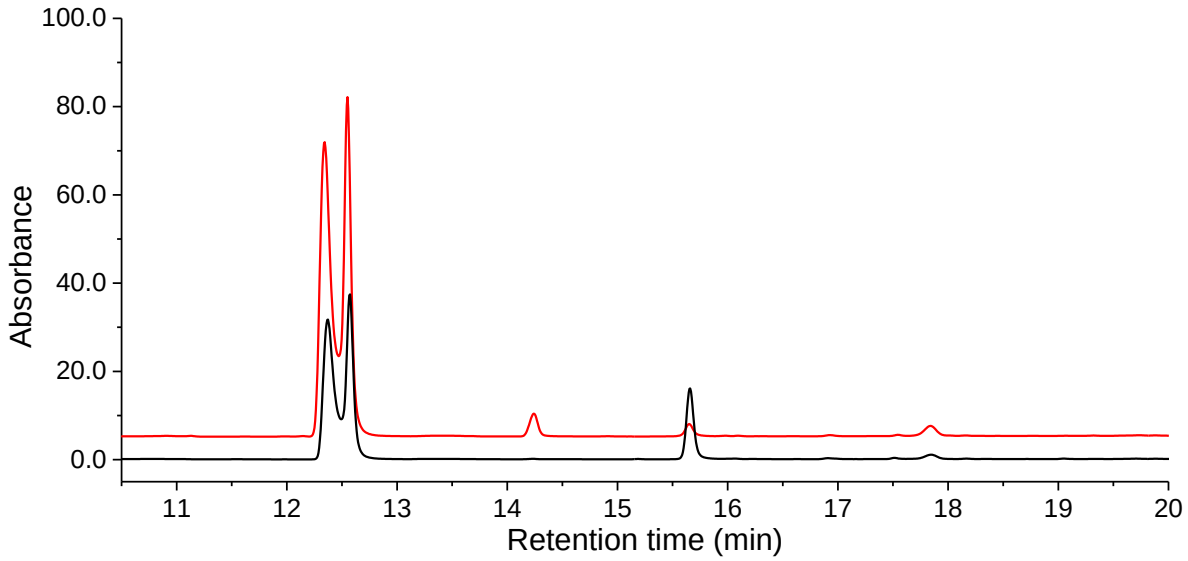

Figure S4 (p) HPLC analysis of the *in vitro* turnovers of 4-(ethylamino)methylbenzoic acid with CYP199A4. For clarity the chromatograms have been offset along the y axis. black = *in vitro* turnover, red = no p450 control.

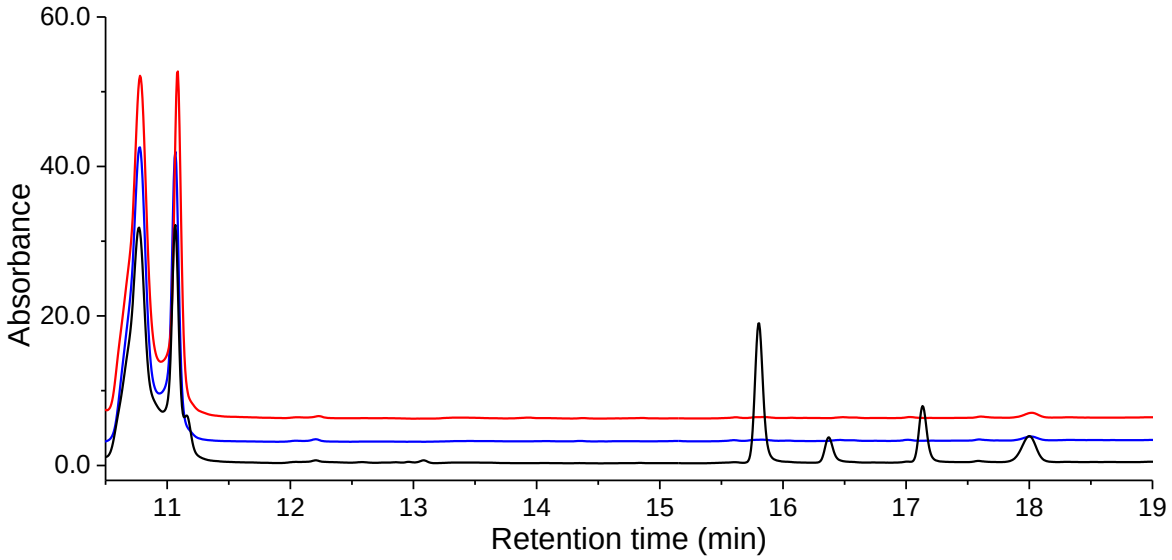

Figure S4 (q) HPLC analysis of the *in vitro* turnovers of 4-aminomethylbenzoic acid with CYP199A4. For clarity the chromatograms have been offset along the y axis. black = *in vitro* turnover, red = no p450 control.

List of reverse phase HPLC retention times. A: H_2O, B: acetonitrile. The gradient used is given in parentheses.

Internal standard – 9-hydroxyfluorene: 16.6 min (20-95%)

4-Ethoxybenzoic acid: 14.3 min (20-95%)

4-Hydroxybenzoic acid: 6.6 min (20-95%)

4-Methylthiobenzoic acid: 14.7 min (20-95%)

4-Methylsulfinylbenzoic acid: 5.3 min (20-95%)

4-Ethylthiobenzoic acid: 16.3 min (20-95%)

4-Ethylsulfinylbenzoic acid: 6.7 min (20-95%)

3,4-Ethylenedioxybenzoic acid: 19.9 min (20-95%)

4-Mercaptobenzoic acid: 17.2 min (20-95%)

6-Carboxy-2,3-dihydro-2-hydroxy-1,4-benzodioxin: 15.6 min (20-95%)

3-(Methylthio)benzoic acid: 17.5 min (20-95%)

3-(Methylsulfinyl)benzoic acid: 3.5 min (20-95%)

Internal standard – 9-hydroxyfluorene: 26.1 min (0-50%)

4-Diethylaminobenzoic acid: 16.8 min (0-50%)

4-Ethylaminobenzoic acid: 16.5 min (0-50%)

4-Acetamidobenzoic acid: 15.3 min (0-50%)

4-Dimethylaminobenzoic acid: 18.3 min (0-50%)

4-Methylaminobenzoic acid: 14.9 min (0-50%)

4-Aminobenzoic acid: 9.4 min (0-50%)

4-Aminomethylbenzoic acid: 10.8 min (0-50%) (second peak at 11.1 min)

Terephthalic acid: 15.7 min (0-50%)

4-Formylbenzoic acid: 17.9 min (0-50%)

4-(Methylamino)methylbenzoic acid: Double peak 11.5 min & 11.8 min (0-50%)

4-(Dimethylamino)methylbenzoic acid: Double peak 11.6 min & 11.9 min (0-50%)

4-(Ethylamino)methylbenzoic acid: Double peak 12.4 min & 12.6 min (0-50%)

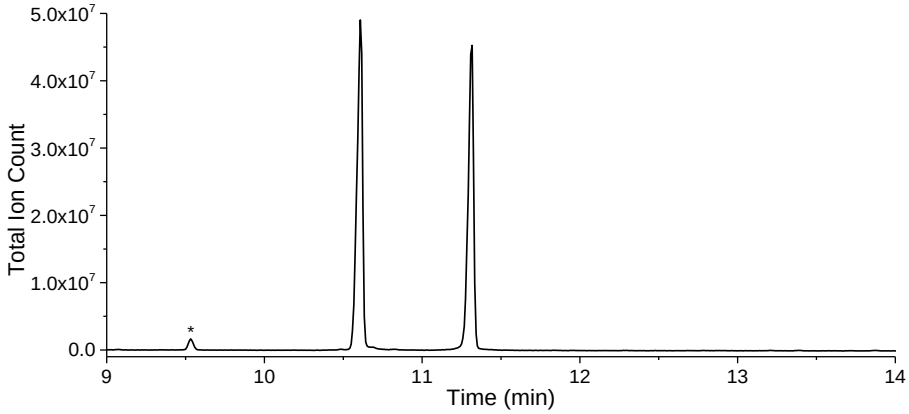

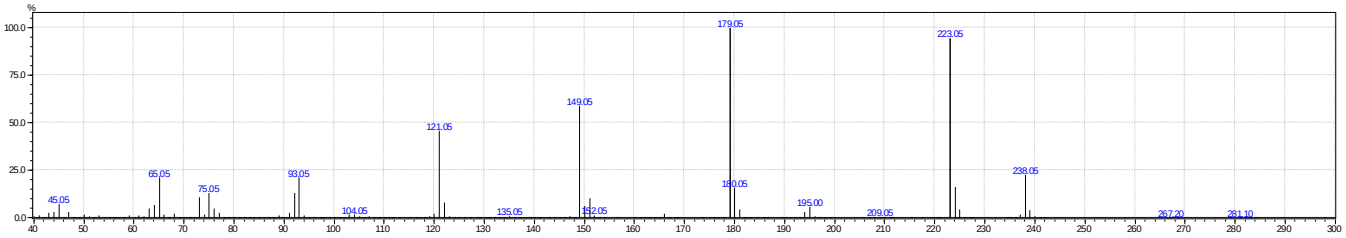

4-EthoxyBA substrate (singly derivatised): m/z = 238.05 (exp. m/z = 238.1025).

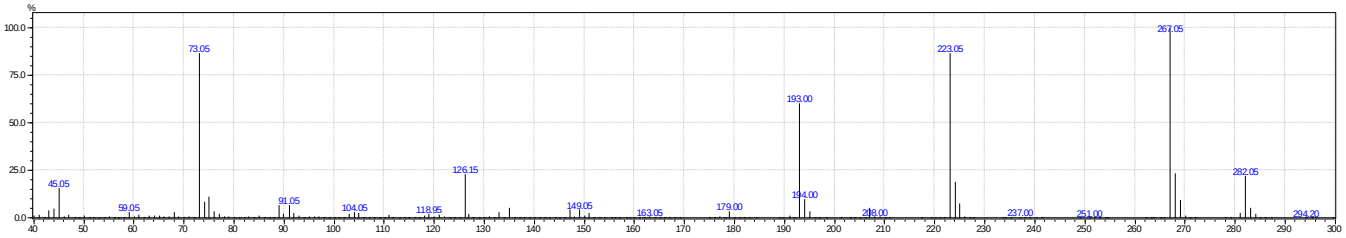

4-Hydroxybenzoic acid (doubly derivatised): m/z = 282.05 (exp. m/z = 282.1107).

Figure S5 (a) GC-MS chromatogram of the *in vitro* turnover of 4-ethoxybenzoic acid with CYP199A4 and the MS data. GC retention times of the trimethylsilyl chloride derivatised substrates and products; 4-ethoxybenzoic acid: 10.6 min; 4-hydroxybenzoic acid: 11.3 min.

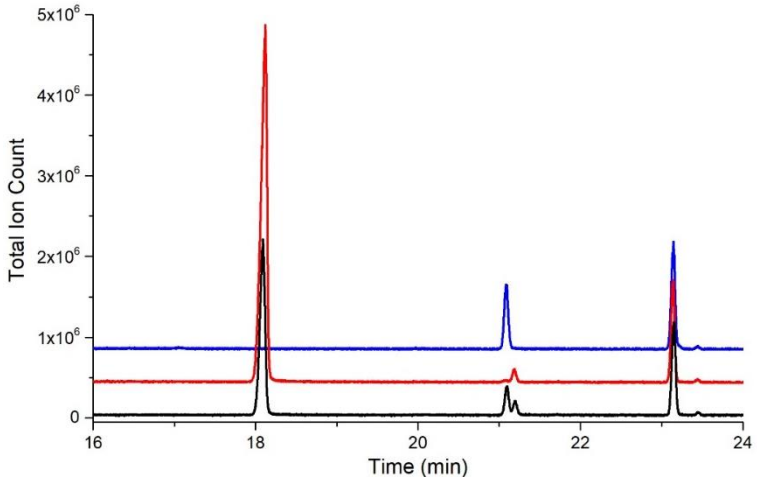

Black = *in vitro* turnover, red = no P450 control, blue = 3-aminoBA control (doubly derivatised)

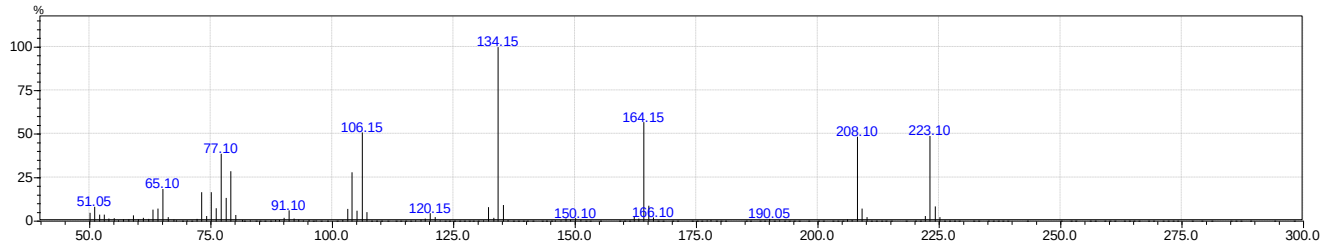

3-Methylaminobenzoic acid substrate (singly derivatised): m/z = 223.10 (exp. m/z = 223.1029)

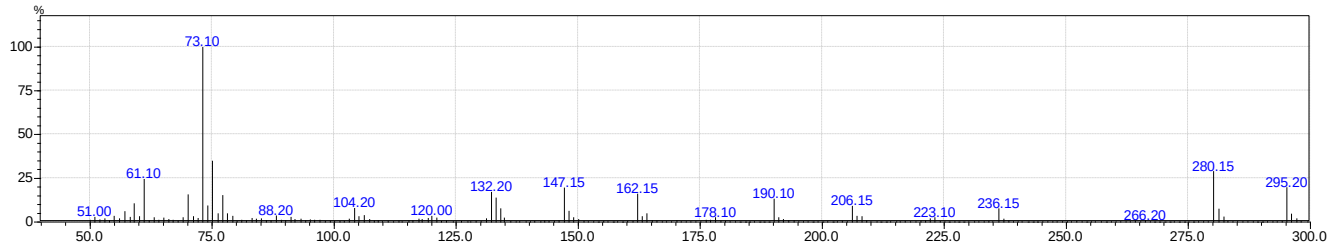

3-Methylaminobenzoic acid substrate (doubly derivatised): m/z = 295.20 (exp. m/z = 295.1424).

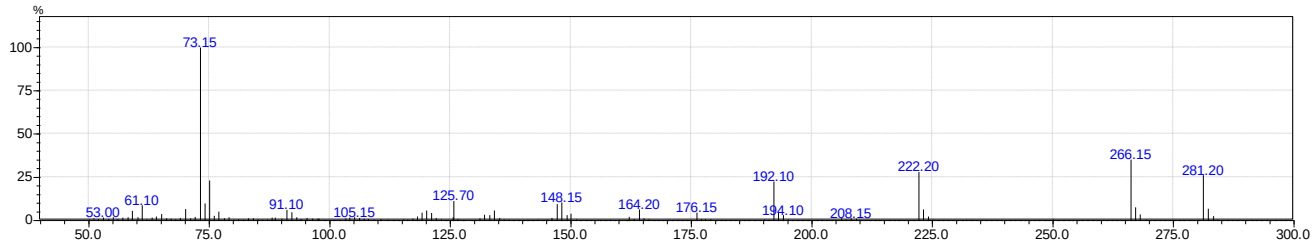

3-Aminobenzoic acid product (doubly derivatised): m/z = 281.20 (exp. m/z = 281.1267).

Figure S5 (b) GC-MS chromatogram of the *in vitro* turnover of 3-methylaminobenzoic acid with CYP199A4 and the MS data. GC retention times of the trimethylsilyl chloride derivatised substrates and products; 3-methylaminobenzoic acid substrate (singly derivatised): 18.1 min; 3-aminobenzoic acid product (doubly derivatised): 21.1 min; 3-methylaminobenzoic acid substrate (doubly derivatised): 21.2 min; internal standard (derivatised 9-hydroxyfluorene): 23.2 minutes.

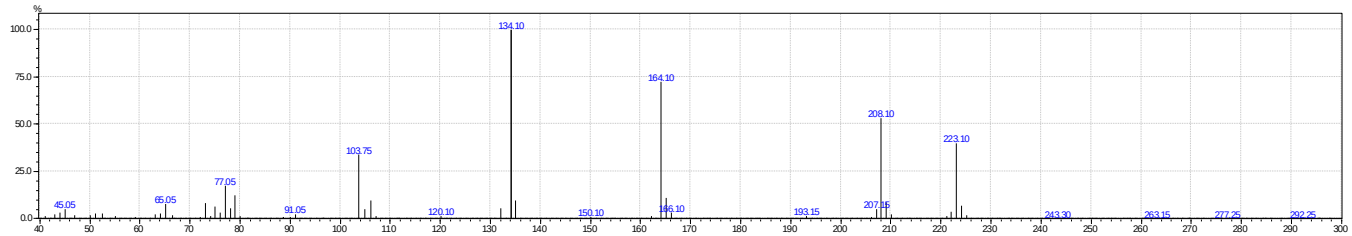

4-methylaminobenzoic acid substrate (singly derivatised): m/z = 223.10 (exp. m/z =223.3437), RT = 13.5 min

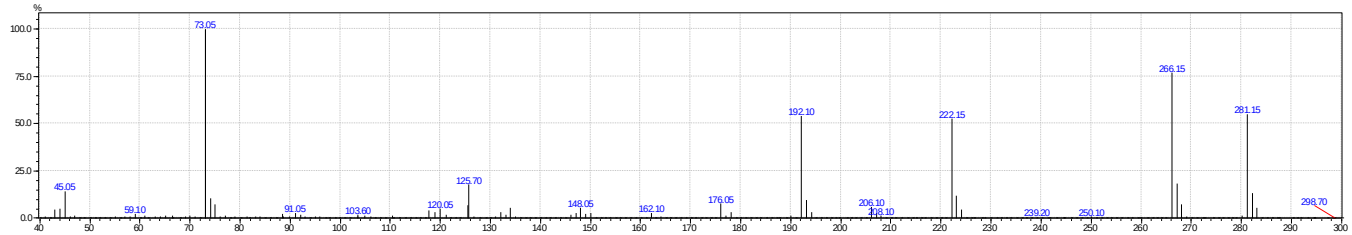

4-aminobenzoic acid (doubly derivatised): m/z = 281.15 (exp. m/z =281.1267), RT = 15.1 min

Figure S5 (c) MS data for 4-methylaminobenzoic acid turnovers with CYP199A4.

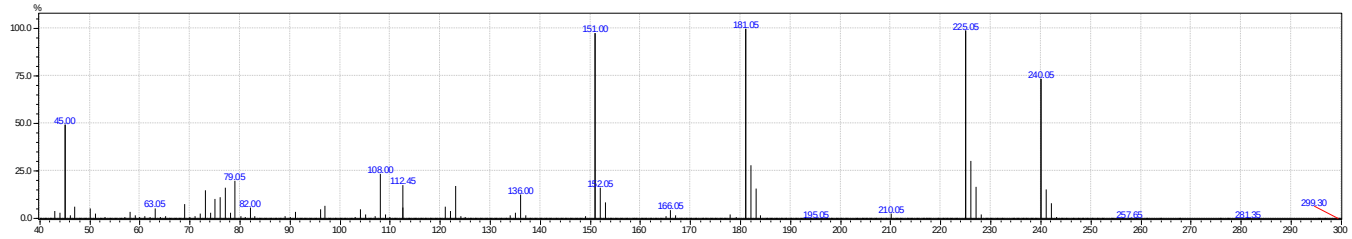

4-methylthiobenzoic acid substrate (singly derivatised): m/z = 240.05 (exp. m/z = 240.0640), RT = 12.6 min

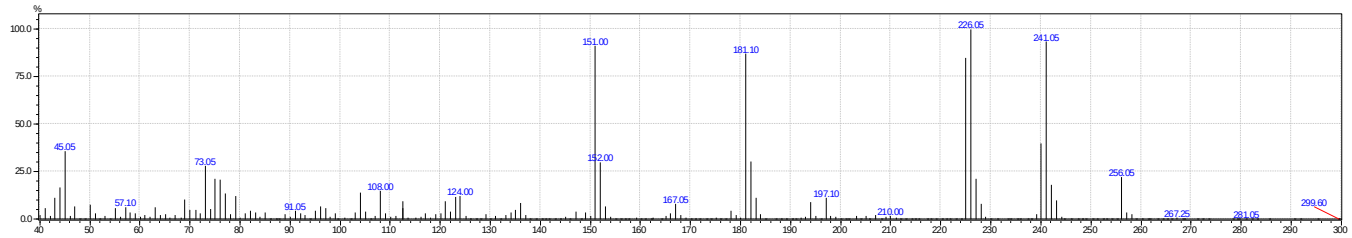

4-methylsulfinylbenzoic acid (singly derivatised): m/z = 256.05 (exp. m/z = 256.0589), RT = 16.2 min

Figure S5 (d) MS data for 4-methylthiobenzoic acid turnovers with CYP199A4.

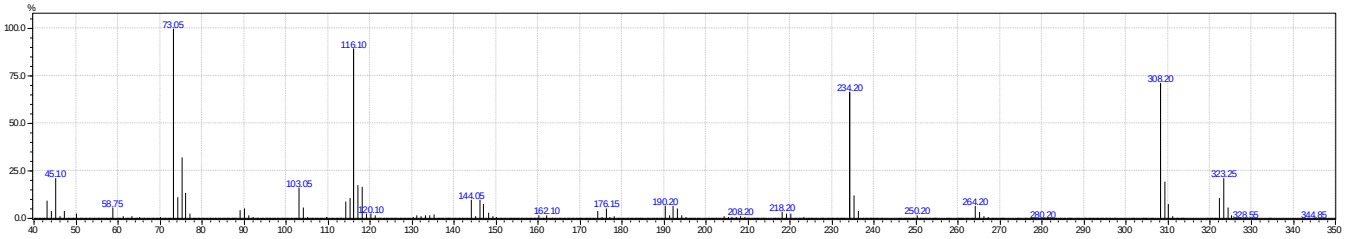

4-acetamidobenzoic acid substrate (doubly derivatised): m/z = 323.25 (exp. 323.1373), RT = 15.4 min

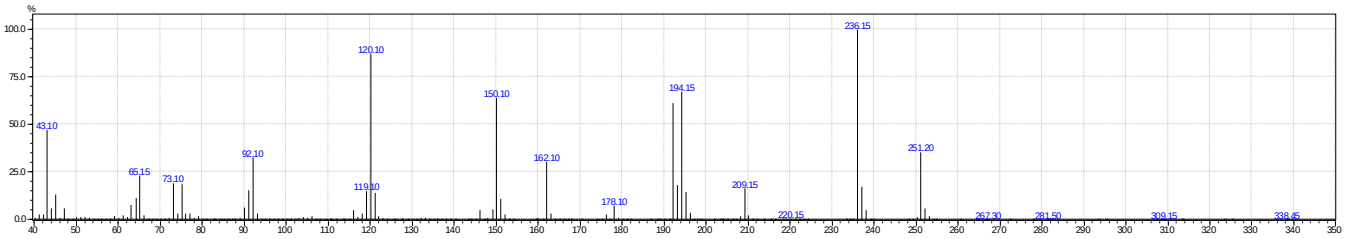

4-acetamidobenzoic acid substrate (singly derivatised): m/z = 251.20 (exp. 251.0978), RT = 17.8 min

Figure S5 (e) MS data for 4-acetamidobenzoic acid product arising from the turnovers with CYP199A4.

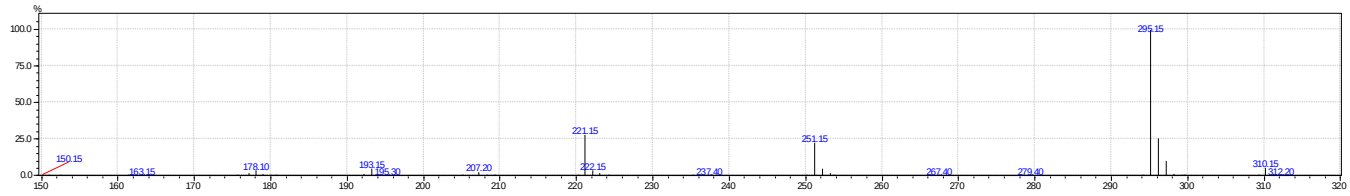

terephthalic acid product, doubly derivatised m/z = 310.15 (-Me -> 295.15; vs exp. 310.1057)

RT 14.2 min

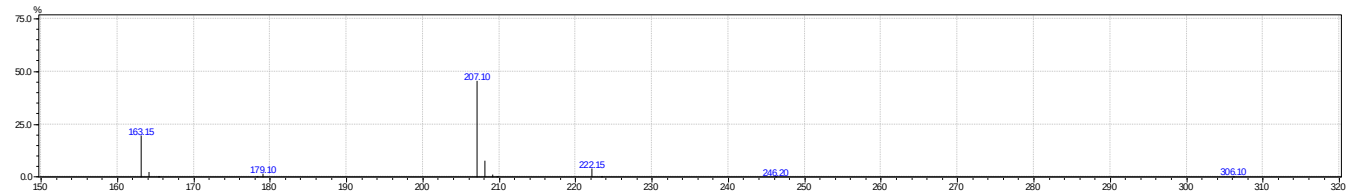

4-formylbenzoic acid, derivatised m/z = 222.15 (exp. 222.0712)

RT 7.8 min

Figure S5 (f) MS data for 4-aminomethylbenzoic acid products arising from the turnovers with CYP199A4.

3-Methylthiobenzoic acid MS data

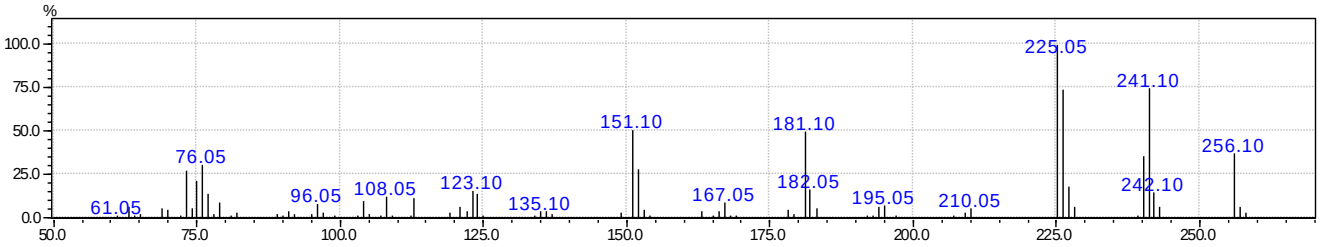

3-(Methylsulfinyl)benzoic acid (singly derivatised): m/z = 256.10 (exp. 256.0589), RT = 17.0 min

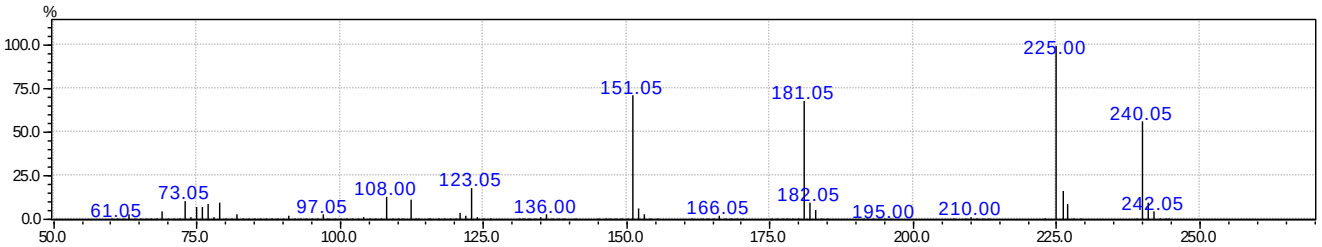

3-(Methylthio)benzoic acid substrate (singly derivatised): m/z = 240.05 (exp. 240.0640), RT = 12.2 min

Figure S5 (g) MS data for 3-methylthiobenzoic acid turnovers with CYP199A4.

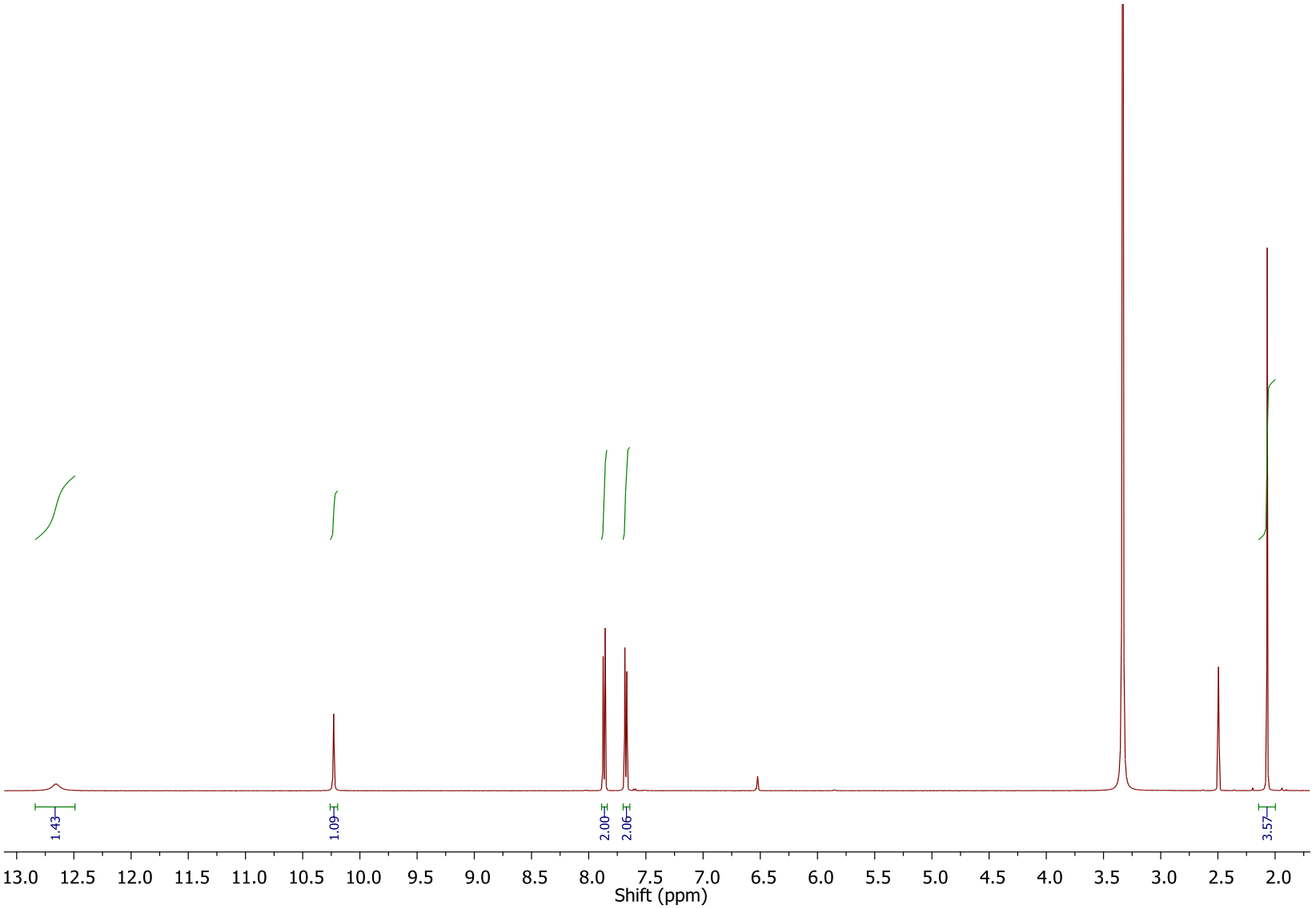

Figure S6 (a) ^{1}H NMR of 4-acetamidobenzoic acid.

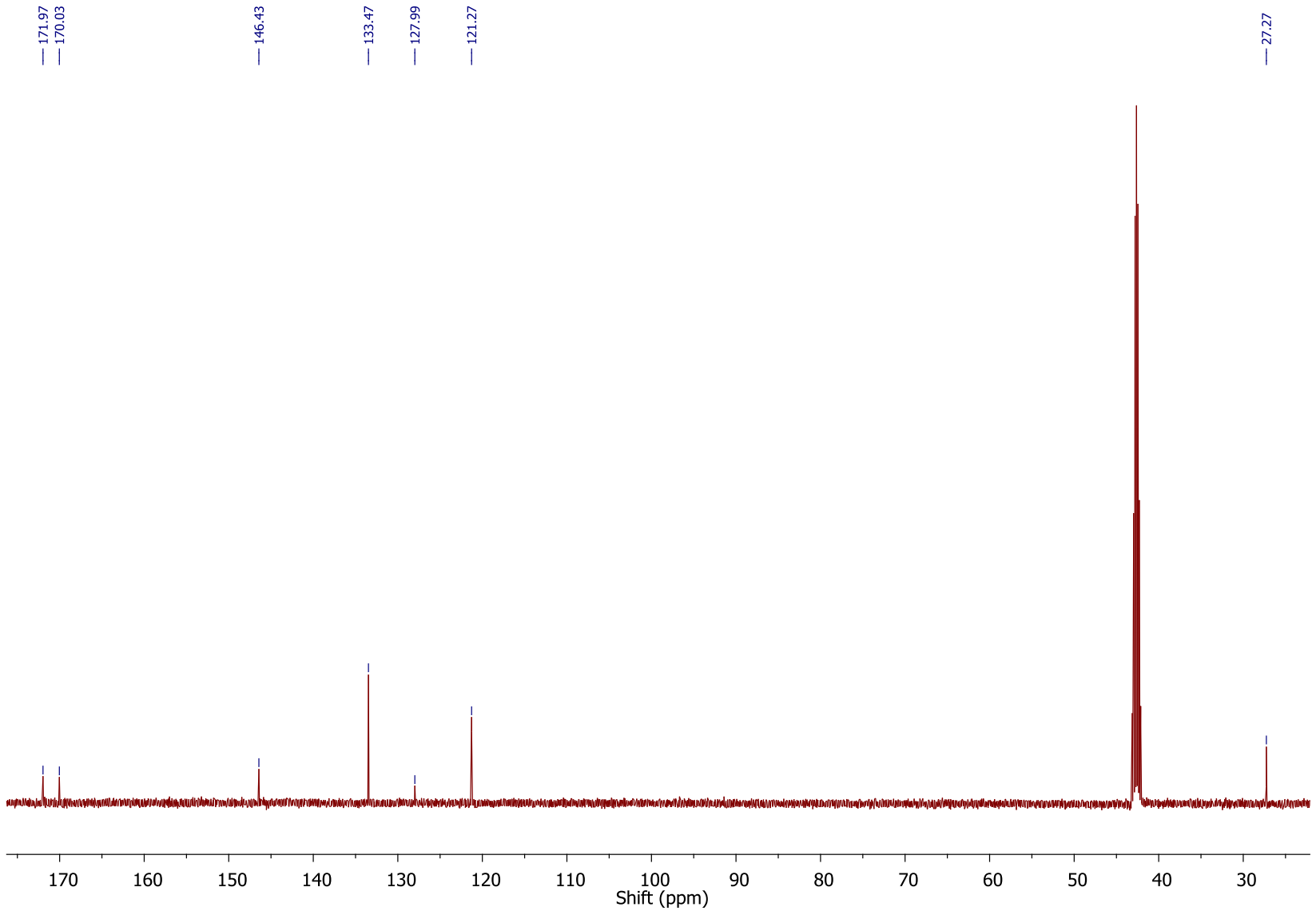

Figure S6 (b) ^{13}C NMR of 4-acetamidobenzoic acid.

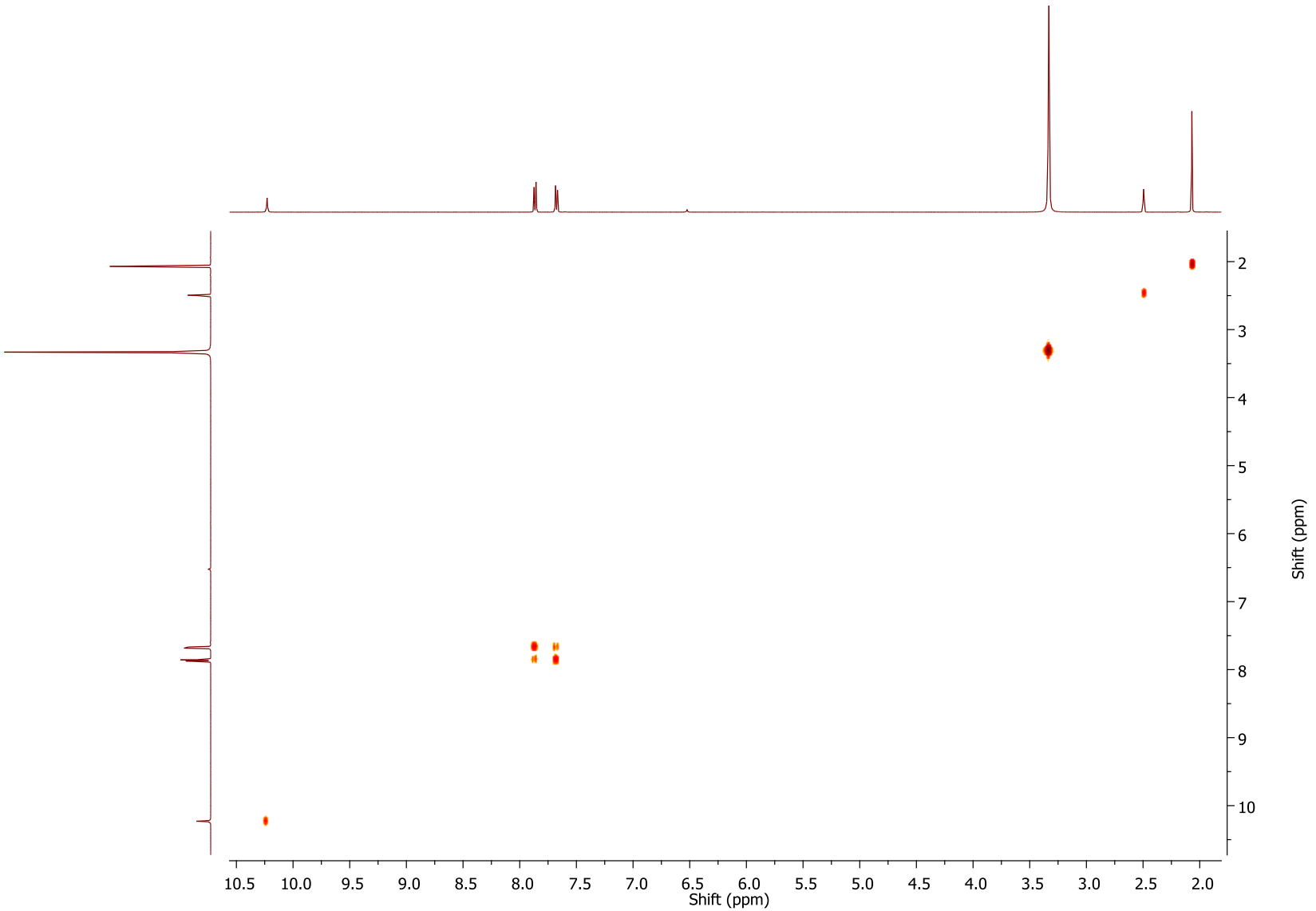

Figure S6 (c) COSY NMR of 4-acetamidobenzoic acid.

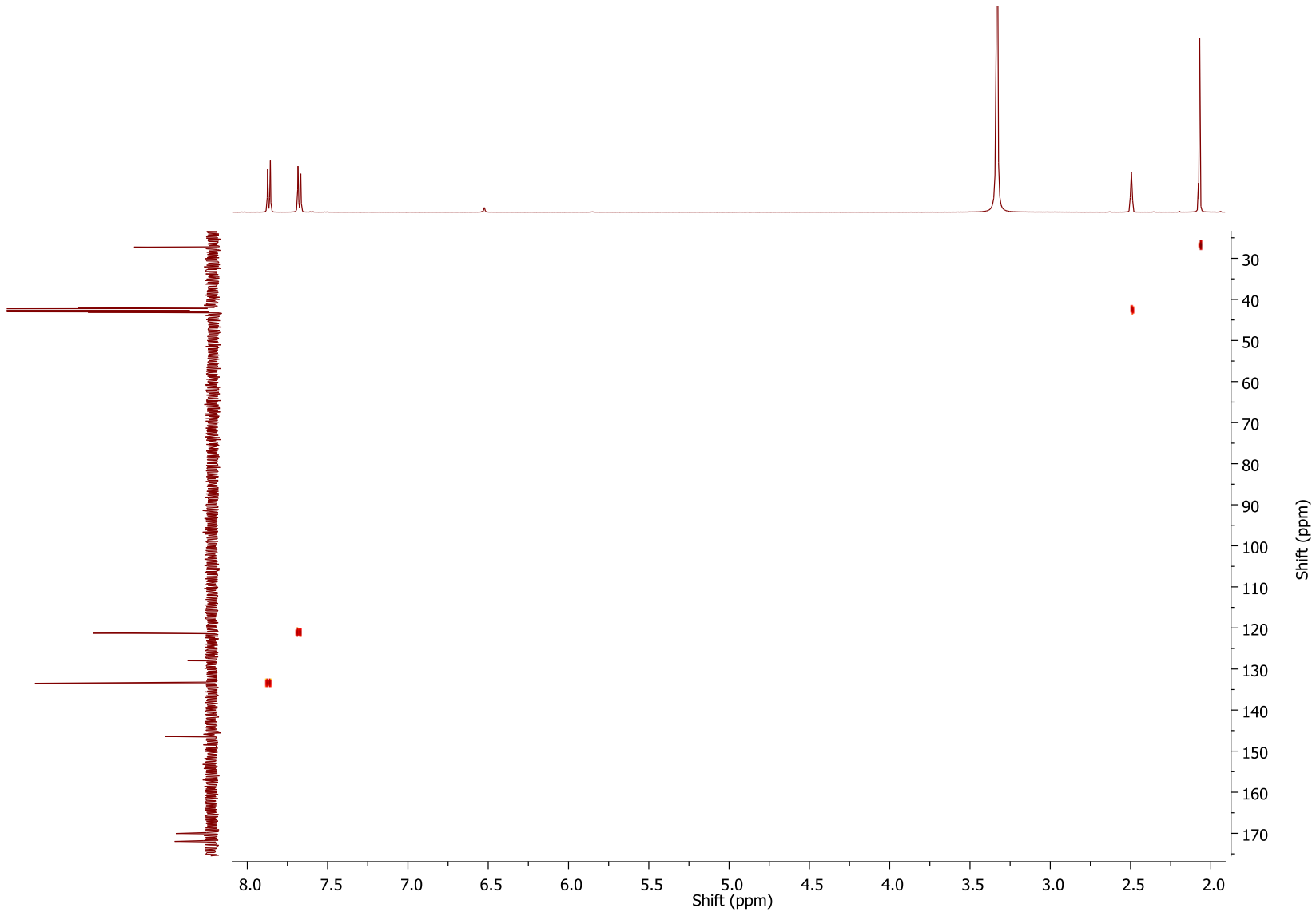

Figure S6 (d) HSQC NMR of 4-acetamidobenzoic acid

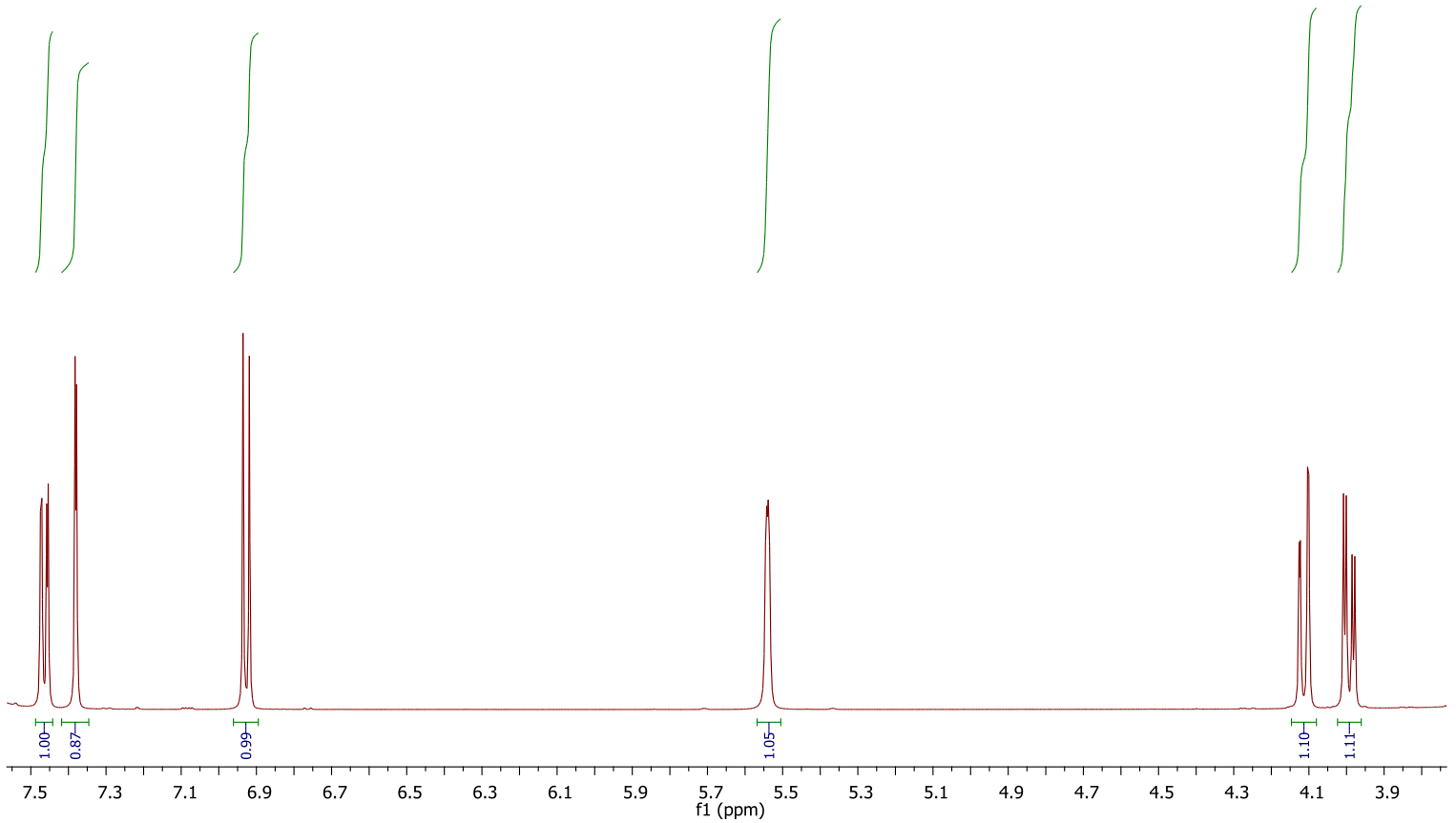

Figure S6 (e) NMR data for product from *in vitro* turnover of 3,4-ethylenedioxybenzoic acid to 6-carboxy-2,3-dihydro-2-hydroxy-1,4-benzodioxin. ^{1}H NMR of 4-- 6-carboxy-2,3-dihydro-2-hydroxy-1,4-benzodioxin.
^{1}H NMR (500 MHz, dmso) δ 7.46 (dd, *J* = 8.4, 2.0 Hz, 1H), 7.38 (d, *J* = 2.0 Hz, 1H), 6.93 (d, *J* = 8.4 Hz, 1H), 5.54 (dd, *J* = 3.7, 1.7 Hz, 1H), 4.11 (dd, *J* = 11.3, 1.7 Hz, 1H), 3.99 (dd, *J* = 11.3, 3.7 Hz, 1H).

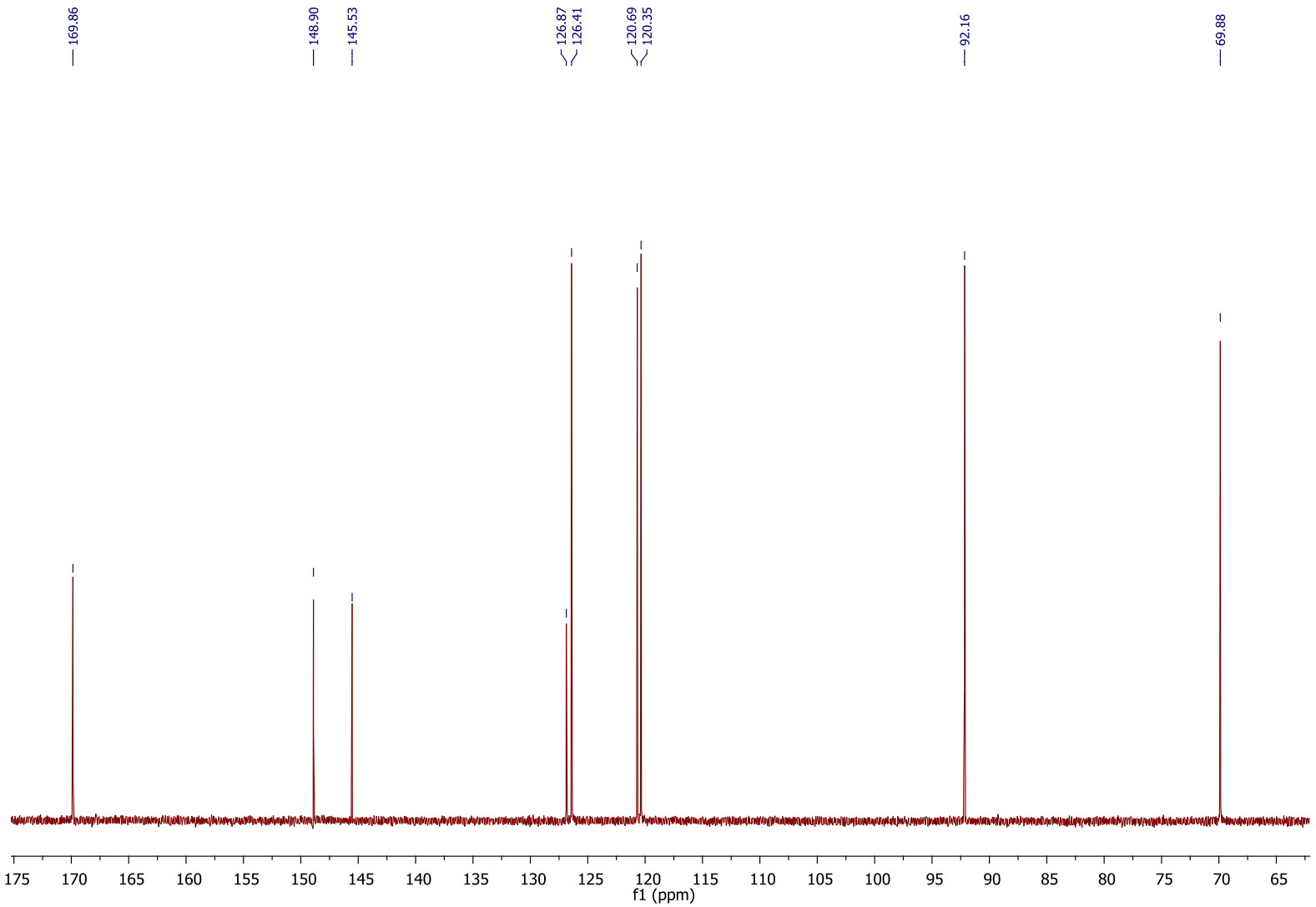

Figure S6 (f) ^{13}C NMR of 6-carboxy-2,3-dihydro-2-hydroxy-1,4-benzodioxin

(500 MHz, DMSO) δ 169.86, 148.90, 145.53, 126.87, 126.41, 120.69, 120.35, 92.16, 69.88.

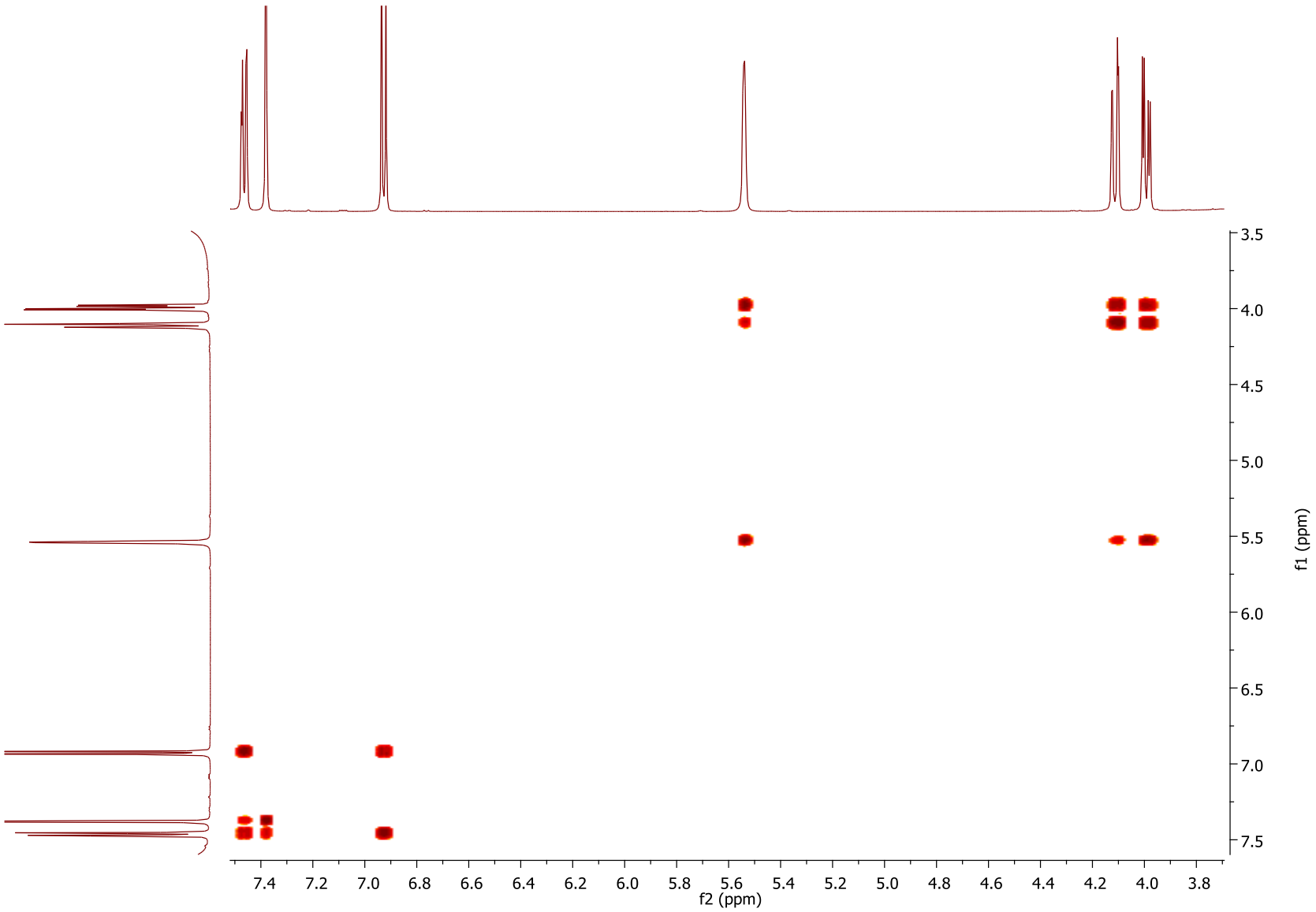

Figure S6 (g) ^{1}H-^{1}H COSY of 6-carboxy-2,3-dihydro-2-hydroxy-1,4-benzodioxin.

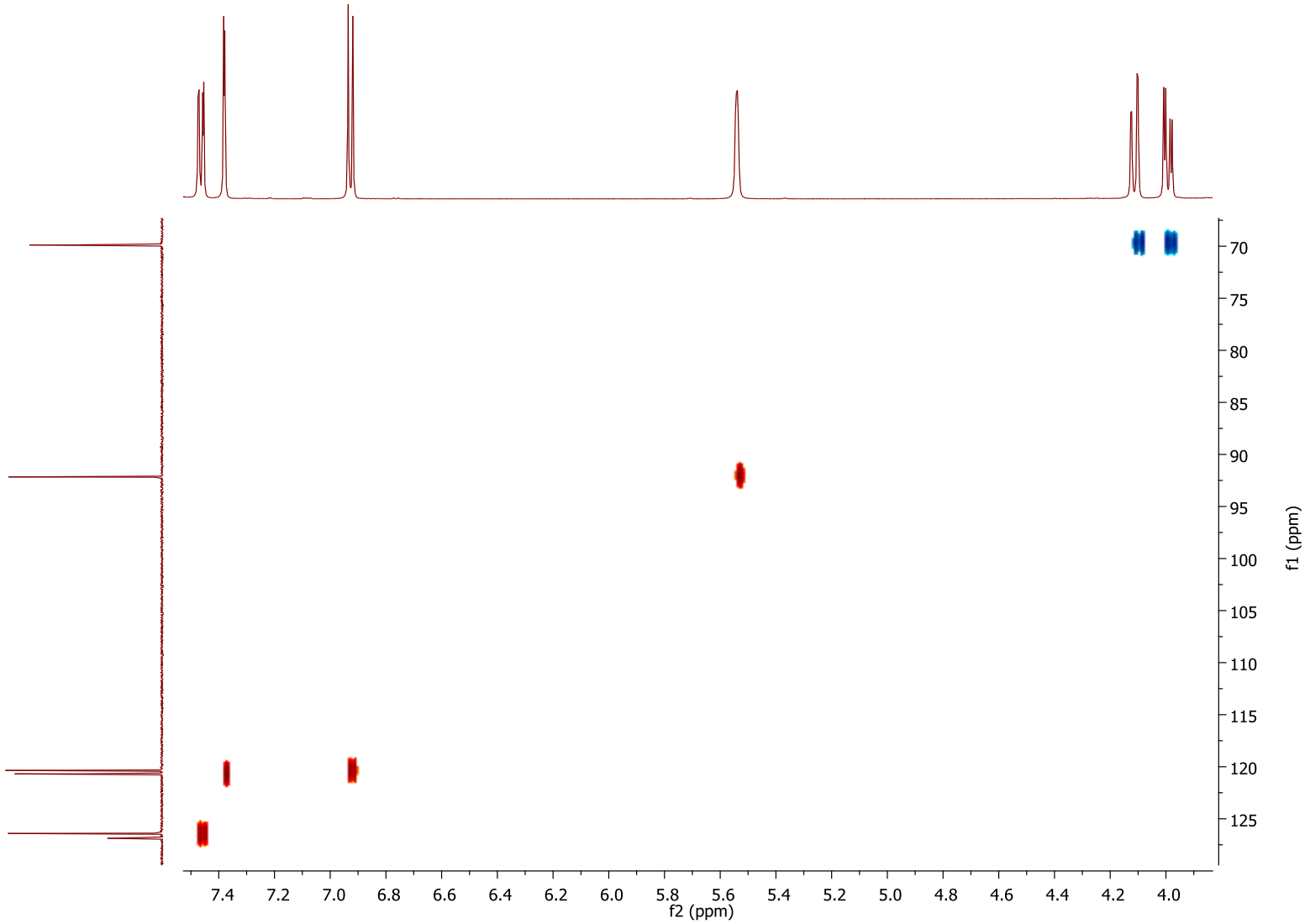

Figure S6 (h) ^{1}H-^{13}C HSQC 6-carboxy-2,3-dihydro-2-hydroxy-1,4-benzodioxin

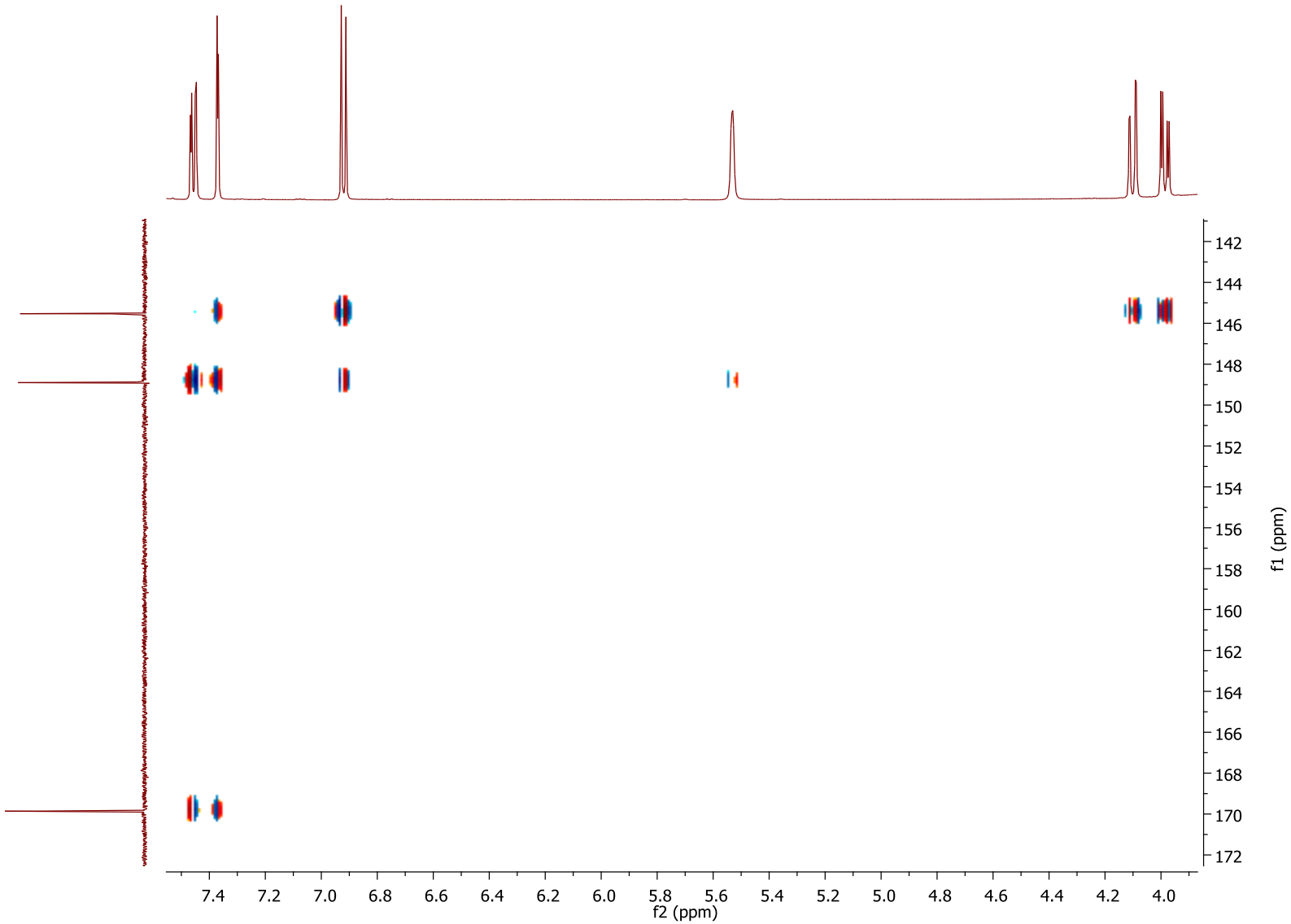

Figure S6 (i) ^{1}H-^{13}C HMBC of 6-carboxy-2,3-dihydro-2-hydroxy-1,4-benzodioxin.

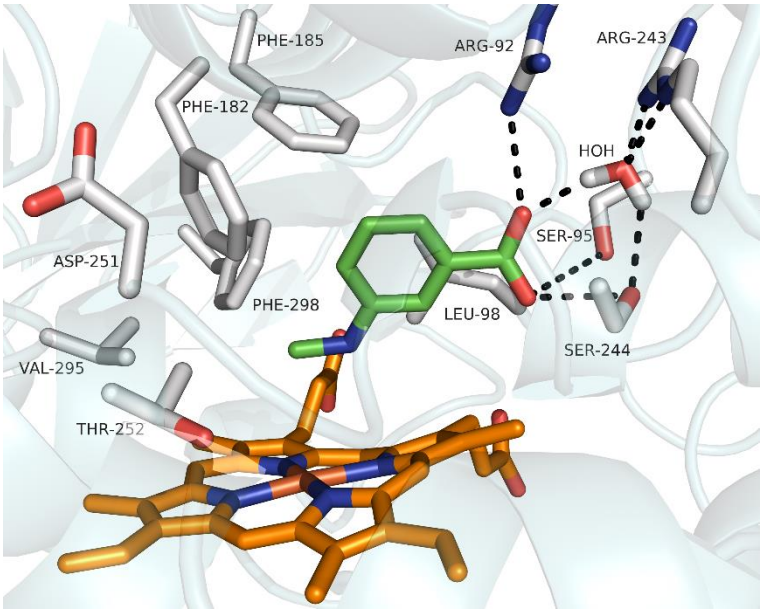

The lowest energy orientation of 3-methylaminobenzoic acid after docking in the active site of CYP199A4 and energy minimisation.

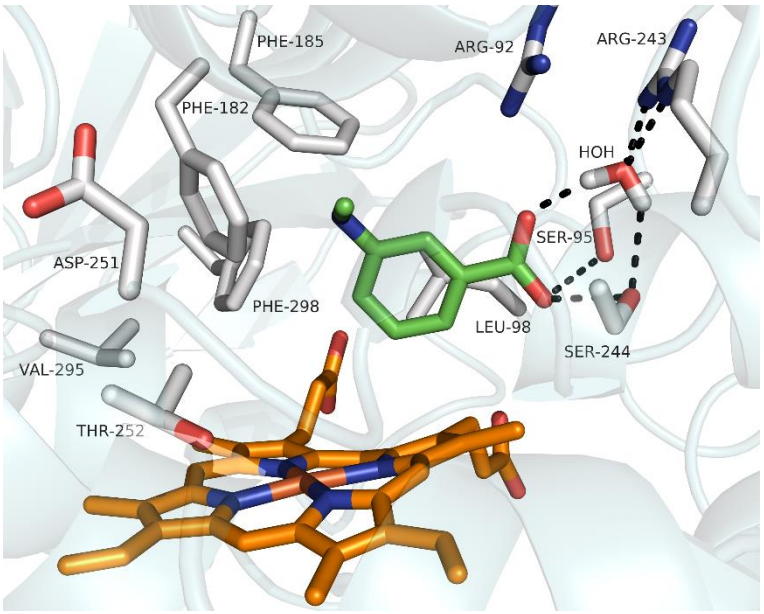

A higher energy orientation of 3-methylaminobenzoic acid after docking in the active site of CYP199A4 in the ‘up’ orientation.

Figure S7 Docking studies with 3-methylaminobenzoic acid

3-Methylaminobenzoic acid, heme and active site residues are depicted in green, orange and grey respectively, with nitrogen atoms shown in blue, oxygen in red and the heme iron in brown. Hydrogen bonds are represented by black dashed lines. Comparative distances and scores from ICM-Pro docking program are given overleaf.

Pose	Score	Vls Score	Strain kcal/mol	Steric	Torsion	Electro	Hbond kcal/mol	Hydroph kcal/mol	Surface
'Down' orientation	-38.03	-40.46	2.421	-16.86	1	-4.597	-9.406	-3.178	6.355
'Up' orientation	-26.73	-36.42	9.698	-6.917	1	-11.1	-10.08	-3.049	6.341

Selected distances between 3-methylaminobenzoic acid in the up or down position and the heme or active site residues of CYP199A4.

	Down	**Up**
CH_3 – Fe	3.9 Å	7.4 Å
N – Fe	4.2 Å	7.2 Å
N – nearest heme N	3.6 Å	n.m.
CH_3 – nearest heme N	3.3 Å	n.m.
CH_3 – nearest heme C	3.4 Å	n.m.
CH_3 – closest C of Phe182	4.1 Å	2.8 Å
N – closest C of Phe182	n.m.	3.1 Å
CH_3 – closest C of Phe298	3.8	5.0 Å
CH_3 – closest C of Phe185	n.m.	3.2 Å

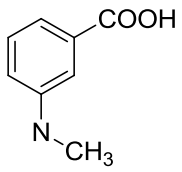

Figure S7 (continued) Docking studies with 3-methylaminobenzoic acid

(a)

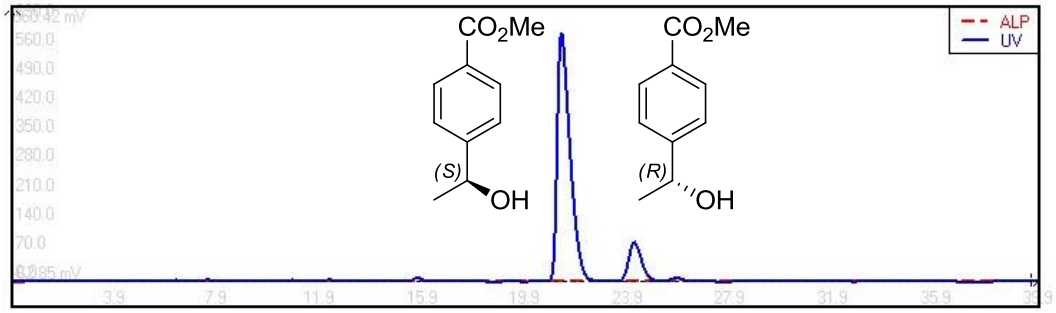

(b)

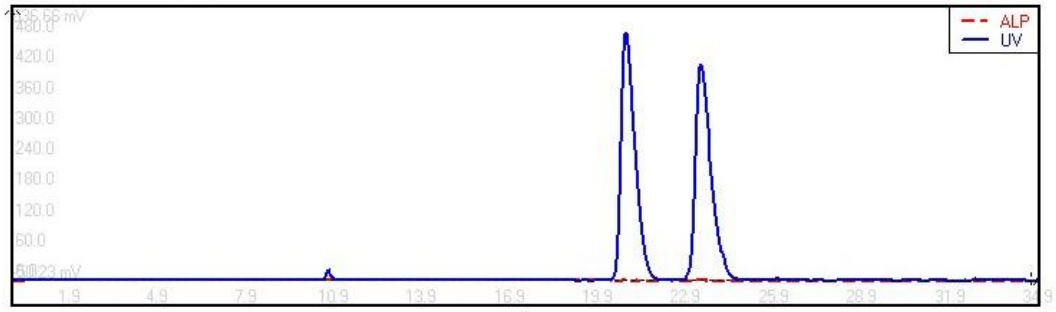

(c)

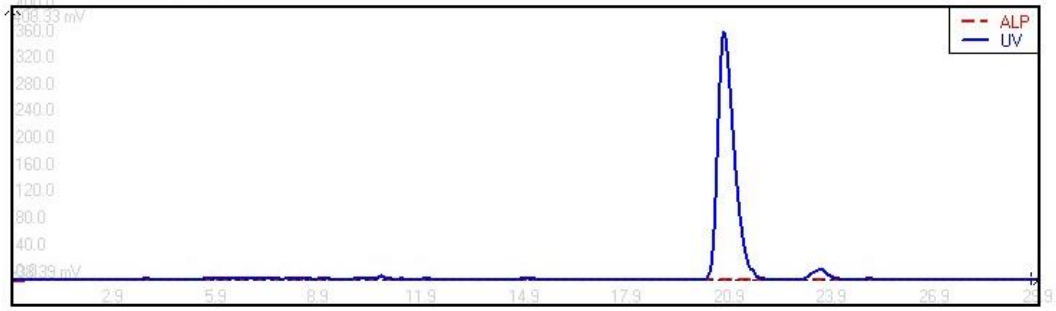

(d)

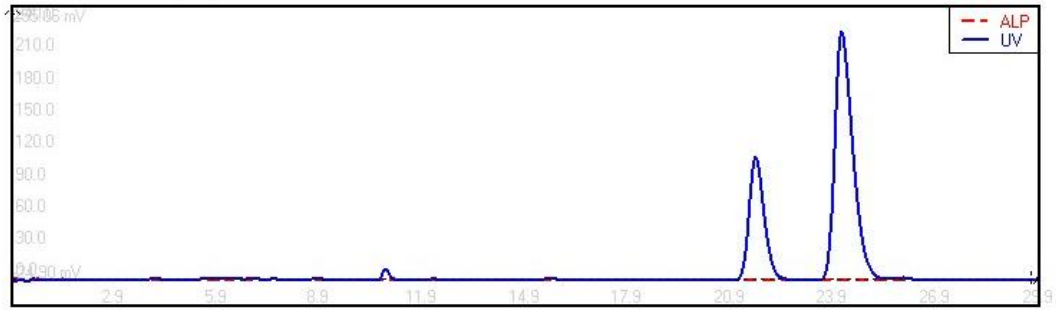

Figure S8 (a) Chiral HPLC data for 4-ethylbenzoic acid. Chiral HPLC analysis of the 4-ethylbenzoic acid alcohol product (methyl ester derivatised). Retention times of the two enantiomers are 20.92 (*S*) and 23.44 (*R*) min. (a)The CYP199A4 turnover of 4-ethylbenzoic acid (86:13 (*S*):(*R*)); (b) the racemic mixture of the alcohol product; (c) e turnover products spiked with the purified (*S*)-alcohol and (d) The turnover products spiked with the purified (*R*)-alcohol.

(a)

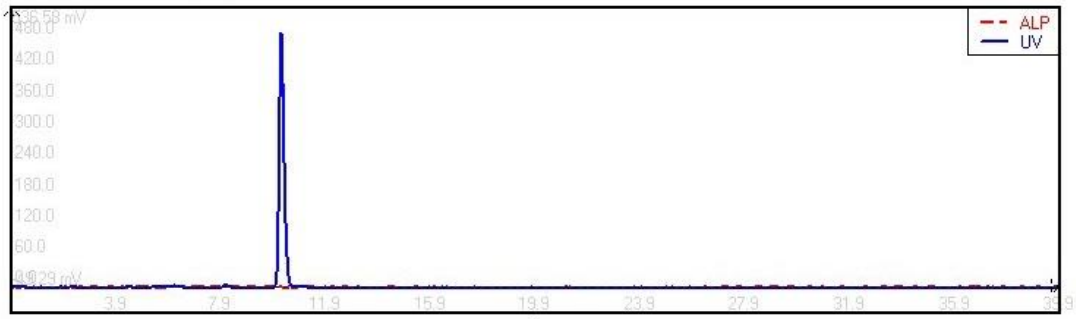

(b)

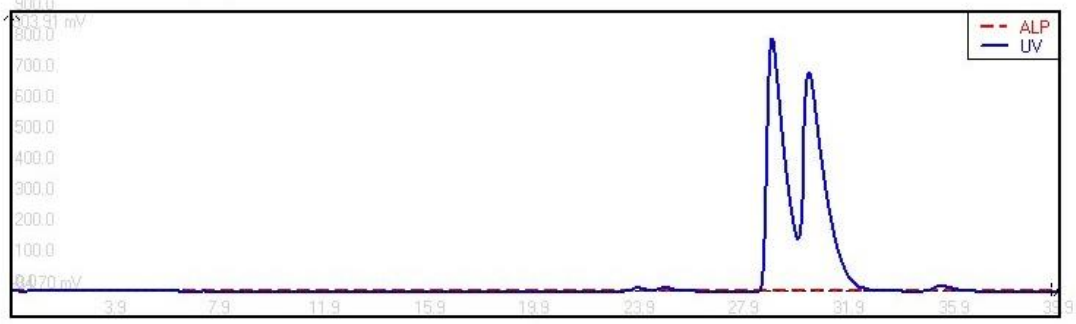

(c)

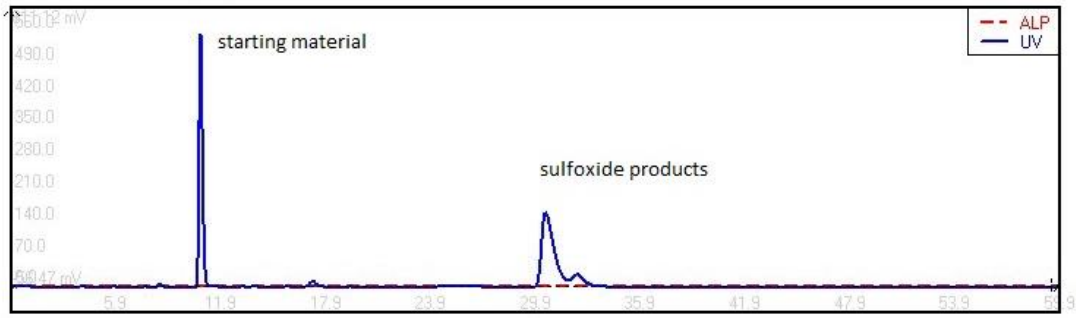

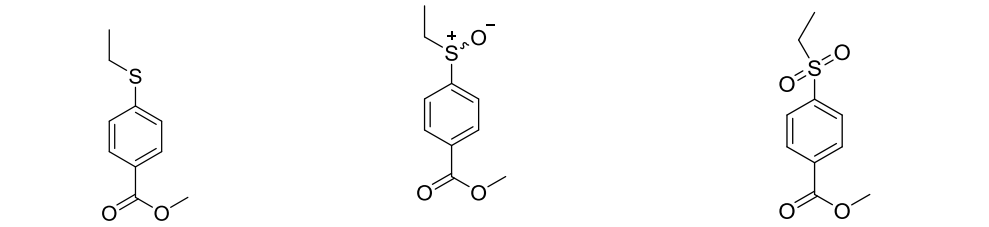

methyl 4-(ethylthio)benzoate methyl 4-(ethylsulfinyl)benzoate methyl 4-(ethylsulfonyl)benzoate

Figure S8 (b) Chiral HPLC data for 4-ethylthiobenzoic acid (methyl ester derivatised); (a) HPLC analysis of methyl 4-(ethylthio)benzoate (substrate, RT 10.3 min); HPLC analysis of methyl 4-(ethylsulfinyl)benzoate (RT 29.0 and 31.5 min). The retention time of methyl 4-(ethylsulfinyl)benzoate was 35.6 min and (c) HPLC analysis of the CYP199A4 turnover of 4-(ethylthio)benzoate (91:9 ratio of the enantiomers).

a)

b)

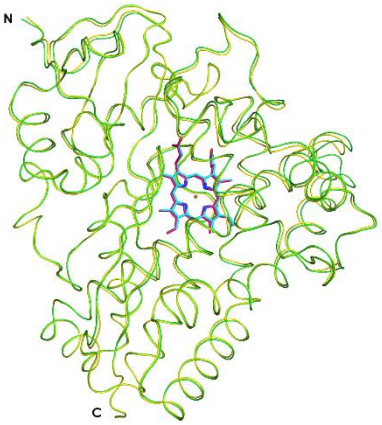

c)

d)

Figure S9 Superimposed structures of the Cα chains of different CYP199A4 structures. The 4-methoxybenzoic acid-bound backbone is shown as green with the heme unit shown as blue in all; the overlaid structure is shown as yellow with a magenta heme unit. Shown are (a) 4-ethoxybenzoic acid, (b) 4-methylaminobenzoic acid, (c) 4-methylthiobenzoic acid and (d) 4-ethylthiobenzoic acid. The N and C terminus is indicated on each. All structures displayed r.m.s.d. <0.60 Å.